

**STRUCTURE-PROPERTY RELATIONSHIP
IN CORE-SHELL RUBBER TOUGHENED EPOXY NANOCOMPOSITES**

A Dissertation

by

KI TAK GAM

Submitted to the Office of Graduate Studies of
Texas A&M University
in partial fulfillment of the requirements for the degree of

DOCTOR OF PHILOSOPHY

December 2003

Major Subject: Mechanical Engineering

STRUCTURE-PROPERTY RELATIONSHIP
IN CORE-SHELL RUBBER TOUGHENED EPOXY NANOCOMPOSITES

A Dissertation

by

KI TAK GAM

Submitted to Texas A&M University
in partial fulfillment of the requirements
for the degree of

DOCTOR OF PHILOSOPHY

Approved as to style and content by:

Hung-Jue Sue
(Chair of Committee)

Abraham Clearfield
(Member)

Chii-Der S. Suh
(Member)

Roger Morgan
(Member)

Dennis L. O'Neal
(Head of Department)

December 2003

Major Subject: Mechanical Engineering

ABSTRACT

Structure-Property Relationship in Core-shell Rubber Toughened

Epoxy Nanocomposites. (December 2003)

Ki Tak Gam, B.S., Pusan National University;

M.S., Pusan National University

Chair of Advisory Committee: Dr. Hung-Jue Sue

The structure-property relationships of epoxy nanocomposites with inorganic layer-structure nanofillers have been studied to obtain the fundamental understanding of the role of nanofillers and the physics of polymer nanocomposites in this dissertation. Several polymer nanocomposite systems with modified montmorillonite (MMT) or α -zirconium phosphate (ZrP) nanofillers were prepared with epoxy matrices of different ductility and properties. The successful nanofiller's exfoliations were confirmed with X-ray diffraction and transmission electronic microscopy (TEM). Dynamic mechanical analysis (DMA) on the prepared epoxy nanocomposites revealed the significant increase in rubbery plateau moduli of the epoxy nanocomposite systems above T_g , as high as 4.5 times, and tensile test results showed improved modulus by the nanofiller addition, while the fracture toughness was not affected or slightly decreased by nanofillers. The brittle epoxy nanocomposite systems were toughened with core shell rubber (CSR) particles and showed remarkable increase in fracture toughness (K_{IC}) value up to 270%. The CSR toughening is more effective at ductile matrices, and TEM observation indicates that

major toughening mechanisms induced by the CSR addition involve a large scale CSR cavitation, followed by massive shear deformation of the matrix.

**To my Lord Jesus, my parents,
and my wife Kyeong Eun.**

ACKNOWLEDGEMENTS

I would like to express my sincere gratitude and respect to my dissertation committee chairperson, Dr. Hung-Jue Sue, for his intellectual advises and steadfast encouragement and support during my Ph.D. program. I also want to give thanks to my dissertation committee member, Dr. Abraham Clearfield for his helpful discussions and insightful suggestions and excellent technical guidance. Thanks are also extended to my dissertation committee members, Dr. Roger Morgan, and Dr. Steve Suh, for their support and understanding.

I would express my gratitude to Dr. Walter Bradley and Dr. Leila Bonnaud for helpful discussions and suggestions and for their encouragement as well. Special thanks are given to Dr. Naima Bestaoui and Mr. Nick Spurr in the Chemistry Department for their valuable work on nanofiller preparation and surface modification. I extend my appreciation to Dr. Zhiping Luo in the Microscopy and Imaging Center for his professional assistance for TEM microscopy.

The research funding by the Defense Logistic Agency (Contract #SP0103-02-D-003) and KANEKA Corporation are greatly appreciated.

I have benefited from working with my precious colleagues in my research group, Guangxue Wei, Jim Lu, Zhiyong Xia, Al Estrada, Chao Li, Chen Xiang, Yanmei Li, Jana Weaver, Buc Slay, Jongil Weon, David Li, and Minhao Wong. Their friendship and unconditional support will always be remembered. I wish them the best in all their future endeavors.

TABLE OF CONTENTS

	Page
ABSTRACT.....	iii
DEDICATION.....	v
ACKNOWLEDGEMENTS.....	vi
TABLE OF CONTENTS.....	vii
LIST OF TABLES.....	x
LIST OF FIGURES.....	xi
 CHAPTER	
I INTRODUCTION.....	1
1.1 Background.....	1
1.2 Objectives of This Research.....	3
1.3 Overview of This Research.....	4
II BACKGROUND AND LITERATURE REVIEW	5
2.1 Introduction.....	5
2.2 Nanofillers for Polymer Nanocomposites.....	7
2.3 Clay Purification and Nanofiller Surface Modification.....	9
2.4 Preparation of Polymer Nanocomposites.....	11
2.5 Mechanical Properties and Fracture Toughness of Polymer Nanocomposites.....	12
2.6 Rubber Toughening of Polymers.....	14
III FRACTURE BEHAVIOR OF CORE-SHELL RUBBER-MODIFIED CLAY-EPOXY NANOCOMPOSITES.....	17
3.1 Introduction.....	17
3.2 Experimental.....	19
3.2.1 Materials.....	19

CHAPTER	Page
3.2.2 Preparation of Nanocomposites.....	20
3.2.3 X-Ray Scattering Study.....	22
3.2.4 Mechanical Properties.....	22
3.2.5 Morphology and Fracture Mechanisms.....	23
3.3 Results and Discussion.....	24
3.3.1 Morphology Characterization.....	24
3.3.2 Mechanical Properties and Fracture Toughness.....	26
3.3.2.1 System-1 Epoxy System.....	26
3.3.2.2 System-2 Epoxy System.....	34
3.3.3 Toughening Using CSR Particles.....	36
3.4 Conclusions.....	45
IV EPOXY NANOCOMPOSITES BASED ON THE SYNTHETIC α -ZIRCONIUM PHOSPHATE LAYER STRUCTURE.....	46
4.1 Introduction.....	46
4.2 Experimental.....	48
4.2.1 Materials.....	48
4.2.2 Synthesis.....	48
4.2.2.1 Preparation of ZrP.....	48
4.2.2.2 Intercalation of ZrP with Jeffamine M715.....	50
4.2.2.3 Preparation of ZrP-Based Epoxy Nanocomposites.....	51
4.2.3 Characterization.....	53
4.2.4 Mechanical Property Characterization.....	54
4.3 Results and Discussion.....	55
4.3.1 Characterization of M-ZrP.....	55
4.3.2 Characterization of M-ZrP/Epoxy Nanocomposites.....	59
4.3.3 Dynamic Mechanical Behavior.....	65
4.3.4 Mechanical Property Characterization.....	68
4.4 Conclusions.....	71
V MECHANICAL PROPERTY OF α -ZIRCONIUM PHOSPHATE-EPOXY NANOCOMPOSITES AND THEIR TOUGHENING MECHANISMS.....	73
5.1 Introduction.....	73
5.2 Experimental.....	75
5.2.1 Materials.....	75
5.2.2 Surface Modification of α -ZrP.....	76
5.2.3 Preparation of α -ZrP-Based Epoxy Nanocomposites.....	76
5.2.4 Characterization.....	77

CHAPTER	Page
5.2.5 Mechanical Property Characterization.....	79
5.2.6 Viscosity Measurement.....	79
5.2.7 Toughening Mechanism Investigation.....	80
5.3 Results and Discussion.....	81
5.3.1 Characterization of the Intercalate α -ZrP and M1-ZrP/Epoxy Nanocomposites.....	81
5.3.2 Dynamic Mechanical Behavior	84
5.3.3 Mechanical Property of ZrP/Epoxy Nanocomposites.....	90
5.3.4 Viscosity of Liquid Epoxy Resin with ZrP Particles.....	92
5.3.5 Epoxy-II Nanocomposite System with CSR.....	94
5.3.5.1 Mechanical Properties.....	94
5.3.5.2 Toughening Mechanisms of CMZE System.....	95
5.4 Conclusions.....	107
VI CONCLUDING REMARKS AND RECOMMENDATIONS.....	109
6.1 Intercalation and Exfoliation of the Inorganic Layer Structures in Epoxy Matrices.....	109
6.2 Mechanical Properties of the Epoxy Nanocomposites.....	110
6.2.1 Clay Epoxy Nanocomposites.....	110
6.2.2 ZrP-Epoxy Nanocomposites.....	110
6.3 Fracture Behavior and Toughening Mechanisms of Epoxy Nanocomposites.....	111
6.3.1 Clay Epoxy Nanocomposites.....	111
6.3.2 ZrP-Epoxy Nanocomposites.....	112
6.4 Recommendations for Future Research.....	112
REFERENCES.....	115
VITA.....	122

LIST OF TABLES

TABLE		Page
3-1	Compositions of Clay-Epoxy Nanocomposites.....	21
3-2	Mechanical Properties of System-1 Nanocomposites	29
3-3	Fracture Toughness (K_{IC}) of System-1 Nanocomposites.....	33
3-4	Mechanical Properties & Fracture Toughness (K_{IC}) of System-2 Nanocomposites.....	42
4-1	Compositions of α -ZrP-Epoxy Nanocomposites.....	52
4-2	DMA Results of α -ZrP-Epoxy Nanocomposites.....	66
4-3	Mechanical Properties and Fracture Toughness.....	69
5-1	Compositions of ZrP-Epoxy Nanocomposite System-1,-2.....	78
5-2	Tensile Properties and Fracture Toughness of ZrP-Epoxy Nanocomposites.....	92
5-3	Tensile Properties and Fracture Toughness of ZrP-Epoxy-II Nanocomposites.....	98

LIST OF FIGURES

FIGURE		Page
3-1	WAXS of System-1 Nanocomposites.....	25
3-2	TEM of System-1N Nanocomposite.....	27
3-3	TEM of System-1NR Nanocomposite.....	28
3-4	DMA of System-1 Nanocomposites.....	30
3-5	Tensile Properties of System-1 Nanocomposites.....	32
3-6	DMA of System-2 Nanocomposites.....	35
3-7	Optical Microscopy of System-1NR Nanocomposite with a Crack.....	37
3-8	TEM of System-1NR Nanocomposite Showing Delamination of Nanofillers with 1 μm Scale Bar.....	38
3-9	TEM of System-1NR Nanocomposite Showing Delamination of Nanofillers with 100 nm Scale Bar.....	39
3-10	TEM of System-1NR Nanocomposite Showing Crack Bifurcation and Crack Deflection.....	40
3-11	TEM of System-2NR Nanocomposite Showing Crack Bifurcation and Bridging of CSR.....	43
3-12	TEM of System-2NR Nanocomposite Showing CSR Cavitation.....	44
4-1	X-ray Powder Pattern of α -Zirconium Phosphate.....	49

FIGURE	Page
4-2	Scanning Electron Micrographs of α -Zirconium Phosphate..... 50
4-3	X-ray Powder Pattern of α -Zirconium Phosphate Intercalated with Jeffamine M715..... 51
4-4	(a) ^{31}P NMR of α -Zirconium Phosphate. (b) ^{31}P NMR of α -Zirconium Phosphate Intercalated with M715..... 57
4-5	Infrared Spectrum of Jeffamine M715 and α -Zirconium Phosphate Intercalated with Jeffamine M715..... 58
4-6	X-ray Powder Pattern of (a) α -ZrP/Epoxy (b) Neat/Epoxy (c) M- α -ZrP/Epoxy 60
4-7	Photographs of (a) Transparent M- α -ZrP/Epoxy and (b) Opaque α -ZrP/Epoxy Samples..... 61
4-8	TEM of M- α -ZrP/Epoxy Showing (a) Low Magnification and (b) High Magnification of Uniform Dispersion and Exfoliation of α -ZrP Layers 63
4-9	TEM of α -ZrP/Epoxy (a) Low Magnification and (b) High Magnification 64
4-10	DMA of (a) Neat and α -ZrP/Epoxy (b) M/Epoxy and M- α -ZrP /Epoxy Systems..... 67
4-11	Tensile Behavior of Neat and α -ZrP-Modified DGEBA/DDS Epoxy Systems..... 70

FIGURE	Page
5-1	WAXD of Intercalated ZrP particles with 20 mmol of Monoamine M715..... 82
5-2	WAXD of ZrP-Epoxy Composite (top) and M1-ZrP/Epoxy Nanocomposite (bottom) 83
5-3	SEM Pictures on the Failed Surface from SEN-3PB Test (Top: ZrP/Epoxy Composite, bottom: M2-ZrP/Epoxy Nanocomposite) 85
5-4	TEM Pictures of M1-ZrP/Epoxy Nanocomposite Showing (a) Low Magnification and (b) High Magnification of Dispersion and Exfoliation of ZrP Layers..... 86
5-5	DMA Plots of (a) Neat Epoxy and ZrP/Epoxy (b) M2/Epoxy and M2-ZrP/Epoxy Systems..... 88
5-6	DMA Plots of M1/Epoxy and M1-ZrP/Epoxy Systems..... 89
5-7	Tensile Behavior of M1-, M2-ZrP/Epoxy Nanocomposites..... 91
5-8	Viscosity of the ZrP and M1-ZrP in Liquid Epoxy (DER332) at Different Shear Rate..... 94
5-9	Tensile Behavior of M-ZrP/Epoxy-II Nanocomposites..... 96
5-10	TEM of Crack Tip Damage Zone from DN-4PB Test Sample of MZE Epoxy Nanocomposites..... 99
5-11	TEM of Crack from DN-4PB Test Sample of MZE Epoxy Nanocomposites..... 100

FIGURE	Page	
5-12	OM of Crack Tip Damage Zone from DN-4PB Test Sample of CMZE Epoxy Nanocomposite. (top) Bright Field and (bottom) Cross-polarized Field.....	101
5-13	TEM of Crack from DN-4PB Test Sample of CMZE Epoxy Nanocomposite before CSR Staining.....	103
5-14	TEM of Crack Tip Damage Zone from DN-4PB Test Sample of CMZE Epoxy Nanocomposite before CSR Staining.....	104
5-15	TEM of CMZE Epoxy Nanocomposite after CSR Staining Far from Crack.....	105
5-16	TEM of Crack from DN-4PB Test Sample of CMZE Epoxy Nanocomposite after CSR Staining.....	106
5-17	TEM of Crack Tip Damage Zone from DN-4PB Test Sample of CMZE Epoxy Nanocomposite after CSR Staining.....	107

CHAPTER I

INTRODUCTION

1.1 Background

Polymer nanocomposites are composite materials that consist of a polymer matrix with well- dispersed nanofillers, which have at least one dimension at the nanometer scale. Since the report on nylon-clay nanocomposites from Toyota Central Labs was published, much research has been performed, on the syntheses, characterization, and properties of polymer nanocomposites, to understand the fundamentals of nanofiller effects on the matrix polymer resins [1-13]. These polymer nanocomposites show improved properties including enhanced mechanical properties at low loading of nanofillers, increased gas barrier properties while retaining clarity, dimensional stability, etc. The exfoliation of the layered structure nanofillers in the polymer matrix is very important to maximize the reinforcement by the nanofillers for the property improvement [6]. However, many of the reported polymer nanocomposites have not convincingly proved the complete exfoliation of layer structures in the polymer matrix, and some intercalation and aggregated layer structures unavoidably remained with their repeatable regular structures in the composite materials. The exfoliation

This dissertation follows the style of *Journal of Materials Science*.

mechanisms of the nano-layer structure in the polymer nanocomposites are still under investigation for many polymer nanocomposite systems.

Epoxy resins are used in many different applications in the automotive, construction, and aerospace industries for their appropriate materials properties including mechanical properties and thermal and chemical stability [14]. On the other hand, because of their high crosslinking density epoxy resins are inherently brittle. This brittleness of epoxy resin is one of the major obstacles preventing epoxy's wider application use in industries. To overcome the lack of toughness in brittle and notch sensitive polymers, elastomer fillers have been incorporated [15-25]. However elastomer filler use in polymer resins reduces stiffness, strength, and creep resistance of the toughened polymer system. There are several available methods to toughen polymer matrices with additives, namely rigid-rigid polymer toughening, rubber toughening, etc. Preformed core-shell rubber (CSR) was introduced to toughen polymer matrices most efficiently among available rubber toughening methods [26], and it was reported that CSR particles significantly enhance the toughness of epoxy resins with only around 3 wt% addition [27, 28]. This amount of CSR does not significantly reduce the stiffness and strength of matrix resins, however it does improve the fracture toughness of the matrix.

Many researchers extensively studied the preparation and physical property improvements of epoxy-clay nanocomposites with the nanofiller additions [6, 29]. But, toughness and fracture mechanisms of polymer nanocomposites were not well understood. It is worthwhile to study the effect of nanofiller addition in epoxy clay

nanocomposites on strengthening mechanism and fracture behaviors and toughening mechanisms of the nanometer scale CSR particles.

1.2 Objectives of This Research

This research is part of a large effort towards the fundamental understanding of the physics of polymer nanocomposites, especially on the preparation of polymer nanocomposites with layer-structure nanofillers and their effects on the mechanical properties of polymer nanocomposites with fracture toughness and toughening mechanisms. To achieve these goals, several epoxy clay nanocomposite systems are carefully prepared with different nanofillers and matrices of different ductility, and characterized to confirm the nanolayer's exfoliation. Dynamic mechanical analysis and tensile tests were performed with microscopy to understand the effects of nanocomposites morphology on their mechanical properties. The extensive investigations of fracture toughness and toughening mechanisms of the prepared polymer nanocomposites and toughened systems are involved with a variety of microscopy techniques. The present work is expected to significantly contribute to the fundamental understanding of the role of nanofillers in polymer nanocomposites and to the fracture behavior and toughening mechanisms of polymer nanocomposites with CSR fillers.

1.3 Overview of This Research

As part of a large effort to understand the fundamental physics of polymer nanocomposites, current research covers preparations of several different epoxy nanocomposite systems, characterizations, mechanical property evaluation and toughness, and investigation of toughening mechanisms of toughened polymer nanocomposite systems.

In Chapter II, background knowledge relevant to polymer nanocomposite research and general review of related literature is provided. Chapter III addresses the preparation, characterization, and the mechanical properties and toughening mechanisms of epoxy-clay nanocomposites with CSR of different ductility.

The preparation of epoxy nanocomposites based on the intercalated α -Zirconium Phosphate (α -ZrP) and their mechanical properties are discussed in Chapter IV. Chapter V reports that the effects on the mechanical properties of the α -ZrP-epoxy nanocomposites by the different amount of surface modifier for the intercalated α -ZrP, and the toughening mechanisms of the CSR resulted in toughened α -ZrP-epoxy nanocomposites. In Chapter VI, an overall summary of present research is given with some recommendations for future research. General conclusions of the work accomplished in this thesis are drawn in this chapter.

CHAPTER II

BACKGROUND AND LITERATURE REVIEW

2.1. Introduction

Polymer nanocomposites with well-dispersed inorganic nanometer-scale particles, which have at least one dimension in the nanometer range, have been studied extensively. For example, clay-epoxy nanocomposites have been shown to exhibit remarkably improved mechanical and gas barrier properties.[4~9] Clay-nylon 6 nanocomposite was also reported to possess greatly improved tensile strength, modulus, and heat distortion temperature.[1~3, 10~13] At present, despite the concept of polymer nanocomposites being in existence for almost two decades, there are still considerable efforts to be carried out which includes effective toughening of polymer nanocomposites.

There are several ways to define nanocomposites. First of all, many different nano-fillers can be found including zero-dimensional nano-particles, one-dimensional linear chain structure nano-materials (e.g., nanofibers), two-dimensional layered structures (e.g., exfoliated layer-structure montmorillonite (MMT) clay), and three-dimensional network structures with nanometer-scale channels (e.g., zeolite). In general, these nanofillers have sizes in the range of 1~100 nm, and they are well-dispersed in

matrix materials to create nanocomposites. When polymer materials are used in the matrix, the composites are named polymer nanocomposites.

In current papers, the terminology for nanocomposites can be defined as follows. If the layer-structure filler is not intercalated nor exfoliated, the nanocomposite can be designated a conventional composite material. If the layer-structure fillers are partially intercalated or exfoliated in the matrix, but not completely exfoliated or shows some aggregated layer structure in the matrix, the nanocomposite can be called an intercalated nanocomposite. If the layer-structure of the nanofillers is well delaminated, randomly oriented and homogeneously dispersed layer-by-layer without remaining repeated layer structures detected by X-ray diffraction or transmission electronic microscopy, the nanocomposite is referred as an exfoliated nanocomposite.

Two main applications of polymer nanocomposites are engineering polymers and packaging materials. Because of the increase in modulus, tensile strength, heat distortion temperature and retention of impact strength, polymer nanocomposites have many possibilities for engineering polymers applications, e.g., automobile parts (especially under-the-hood applications). The packaging materials application, such as food, beverage, and pharmaceutical packaging, is also a good area for nanocomposite use due to increased gas barrier properties against O₂, CO₂, and water vapor while retaining clarity. Material properties serve as a foundation of practical engineering applications of nanocomposites including these two major applications. They also are pivotal for further research and development of polymer nanocomposite materials. Thus, materials

properties need to be explained alongside the fundamental understanding of the role of nanofillers in nanocomposites.

In this chapter, background knowledge relevant to polymer nanocomposites and a general review of related literature is provided. Nanofillers for polymer nanocomposites and their purification, surface modification, and preparation of polymer nanocomposites is discussed, and mechanical properties and rubber toughening for polymer materials will be reviewed.

2.2. Nanofillers for Polymer Nanocomposites

Polymer nanocomposites with matrices based on epoxy [4~9, 30~32], polyamide-6 [1~3, 10~13], polypropylene (PP) [11, 33], polystyrene [34], and nanofillers based on montmorillonite clay, TiO_2 , CaCO_3 , SiO_2 [35~37], have been extensively studied. Significant efforts have been paid to achieve maximum dispersion of nanofillers in polymer matrices. However, aggregation of nanofillers, to various degrees, is unavoidable. As a result, the cause(s) for the significant drops in ductility and toughness found in polymer nanocomposites cannot be unambiguously determined due to the constraining effect of the nanofiller particles or to the presence of the detrimental aggregates in the polymer matrix, or both.

Montmorillonite clay is among the most widely chosen nanofiller for polymer nanocomposites because of its several advantages. Clays have high ion exchange capacity, which allows modification of the interlayer spacing to achieve better

compatibility with host polymer matrices. It also exhibits high aspect ratio to give better reinforcement effect [38]. Most importantly, clay is abundant and inexpensive. Its potential for large-scale commercial uses is high.

Clay is mined naturally and then purified for filler applications. Therefore the particle size distribution and aspect ratio of clay can be limitedly controlled for specific research purposes to understand the fundamental physics of the polymer nanocomposite. With the exception of nylon 6/clay nanocomposites [39], most of published results on clay-based polymer nanocomposites only exhibit incomplete exfoliation of the clay [40~42]. Many of the inconsistent claims on how nanofillers influence properties, such as T_g , toughness, ductility and strength, may partially be due to imperfect exfoliation or presence of aggregation of clay in the polymer matrix, or some unknown nanofiller surface chemistry and reactions.

For these concerns, synthetic α -zirconium phosphate (α -ZrP), $Zr(HPO_4)_2 \cdot H_2O$ is used as a layer-structure nanofiller in the latter part of this study. Because of the higher ion exchange capacity of α -ZrP as compared to montmorillonite clays, the controllable size and aspect ratio of α -ZrP particles, and the narrow particle size distribution of α -ZrP, we can investigate the fundamental nanofiller effects on the properties of the host polymers.

Crystalline α -ZrP was first prepared in 1964 by Clearfield and Stynes [43]. The crystal structure has been determined to be a layer structure in both $P2_1/n$ and $P2_1/c$ space groups [44]. This layer structure is similar to montmorillonite clay. However, the layers are formed by zirconium atoms connected between them by the oxygen atoms of

the phosphate groups. Each phosphate contributes three of its oxygen atoms to the formation of these layers, leaving one OH group pointing into the interlayer space. Earlier studies have shown that α -ZrP is capable of incorporating 2 moles of n-alkylamines with the formation of a bilayer in the interlayer space [45]. This occurs through an acid-base reaction, where the proton is transferred from the -POH group to the nitrogen or by hydrogen bonding.

So far, only two related research papers were found focusing on the intercalation of α -ZrP particles using amino acids [46] and on α -ZrP modification using equimolar tetra-n-butyl ammonium hydroxide to prepare thin films of α -ZrP [47]. No known effort has been focused on the utilization of α -ZrP to prepare polymer nanocomposites.

2.3. Clay Purification and Nanofiller Surface Modification

There are a few requirements for clay to be used as a nanofiller. First, the purification to remove the 5~35% impurity from the natural montmorillonite is necessary. If these impurities are not removed from the clay, they may act as stress concentrators or increase haze in the final composites. The purification is composed of two steps.[48] The first step is to remove carbonate. Carbonate in gallery of montmorillonite from nature, causes floccuation of phyllosilicate layers, and must be replaced with Na^+ , which tends to disperse soil particles. This process can be achieved with NaOAc. The second step is to remove organic matter and MnO_2 . The organic

matter in the Na^+ saturated samples obtained from the first step aggregate in the soil, so it needs to be removed with an oxidizing agent, such as H_2O_2 .

The purified montmorillonite needs to be surface-modified for exfoliation in the polymer matrix. The Na^+ saturated, pure montmorillonite surface needs to be modified with appropriate surface modifiers to achieve the compatibility with polymer matrices by changing the hydrophilic clay surface to a hydrophobic modifier. The modifier is composed of a non-polar tail on one end and a positive group on the other end. After surface modification, it can be compatible with a non-polar polymer matrix and also this can replace the Na^+ on the negatively charged phyllosilicate surface. There are several available methods to modify the clay surface. Cation exchange is a traditional method since 1949 [49]. This method substitutes onium ions (contain amine functionality) for the exchangeable cations. It is used for Cloisite particles (modified clay products of SCP Inc.), I.24T, I.30TC (products of Nanocor), and usually a reversible chemical reaction takes place in which positive ions in a solution are exchanged for the equivalent ions in a clay solid surface. For example, in the surface treatment of montmorillonite with octadecyl amine, the reaction occurs between the Na^+ ions binding on negatively charged montmorillonite surfaces and the positively charged ammonium (NH_3^+) groups from octadecyl amines. Ion dipole interaction is another method. It is a relatively new method, involving attaching organic molecules (containing alcohol, carbonyl, ether groups) to the exchangeable cations. The modified clay product from Nanocor, I.35K and I.46D is prepared with this method [50]. Several reports on the study of the effects of surface modification to prepare nanocomposites reveals that the exfoliation of layer

structures need enough length of the surface modifier to avoid restrictive diffusion of layer structures, and prefer more acidic ammonium exchange ions.[29, 51]

Synthesized α -ZrP is dried and powdered for surface modification without further purification. Monoamine surface modifier, Jeffamine M-715 is used for surface modification of synthesized α -ZrP particles. [43, 52]

2.4. Preparation of Polymer Nanocomposites

In-situ intercalative polymerization is a common way for preparing epoxy-clay nanocomposites with intercalated organic monomers in the inorganic layered host undergoing polymerization. The in-situ intercalative polymerization is typically performed from the start with the mixing of modified clay with liquid epoxy resin, sonication of the mixture, addition of a curing agent to the mixture and degassing, followed by two-step curing at elevated temperatures. Another way to prepare nanocomposites is melt blending the polymer resin with modified inorganic fillers and compatibilizers, as in the PP-clay nanocomposites with PP and maleic anhydride modified PP as compatibilizer [33]. The procedure is started by dry mixing the three components, which are modified clay, maleic anhydride modified PP oligomer, and PP matrix resin. Then, they are melt blended at 210 °C using twin screw extruders to make the nanocomposites.

Many researchers study the polymer nanocomposites report on the major factors affecting the exfoliation of the layer-structure nanofillers in polymer matrices. Ion

exchange capacity of the silicate layers, chemical nature of interlayer cations, polarity of the organic cations, polarity of medium and polarity of the monomer are among the important factors they investigate.[29, 53] Also, the curing agents, the diffusion of monomers and curing agents, the preparation conditions, such as temperature, mixing or stirring conditions, sonication, etc, can affect the successful exfoliation of the nanolayers in polymer nanocomposites.[29, 54, 55]

2.5. Mechanical Properties and Fracture Toughness of Polymer Nanocomposites

Improvement in various mechanical properties is one of most interesting aspects of polymer nanocomposites. The reinforcement of tensile modulus by addition of layer-structure nanofiller was broadly investigated by researchers with many different polymer matrices including poly(amide-6) [1~3, 10~13], PP [33], poly(amide-6)/PP [11], polysulfone [56], polystyrene[11, 34], poly (ethylene terephthalate-co-ethylene naphthalate)(PETN) [57], poly (vinylalcohol)(PVA) [58], epoxy resin [4, 6, 29, 51], polyimide film [35, 59~62], and polyurethane [63~65].

The most significant enhancements of the moduli were found in the MMT - PETN nanocomposite and MMT-PVA nanocomposite. The MMT-PETN nanocomposite with 4wt% MMT showed improved modulus of 4.34 GPa from 1.57 GPa of neat PETN, and MMT-PVA nanocomposite with 2.11 wt% of MMT yielded modulus of 212 MPa whereas neat PVA has a modulus of 69 MPa. Many other prepared nanocomposites

show moderately improved tensile moduli with the addition of the nanofillers, however they are not so significant as these two systems. It is possibly due to the incomplete exfoliation of the nanofillers in polymer resins as clearly found in several reports [10, 61] and supported with micro-mechanics view point with model system [66], and the matrix rigidity also may affect this not-significant improvement of the tensile modulus of matrix.

The most common approach to investigate the fracture toughness of polymer materials are Single-edge notch 3 point bending (SEN-3PB) tests as described in ASTM D5045-96 method to acquire the mode I critical stress intensity factor, K_{IC} . The sequence of damage or events leading to the toughening of the polymer is crucial in understanding the role the toughener plays. Values alone do not allow observation of damage zones or toughening mechanisms. The double-notch 4 point bending (DN-4PB) test studies the crack tip damage zone. From this morphology study at the damage zone the information of the fracture behavior of the materials can be obtained. It is imperative that this method is utilized to validate the values obtained from other mechanical tests.

For the fracture toughness of the polymer nanocomposites, only a few studies exist [32, 67]. A report on the clay nanocomposites with nylon6 and PP matrices addressed fracture behavior [67]. The extensive cavitation behavior was found at the temperature above its T_g and for nylon6 the typical shear banding deformation is changed at least in the initial stage, and localized interfacial damage provokes significant matrix fibrillation and failures were mainly found where the clay exfoliation was not completely achieved. However, not many studies were performed to understand the

fracture behaviors of polymer nanocomposites, and the fundamental understanding of the role of nanofillers in fracture and toughening mechanisms of polymer nanocomposites is not yet established.

2.6. Rubber Toughening of Polymers

Several methods have been employed in past research to toughen different material systems. These methods have led to different toughening mechanisms that can be evaluated and shown to improve properties significantly. As mentioned before, the rigid-rigid polymer toughening method has proven advantageous in improving properties in different material systems including bismaleimide(BMI) resin toughened with preformed polyphenylene oxide (PPO) particles and isotactic polypropylene toughened with Noryl (a mixture of PPO and high impact polystyrene) particles. It was found that PPO could be utilized to greatly increase the toughness of BMI without compromising its stiffness [68]. This has been evidenced by dilatation band formation and crack tip blunting [69, 70]. This concept is actually derived from the rubber toughening approach. This method suggests that a second-phase rigid polymer can help relieve tension and can generate stress concentration sites, similarly as rubber-toughened epoxy systems do to toughen a rigid polymer matrix [69]. Other techniques for toughening brittle epoxies include making a chemical modification of a given epoxy backbone to a more flexible backbone structure, an increase of epoxy monomer molecular weight, and lowering of

the cross-link density [71]. Each toughening approach exhibits unique advantages over the others.

Rubber is typically used as a toughening agent. For the rubber modified epoxies, Garg and Mai [72] found more than 14 toughening mechanisms available around developing cracks. Shear-banding, crazing, crack bridging, micro-cracking, crack-bifurcation, crack deflection, and crack pinning are the important toughening mechanisms. The particle size is another other important factor in generating effective toughening mechanisms such as massive crazing and shear banding. As demonstrated by both Kramer [73] and Bucknall [16], the optimum toughness of PS was achieved at the size of rubber particles about 0.5 ~2 μm . Jang [74] also demonstrated that larger rubber particles mainly led to massive crazing while smaller rubber particles caused matrix shear yielding.

A study using an epoxy resin showed that the CSR modified system exhibited the most effective toughening among all available rubber tougheners [27]. The preliminary work has also shown significant increase in fracture toughness [75]. The significant improvements in toughness (G_{IC}) by CSR addition (490~640 J/m^2) compared with DAR (Dispersed Acrylic Rubber) addition (420 J/m^2) in the Diglycidyl ether bisphenol-A/4,4'-diamino diphenylsulfone(DGEBA/DDS) epoxy system, which has G_{IC} value of 180 J/m^2 was reported [27].

It was found that between three to five percent of CSR had the greatest effect on the epoxy matrix [27, 28]. Studies compared the effect of the variation of particle size, particle size distributions and particle distribution [27, 28]. It was found that smaller

particles provided a greater increase in toughness by cavitation-induced shear banding. It has also been found that it is preferable to obtain a globally, randomly dispersed system of particles that may be locally clustered in order to obtain higher toughness [27]. Because of this promising work of using CSR to toughen epoxy-based resin systems, it is believed that this same technology can be applied to the clay-polymer nanocomposites as a toughening agent.

To strengthen polymer matrices, we can apply the nanocomposite technology via the surface modified montmorillonite clay particles, which have proven to effectively increase modulus and strength of the epoxy resin [5, 6, 29]. Also, if combined with the CSR particles, the material can have an increased modulus with improved toughness. From this finding, it is possible that the toughness of polymer matrices can be further improved while maintaining, not compromising, the modulus of the material.

In summary, the study up to date still does not allow for establishment of the mechanical behavior and toughening mechanisms of polymer nanocomposites. There is much work to be done to gain knowledge of the unambiguous fundamental structure-properties relationship of polymer nanocomposites and the understanding of the role of nanofillers in the nanocomposite materials.

CHAPTER III

FRACTURE BEHAVIOR OF CORE-SHELL RUBBER-MODIFIED CLAY-EPOXY NANOCOMPOSITES*

3.1 Introduction

Toughness is one of the most important material properties to be considered for engineering applications. Unfortunately, fracture toughness and ductility of nanocomposites usually are known to deteriorate due to the presence of the rigid, inorganic nanofillers. It is not yet known the exact fundamental causes for such significant drops in fracture toughness and ductility. It is possible that either polymer nanocomposites inherently contain incomplete dispersion of nanoparticles, which form aggregates, that cause premature crack formation or the presence of exfoliated nanoparticles restricts molecular mobility of the surrounding matrix material, which lead to embrittlement, or both.

Many researchers have reported that polymer nanocomposites exhibit improved modulus and strength. However, toughness and fracture mechanisms of polymer nanocomposites have not been systematically investigated.[10, 29, 76] Several methods

* Reprinted from accepted paper for *Polymer Engineering & Science*, SPE as "Fracture Behavior of Core-Shell Rubber-Modified Clay-Epoxy Nanocomposites" by K. T. Gam, M. Miyamoto, R. Nishimura and H.-J. Sue.

have been successfully employed in the past to toughen different polymeric systems.[68~72] A study using an epoxy resin has shown that among all the available rubber tougheners, preformed core-shell rubber (CSR) particles are most effective in toughening epoxy.[26] As a result, CSR is chosen for this work to toughen epoxy nanocomposites.

In this study the mechanical properties of two model clay-modified epoxy nanocomposites and the toughening effects of CSR on epoxy nanocomposites were investigated. The tools utilized for characterizing the state of clay dispersion of the two model epoxy nanocomposites include wide angle X-ray diffraction (XRD), and transmission electron microscopy (TEM). Tensile and dynamic mechanical properties of the model epoxy nanocomposites were studied. Fracture toughness and failure mechanisms of the clay-epoxy nanocomposites at different temperatures were also investigated. The fracture and toughening mechanisms of the clay-epoxy nanocomposite with and without the addition of CSR particles were investigated by probing the crack tip damage zones of the double-notch four-point-bend (DN-4PB) specimens [26], using transmitted light optical microscopy (TOM) and TEM. The effectiveness of CSR on epoxy nanocomposite toughening is investigated. The physics of why and how epoxy nanocomposites become brittle is also discussed.

3.2 Experimental

3.2.1 Materials

Two epoxy systems, having two distinctively different glass transition temperatures (T_g) and ductilities, were chosen to study how the nanoclay and CSR affect the mechanical properties of epoxy. The first epoxy resin (System-1) used for the epoxy-clay nanocomposite preparation was diglycidyl ether of bisphenol-A (DGEBA) epoxy resin (DER332[®], Dow Chemical). Diamine terminated polyether (Jeffamine D-400[®], Huntsman Performance Chemicals) was used as the curing agent for System-1. For the 2nd epoxy matrix resin (System-2), a mixture of DGEBA based epoxy and cycloaliphatic epoxy was used. A mixture of substituted phthalic anhydride curing agents with substituted amine catalyst was used to cure epoxy for the 2nd model epoxy system.

Montmorillonite clay particles having surface modification with octadecyl amine (Nanomer I.30E[®], Nanocore) were used as the nanofiller of System-1. The pure montmorillonite clay particle before surface treatment (PGW[®], Nanocor) was used as a reference. Since the I.30.E nanoclay particles cannot withstand high temperature curing steps, the more heat-stable montmorillonite, modified with a ternary ammonium salt (Cloisite 30B[®], Southern Clay Product Inc.), was used as the nanoclay filler for System-2.

Preformed CSR particles from KANEKA Corporation were used to investigate the toughenability of clay-epoxy nanocomposites. These CSR particles have a rubber

core size of 80~90 nm in diameter, and is covered with a compatibilizer copolymer shell of 10~20 nm in thickness [26].

3.2.2 Preparation of Nanocomposites

After mixing System-1 epoxy resin with I.30E[®] clay particles at 60°C, the mixture was sonicated and degassed under vacuum. Curing agent was then added to the mixture with stoichiometric ratio at ambient temperature and stirred and degassed again before pouring into a glass mold. To prepare nanocomposite plaques, pre-curing of the resin mixture was performed at ambient temperature for 2 hrs to avoid precipitation of the surface-treated clay particles in the epoxy matrix. After pre-curing, the resin mixture was cured in an oven at 75°C for 2 hrs, followed by 3 hrs post-cure at 120°C.

System-2 epoxy resin, which has a higher T_g than System-1 epoxy resin, was prepared using the same procedure as System-1, but with different curing schedule, i.e., at 125°C for 30 minutes followed by 165°C for 1.5 hrs.

Preformed CSR particles were extracted from aqueous emulsion of CSR using methyl ethyl ketone (MEK) to remove water and surfactant. Both System-1 and System-2 epoxy resins were mixed with CSR in MEK at ambient temperature. Afterwards the solvent was removed with a rotavapor (Buchi R-114[®]) in water bath at 90°C under vacuum. The epoxy-CSR mixture was later used to make CSR-toughened epoxy nanocomposites.

Specimens having thicknesses of 6.35 mm (0.25 inch) and 3.12 mm (0.125 inch) were cast for clay-epoxy nanocomposites with CSR, which are designated as System-1NR and System-2NR, respectively.

Table 3-1. Compositions of Clay-Epoxy Nanocomposites.

		Clay (wt% of Inorganic part)	CSR (wt%)
System-1	[Neat resin Epoxy1]	None	None
System-1N	[Epoxy1/clay]	5.4	None
System-1NR	[Epoxy1/clay & CSR]	5.4	3.0
System-1C	[Epoxy1/PGW]	5.0	None
System-2	[Neat resin Epoxy2]	None	None
System-2NR	[Epoxy2/clay & CSR]	2.0	3.0
System-2R	[Epoxy2/CSR]	None	3.0

The as-received nanoclay particles from Nanocor have 28 wt% of organic surface modifier, i.e., octadecyl amine. Consequently, a composite with 7.5 wt% of nanoclay particles (System-1N and System-1NR) has only 5.4 wt% of inorganic clay particles. System-1C, which contains untreated montmorillonite clay particles, was prepared as a reference. The compositions of all the clay-epoxy nanocomposites investigated are summarized in Table 3-1.

3.2.3 X-Ray Scattering Study

The nanofiller dispersion in clay-epoxy nanocomposites was investigated using XRD. The Seifert Scintag PAD-V with Cu-K α radiation was used for XRD to verify the exfoliation of clay layers in polymer matrices. The WAXD was performed with 2θ ranging from 2 to 10 degrees, which corresponds to the d-spacing ranging from 44.2Å to 8.8Å.

3.2.4 Mechanical Properties

Dynamic mechanical analysis (DMA) was performed using Rheometrics (RDS-II[®]) with a temperature sweep from -150°C to 200°C at 5°C per step and a frequency of 1 Hz. A sinusoidal strain amplitude of 0.225 % was chosen for the analysis. The dynamic storage modulus (G') profiles were recorded against temperature. Tensile test (ASTM D 638-98) was performed using a screw-driven mechanical testing machine (Sintech-2[®]) at a cross-head speed of 0.508 mm/min (0.2" /min) at room temperature.

Single-Edge-Notch 3-Point-Bending (SEN-3PB) test (ASTM D5045-96) was conducted to obtain the mode-I critical stress intensity factor fracture toughness (K_{IC}) of the neat epoxy and clay-epoxy nanocomposite systems. Measurements of K_{IC} at low temperatures (i.e., 0°C and -20°C) were performed using SEN-3PB test in an environmental chamber attached to Sintech-2[®] machine to investigate the toughening effects of epoxy matrices with low ductility.

3.2.5 Morphology and Fracture Mechanisms

The DN-4PB test was performed to investigate the subcritically propagated crack tip damage zone using both TOM and TEM.[27] TOM investigations of nanocomposite fracture damage zones were performed on thin sections having a thickness of about 40 μ m. The specimens were prepared following the procedures described by Holik et al.[77] These thin sections were observed with an Olympus BX60 optical microscope under both bright field and cross-polarization conditions to observe the overall damage zone size and feature.

TEM (JEOL JEM-2010A) was utilized to investigate detailed deformation and fracture mechanisms, such as signs of shear yielding and crazing, operated at an accelerating voltage of 200kV. The crack tip damage zone from DN-4PB test was embedded in an epoxy mount and stained with osmium tetroxide (OsO_4) to harden the rubber phase in epoxy and to obtain sufficient contrast between CSR and epoxy matrix. Thin sections of 70 ~ 100 nm in thickness were prepared for TEM observation.

3.3 Results and Discussion

To study the effect of exfoliated clay particles on the properties of epoxy matrix, System-1 and System-2 series were prepared with the compositions shown in Table 3-1. It should be noted that only 2wt% of clay was incorporated in System-2NR, instead of 5wt% of clay as in System-1 epoxy, because of the difficulty in the sample preparation of System-2.

3.3.1 Morphology Characterization

To characterize the state of clay exfoliation in epoxy matrix, both XRD and TEM were used. The XRD results suggest that the clay particles in both System-1 [Fig. 3-1] and System-2 epoxy nanocomposites have exfoliated.

The XRD patterns of System-1N and the pure clay particles are shown in Fig. 3-1. The original clay has a sharp peak at 7.2° , which corresponds to a d-spacing of 12 \AA [Fig. 3-1a]. This peak was shifted to about 3.8° (23 \AA) after surface treatment of the clay [Fig. 3-1b]. The nanoclay becomes intercalated with a bigger d-spacing (36 \AA) after sequentially being immersed into epoxy resin, high shear mixing, and sonication steps [Figs. 3-1c, 1d, and 1e]. After 2 hrs of pre-curing at ambient temperature the sharp diffraction peak from the clay is significantly shifted to the left and broadened [Fig. 3-1f], and finally exfoliation occurs after 2 hrs of curing at 75°C [Figs. 3-1g and 1h]. These XRD patterns indicate that the clay particles have either highly intercalated or exfoliated

in epoxy nanocomposites to greater than 44\AA ($2\theta = 2^\circ$, the WAXD detection limit) of d-spacing. This finding is further supported by TEM observations, to be shown below.

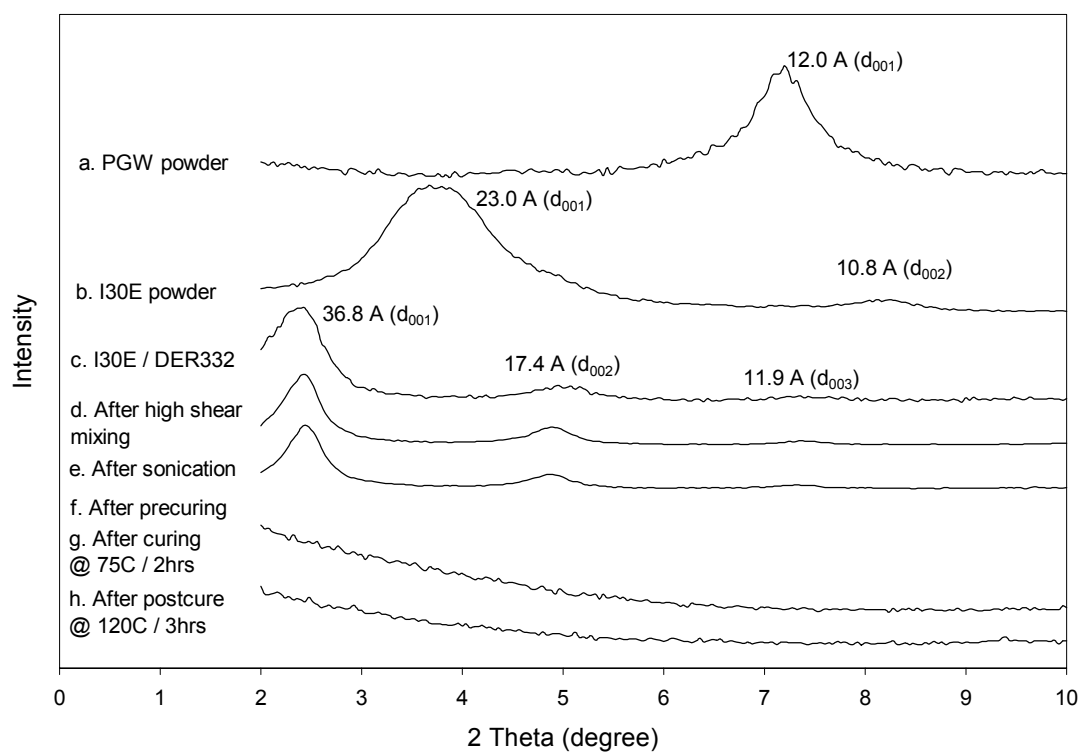


Figure 3-1. WAXS of System-1 Nanocomposites.

TEM micrographs of System-1N, System-1NR, and System-2NR give direct evidence of the exfoliation of nanoclay in the clay-epoxy nanocomposites investigated [Figs. 3-2~3]. These TEM micrographs show that the surface-modified clay is well-dispersed in epoxy matrices with the presence of occasional assembly of wide, loosely spaced intercalated clay particles. Typical clay exfoliation in System-1 epoxy resin is shown in Fig. 3-2. The modified clay is exfoliated layer by layer and clearly appeared as straight or curved lines in the matrix. As shown in Fig. 3-3 for System-1, the good dispersion of exfoliated clay layers or widely spaced intercalated clay particles is not affected by the presence of CSR (shown as dark round phases in the micrographs) in the matrix.

3.3.2 Mechanical Properties and Fracture Toughness

3.3.2.1 System-1 Epoxy System

The storage moduli (G') of the clay-epoxy nanocomposites were studied using DMA. As shown in Table 3-2 and Fig. 3-4, the rubbery plateau modulus of System-1 is significantly increased by 132 % with an addition of 5.4 wt% (3vol.%) of nanoclay. System-1NR shows a moderate rubbery plateau modulus increase by about 50 % of that of the neat resin. This significant increase in rubbery plateau modulus is due to the presence of the exfoliated high surface area, high aspect ratio clay particles, which act as effective physical crosslinkers.

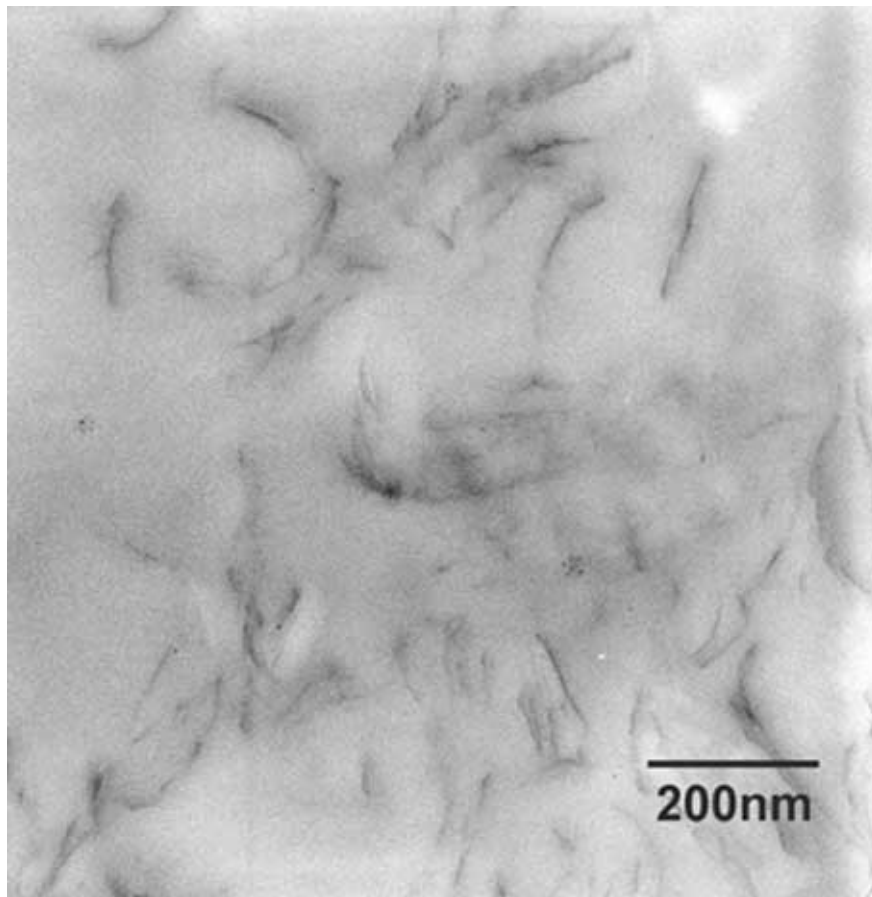


Figure 3-2. TEM of System-1N Nanocomposite.

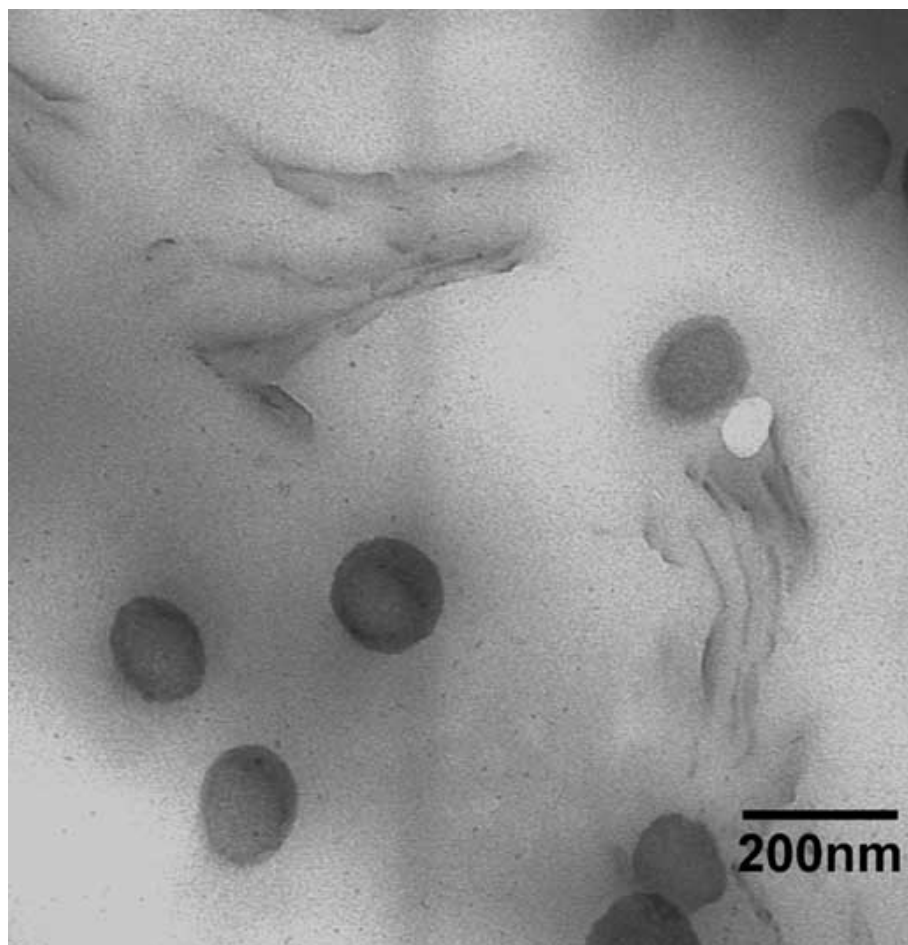


Figure 3-3. TEM of System-1NR Nanocomposite.

Table 3-2. Mechanical Properties of System-1 Nanocomposites.

	System-1	System-1N	System-1NR	System-1C
Tensile Modulus (GPa)	2.38	3.69	3.00	2.52
Yield stress (MPa)	39.9	46.6	38.2	37.9
Flexural modulus [0°C]	3190	3620	3410	-
(MPa) [-20°C]	3540	3860	3650	-
G' from DMA [25°C]	1.15E+09	1.24E+09	1.24E+09	-
(Pa) [120°C]	5.70E+06	1.32E+07	8.72E+06	-

*PGW: montmorillonite clay before surface modification.

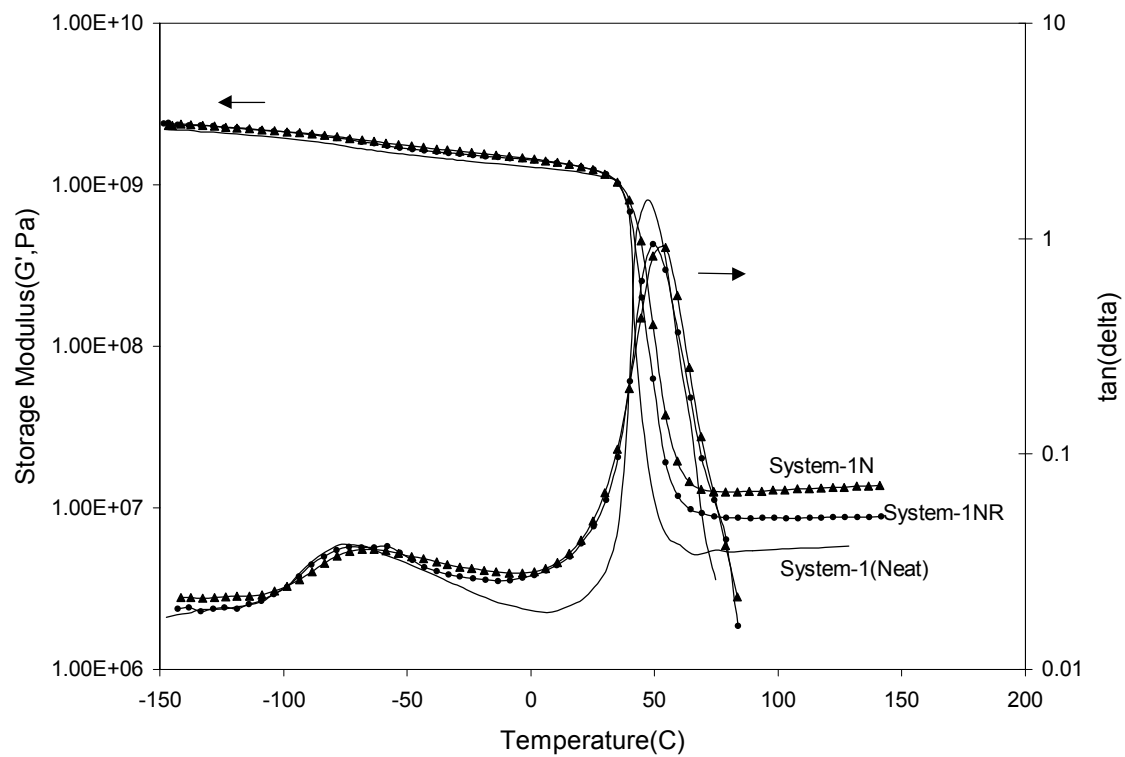


Figure 3-4. DMA of System-1 Nanocomposites.

Based on the DMA analysis, no significant change in T_g is observed by the addition of nanoclay particles to epoxy matrix. Similar findings were also reported by Chen and Curliss.[76] It is worth noting that only ordered intercalated nanocomposites systems are found to be more effective in causing an increase in T_g of epoxy matrices. A higher T_g increase can be obtained if the clay content is increased. However, no significant change in T_g is observed when the clay is exfoliated, at least at low levels of clay loadings.[76] Fully exfoliated nanoclay layers possibly do not effectively hinder the segmental motions of the epoxy matrix, which are known to affect T_g . [78]

The tensile properties of System-1 series are shown in Table 3-2 and Fig. 3-5. It can be seen that, with an addition of only 5.4 wt% (3vol.%) of inorganic nanoclay, the tensile modulus and yield stress of the epoxy are increased from 2.38 GPa to 3.69 GPa and from 39.9 MPa to 46.6 MPa, respectively. These increases are significant when we consider the modulus and yield stress of the reference clay-epoxy system, i.e., System-1C, which gives only slight increase in tensile modulus and a small reduction in yield stress.

The K_{IC} of System-1N is $0.91 \text{ MPa}\cdot\text{m}^{1/2}$, which is lower than the value of the neat epoxy system ($1.12 \text{ MPa}\cdot\text{m}^{1/2}$) [Table 3-3]. The investigation of fracture mechanisms on the clay-epoxy nanocomposite (System-1N) using TOM reveals that the clay addition does not trigger any effective toughening mechanisms, such as shear bands or crazes. The crack propagates in a straight and brittle manner. These results are consistent with

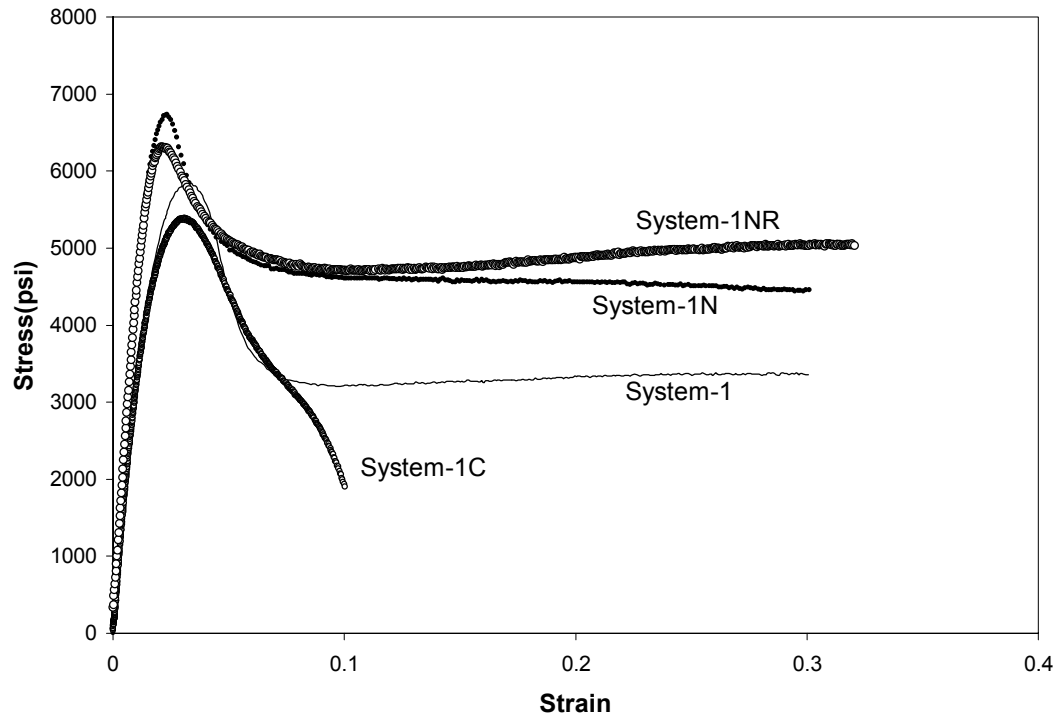


Figure 3-5. Tensile Properties of System-1 Nanocomposites.

Table 3-3. Fracture Toughness (K_{IC}) of System-1 Nanocomposites.

	System-1	System-1N	System-1NR	System-1C
K_{IC} (MPa·m ^{1/2}) [25°C]	1.12	0.91	3.05	1.51
[0°C]	1.19	0.88	1.80	-
[-20°C]	1.07	0.95	1.23	-

the literature finding.[76] The above study indicates that the addition of exfoliated clay in epoxy leads to embrittlement of the ductile epoxy matrix. The main cause for such a disappointing result may be because of the significant increase of the effective rubbery plateau modulus, i.e., high crosslink density. As a result, the ability for the epoxy network structure to undergo plastic deformation is greatly limited. This implies that the presence of exfoliated nanoclay particles can effectively restrict large-scale molecular motions of epoxy molecules, thus leading to embrittlement of the epoxy matrix.

3.3.2.2 System-2 Epoxy System

Although System-1 is good for fundamental study on the effect of nanoclay addition on the modulus and strength of epoxy resin matrices, it has a relatively low T_g (i.e., 50°C), which is not high enough for engineering applications. For high performance structural applications, the material needs to have a higher T_g . This is the reason why System-2 nanocomposites were prepared and their mechanical properties were evaluated.

The DMA result shown in Fig. 3-6 is based on System-2 nanocomposites. The storage modulus (G') and T_g were not changed significantly by adding CSR particles and nanoclay particles. However, the plots show a clear increase of the magnitude of $\tan\delta$ at temperatures from 0 to 150°C after the CSR addition. Although the hump of $\tan\delta$ curve found around 100°C is due to the copolymer shell of the CSR particles, the overall increases in $\tan\delta$ values implies that increased damping is introduced by addition of CSR.

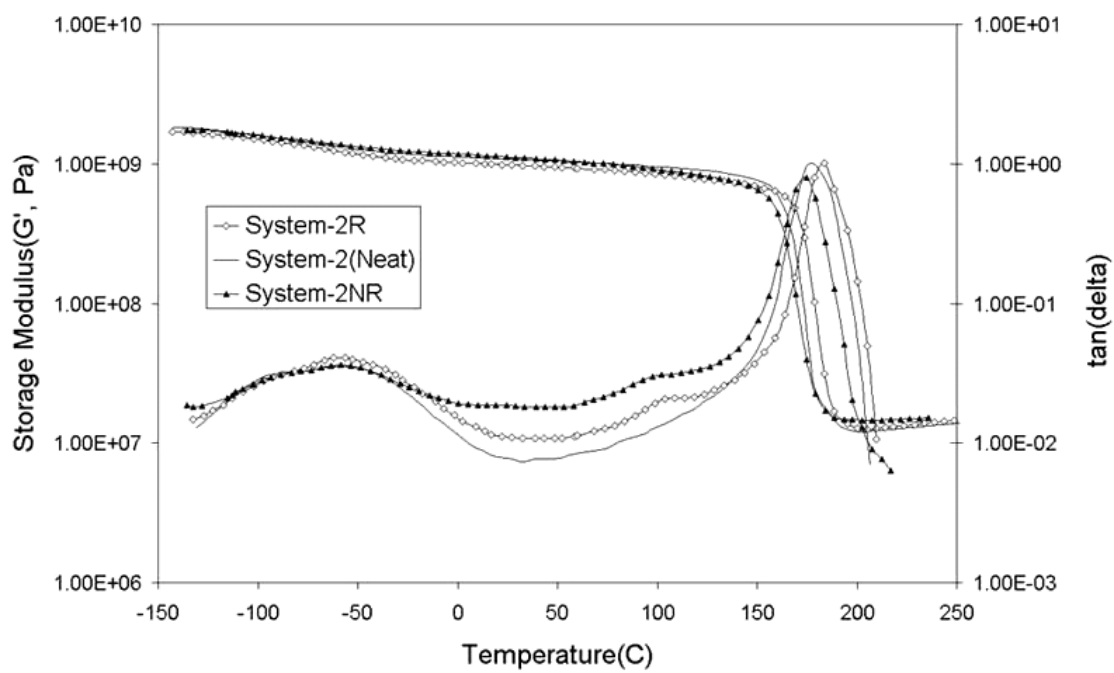


Figure 3-6. DMA of System-2 Nanocomposites.

3.3.3 Toughening Using CSR Particles

When the nanoclay-reinforced System-1 epoxy is toughened using CSR (System-1NR), the tensile modulus is reduced from 3.69 GPa to 3.00 GPa, which is still higher than that of the neat epoxy. The yield stress of System-1NR stays almost the same as that of the neat epoxy [Table 3-2]. However, the K_{IC} of System-1NR is significantly improved by 172 % [Table 3-3].

The System-1N shows only brittle, featureless crack tip damage zone. In comparison, System-1NR shows a much bigger crack tip damage zone [Fig. 3-7]. It is evident that significant plastic deformation has occurred due to the incorporation of CSR. Interestingly, no signs of CSR particle cavitation are found using TEM [Figs. 3-8~10]. We surmise that the low T_g (50°C) of the epoxy matrix may have led to a quick recovery of the dilatational plasticity of matrix, which prevented the cavitated CSR from being observed under TEM. It is noted that many small cavities in the inter-laminar region of the clay layers are still found [Figs. 3-8~10]. These cavities may be formed due either to the weak inter-laminar bonding between clay layers or to the artifact induced from the thin-sectioning process. The TOM micrograph in Fig. 3-7 clearly suggests that massive dilatational process, which scatters light effectively, has taken place in the crack tip region. It is still unclear if such a dilatational zone is formed mainly because of CSR cavitation or clay inter-laminar debonding, or both. Crack bifurcation and crack deflection are also observed from TEM of the nanocomposite System-1NR [Fig. 3-10].

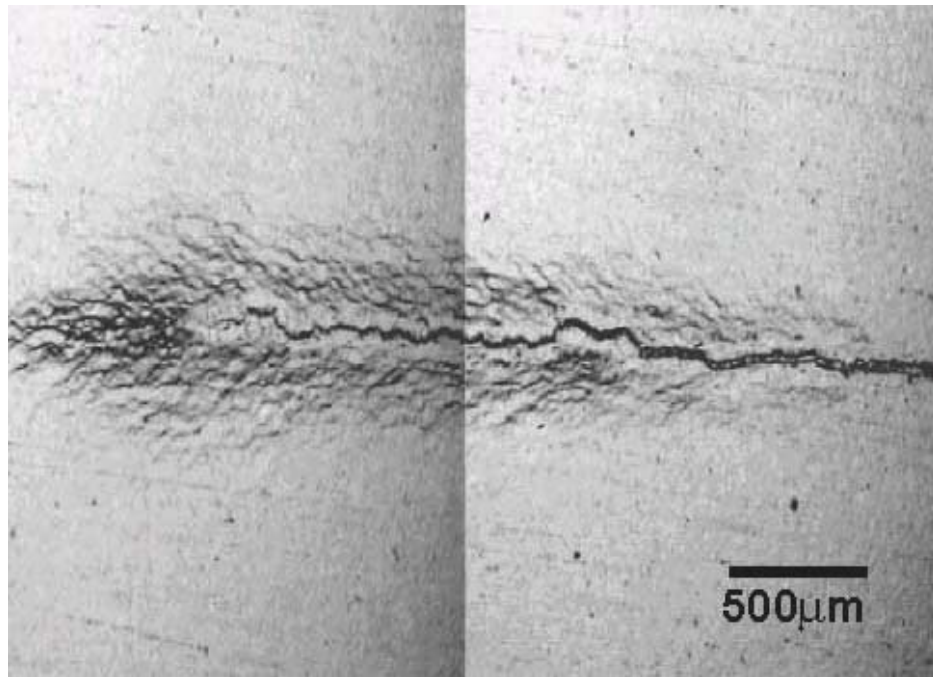


Figure 3-7. Optical Microscopy of System-1NR Nanocomposite with a Crack.

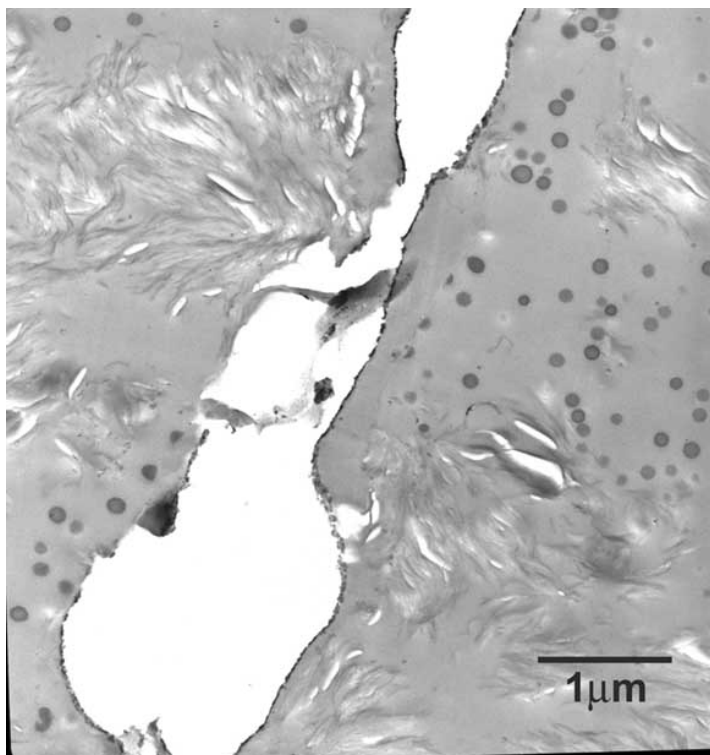


Figure 3-8. TEM of System-1NR Nanocomposite Showing Delamination of Nanofillers with 1 μm Scale Bar.

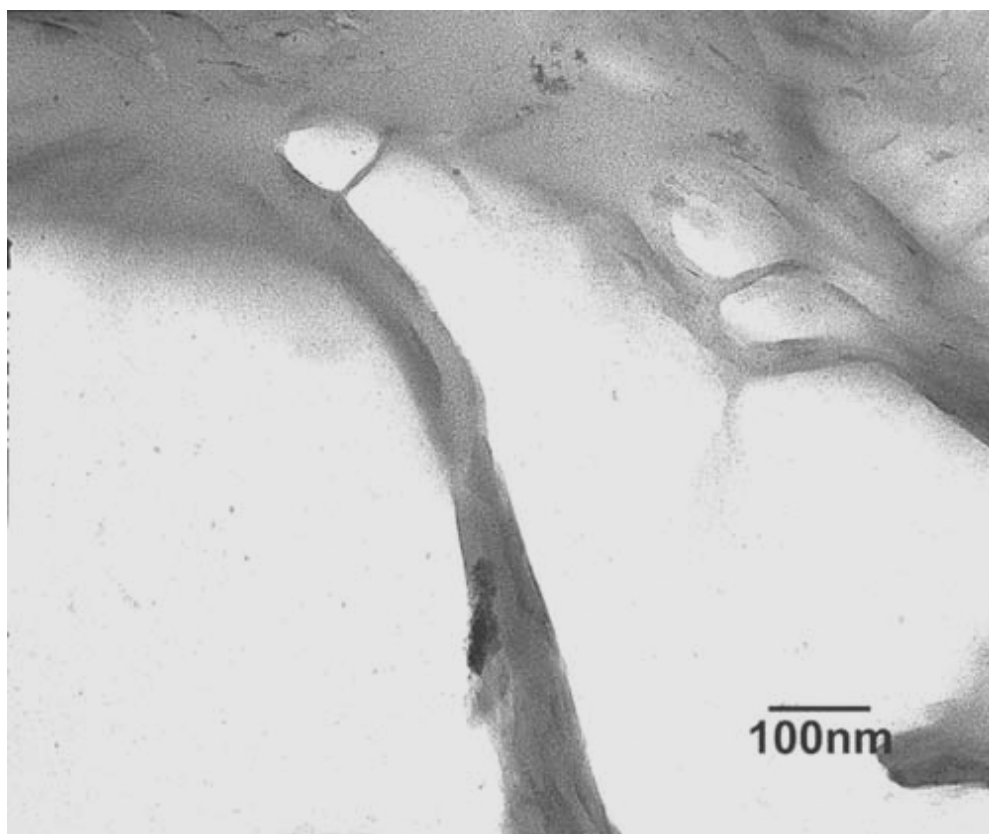


Figure 3-9. TEM of System-1NR Nanocomposite Showing Delamination of Nanofillers with 100 nm Scale Bar.

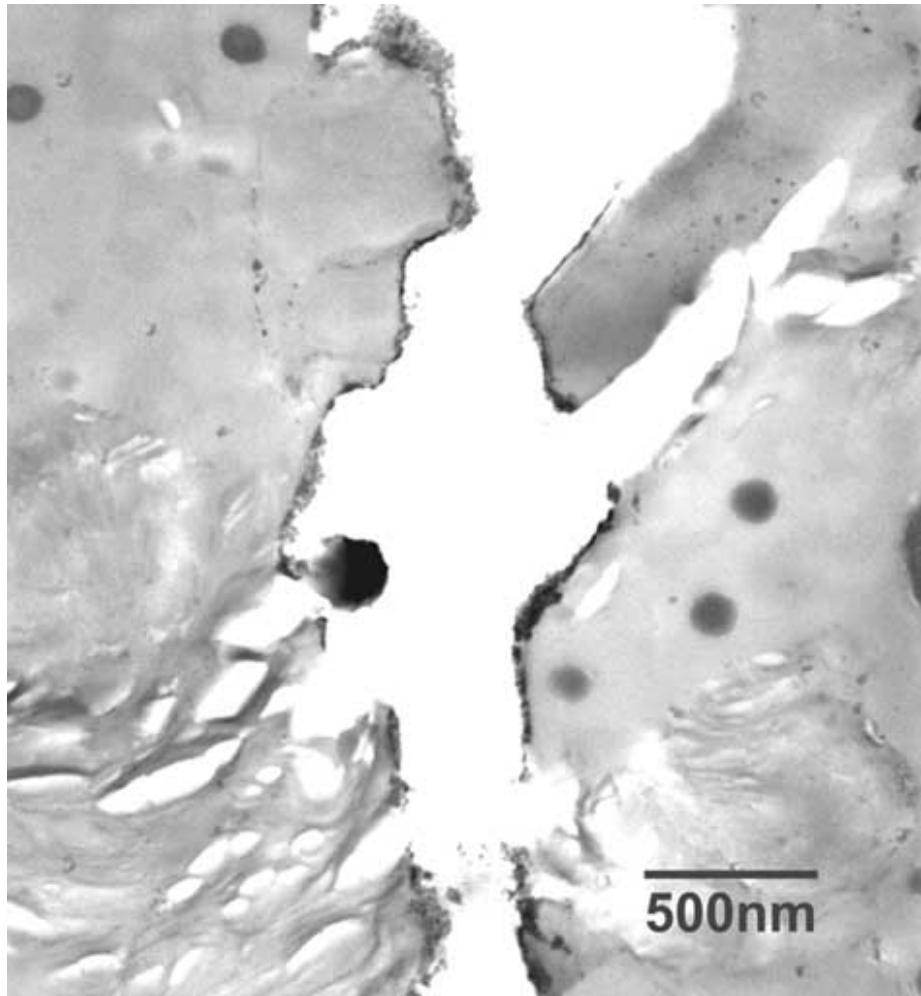


Figure 3-10. TEM of System-1NR Nanocomposite Showing Crack Bifurcation and Crack Deflection.

To assess the toughening effect of CSR for less ductile systems, the SEN-3PB test was performed to evaluate the K_{IC} of System-1 at low temperatures, i.e., 0°C and –20°C. The K_{IC} improvements in System-1NR by addition of CSR at 0 and –20°C are shown in Table 3-3. The toughening effect is significantly reduced upon testing at low temperatures. The above findings suggest that, as expected, the ductility of polymer matrix influences the toughening effect of CSR, which is consistent with literature finding.[79]

Similar findings are observed from the toughness measurement of System-2, which has a lower ductility (higher crosslink density) than System-1. System-2 has a higher T_g and can be considered as a more rigid system than System-1 epoxy at ambient temperature. The addition of the same amount of CSR (3 wt%) to System-2 produces a relatively small increase of K_{IC} from 0.53 to 0.81 MPa·m^{1/2} [Table 3-4]. The big increase in toughness of System-1NR is most likely due to the large scale plastic deformation System-1NR introduced [Fig. 3-7]. This phenomenon is not observed in System-2NR.

The toughening of System-2NR can be attributed to several fracture mechanisms, such as cavitation of CSR, followed by limited shear yielding of the matrix [Figs. 3-11 and 12]. TEM micrographs in Figs. 3-11 and 12 also show that crack bifurcation, deflection, CSR cavitations, and bridging of CSR particles are among the operative toughening mechanisms.

Table 3-4. Mechanical Properties & Fracture Toughness (K_{IC}) of System-2 Nanocomposites.

	System-2	System-2R	System-2NR
Tensile Modulus (GPa)	3.02 ± 0.11	2.70 ± 0.07	3.29 ± 0.09
Bending Modulus (GPa)	2.85 ± 0.02	2.68 ± 0.03	-
K_{IC} (MPa*m ^{1/2}) [25°C]	0.53 ± 0.06	0.83 ± 0.11	0.81 ± 0.03
T _g from DSC (°C)	163.3	171.7	170.9

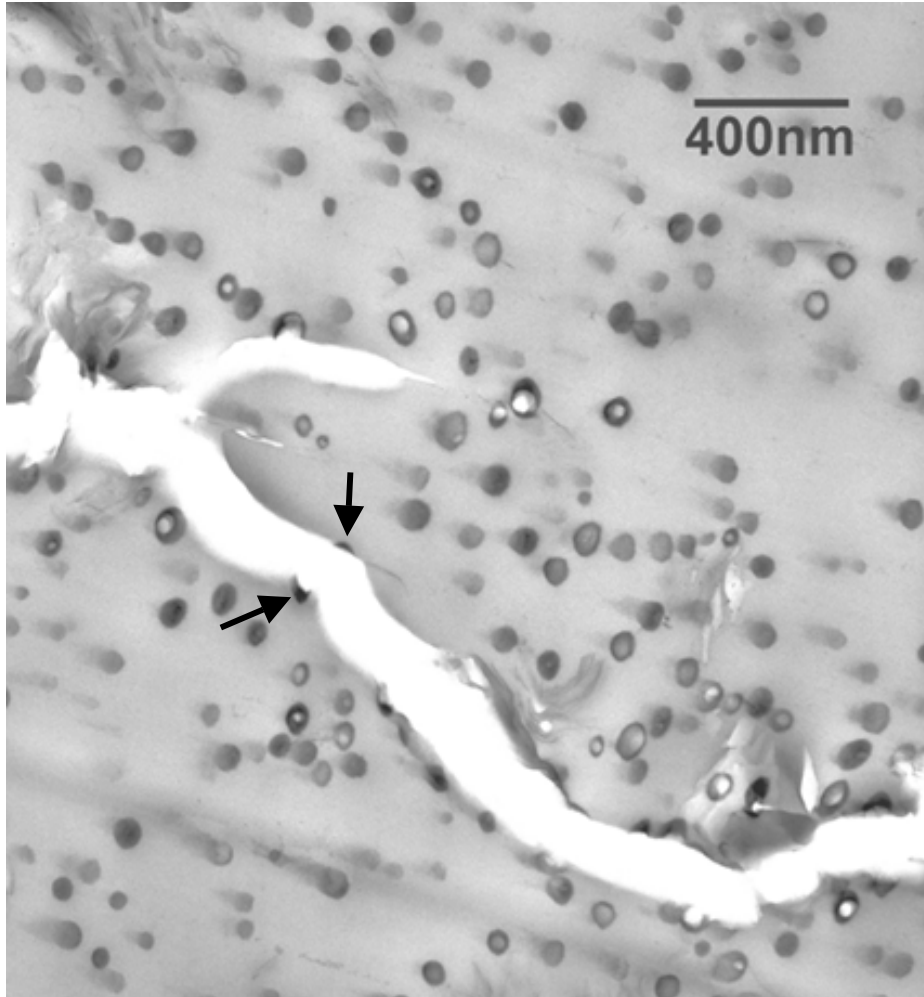


Figure 3-11. TEM of System-2NR Nanocomposite Showing Crack Bifurcation and Bridging of CSR.

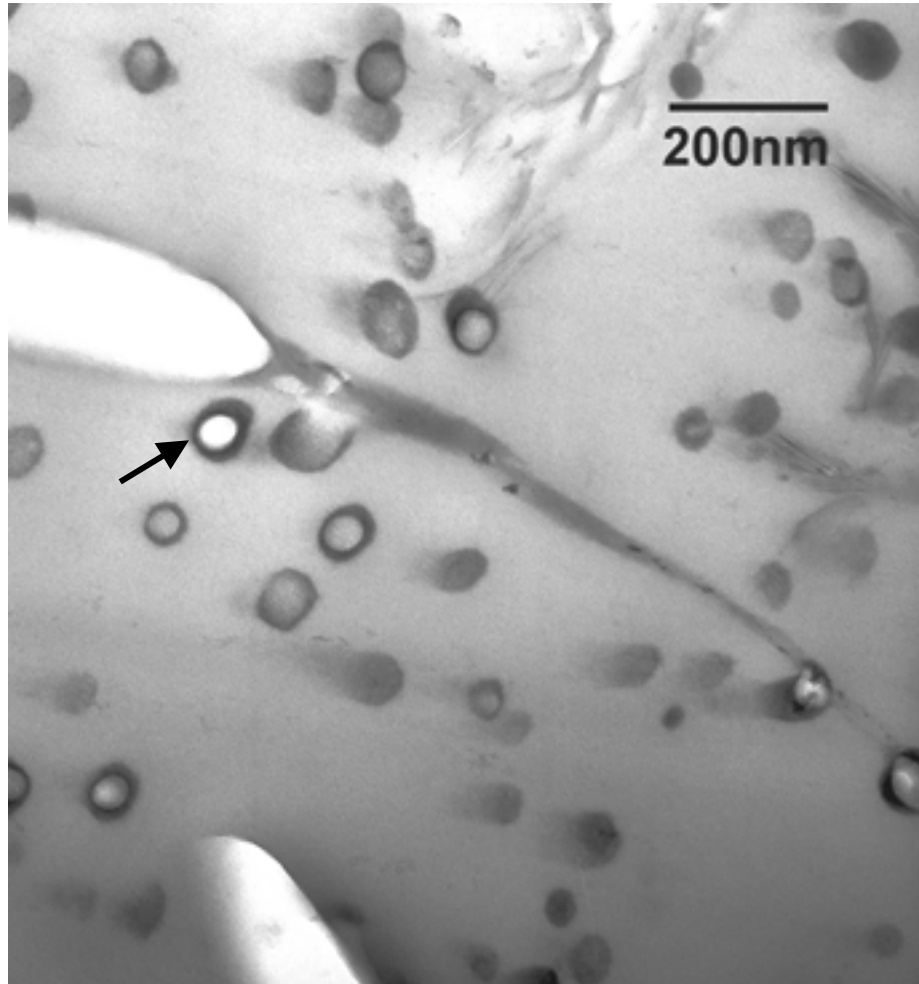


Figure 3-12. TEM of System-2NR Nanocomposite Showing CSR Cavitation.

3.4 Conclusions

To investigate mechanical properties and toughening mechanisms of clay-epoxy nanocomposites by addition of CSR, two model epoxy systems with different T_g (50 and 170°C) were prepared and characterized using XRD and TEM. The T_g of the epoxy nanocomposites based on DMA were nearly identical to that of neat epoxy. The rubbery plateau moduli of the nanocomposites were increased with an addition of nanofiller. The tensile moduli of both System-1N and System-1NR were significantly higher than that of neat resin. The additions of both clay and CSR have improved not only modulus but also fracture toughness. The toughening mechanisms in System-2NR include cavitation of CSR, followed by limited shear yielding of the matrix. Crack bifurcation, deflection, and crack bridging are also observed. In the more ductile System-1NR system, the major toughening mechanisms involve a large scale CSR particle cavitation and/or debonding between the intercalated clay layers, followed by massive shear banding of the matrix. The present study has shown that the ductility of polymer matrix can significantly influence the toughening effect using CSR. CSR is effective in improving the fracture toughness of epoxy nanocomposites.

CHAPTER IV

EPOXY NANOCOMPOSITES BASED ON THE SYNTHETIC α -ZIRCONIUM PHOSPHATE LAYER STRUCTURE

4.1 Introduction

Polymer nanocomposites exhibit significantly better physical and mechanical properties than conventional micrometer scale inorganic filler reinforced polymer composites [1~13, 32~37]. In general, clay-based nanocomposites exhibit greatly enhanced modulus and gas barrier properties of the host polymers [1-13, 32], but cause significant reduction in ductility and toughness.

The main drawback of montmorillonite clay is that it is produced *via* purification and modification of the mined clay. It is extremely difficult, if not impossible, to achieve 100% purity, narrow particle size distribution, and controlled aspect ratio of the clay nanofiller. Consequently, despite the significant research efforts in the past two decades, fundamental knowledge on exactly how the degree of dispersion, aspect ratio and particle size of nanoparticles influence the physical and mechanical properties of polymers is still lacking. It is imperative to prepare model polymer nanocomposites that contain nanofillers with controlled surface functionalities, particle sizes and aspect ratios to gain unambiguous fundamental understanding of mechanical behavior of polymer nanocomposites.

Stemming from the above concerns, as a part of a larger effort to gain fundamental structure-property relationship in polymer nanocomposites, we used α -zirconium phosphate (α -ZrP), $\text{Zr}(\text{HPO}_4)_2 \cdot \text{H}_2\text{O}$, as a nanofiller in this study. α -ZrP has a much higher ion exchange capacity than montmorillonite clays, and the size and aspect ratio of the α -ZrP particles can be controlled by varying reaction time and reactant concentrations [52]. Also, the particle size distribution of α -ZrP has been found to be quite narrow, thus suitable for fundamental study of nanofiller effect on the properties of the host polymers.

In this study, α -ZrP with a large interlayer spacing was synthesized to make α -ZrP/Epoxy nanocomposites. For this purpose α -ZrP was intercalated using a commercially available monoamine-terminated polyether, Jeffamine M715 (M715) with the formula $\text{CH}_3\text{O}(\text{CH}_2\text{CH}_2\text{O})_{14}\text{CH}_2\text{CH}_2\text{NH}_2$. The resulting material is then incorporated into an epoxy polymer. The morphology and mechanical properties of the α -ZrP-reinforced epoxy nanocomposites are studied. The influence of α -ZrP nanoparticles on physical and mechanical properties enhancement of epoxy matrix is investigated. The implication of this research on fundamental understanding of physical, mechanical, and functional properties of polymer nanocomposites is also discussed. A preliminary report as a proceedings account is available [80].

4.2 EXPERIMENTAL

4.2.1 Materials

The reagents were used as received: Zirconium oxychloride octahydrate ($\text{ZrOCl}_2 \cdot 8\text{H}_2\text{O}$), 98% (Aldrich), Phosphoric Acid (EM), Jeffamine M715 (Huntsman Chemical) and Methyl ethyl ketone (Merck). Diglycidyl ether of bisphenol-A (DGEBA) epoxy resin (DER 332[®], Dow Chemical) was mixed with 4,4'-diamino-diphenyl sulfone (DDS, Aldrich), which is a curing agent, as the epoxy matrix for this study. The DGEBA epoxy monomer has a narrow monomer molecular weight distribution of 172-176 g/mole.

4.2.2 Synthesis

4.2.2.1 Preparation of ZrP

The detailed chemistry and procedures for the preparation for α -ZrP can be found elsewhere [81, 82]. Only a brief summary of the α -ZrP preparation is given here. A gel was prepared by addition of $\text{ZrOCl}_2 \cdot 8\text{H}_2\text{O}$ to phosphoric acid and then refluxed 24 hours in 3M phosphoric acid solution. The X-ray powder pattern of this compound is presented in Figure 4-1. The broadened peaks show that the compound is not perfectly crystallized because the acid used is dilute. The interlayer spacing of this compound is about 7.6 Å. The scanning electron micrograph [Figure 4-2] shows the formation of aggregates, which consist of many irregular small particles. The sizes of the aggregated particles vary between 0.3 μm and 2 μm .

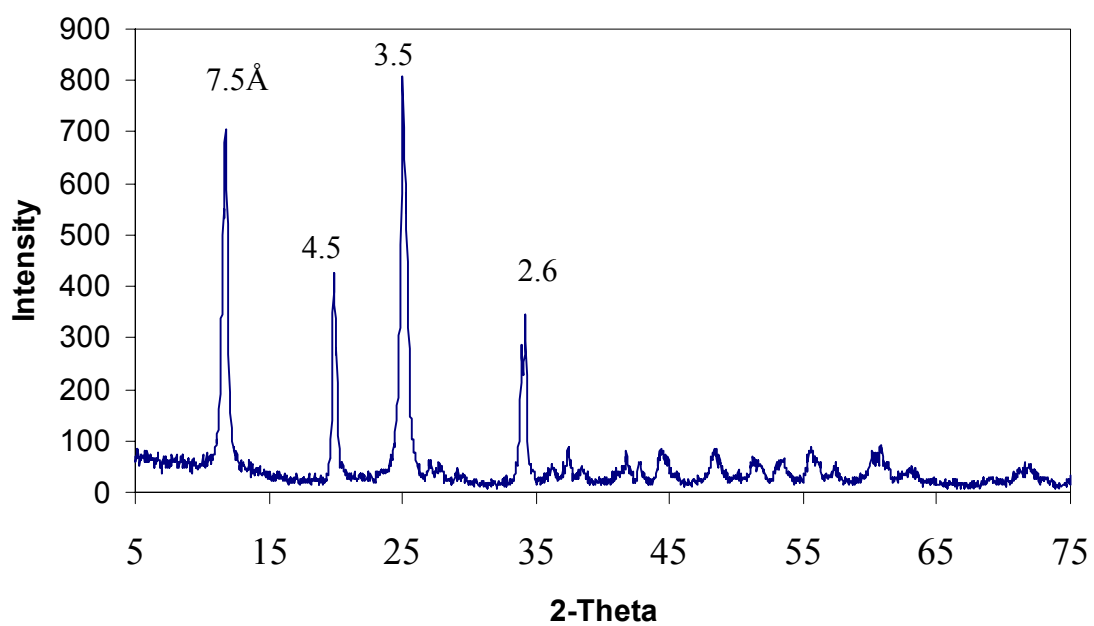


Figure 4-1. X-ray Powder Pattern of α -Zirconium Phosphate.

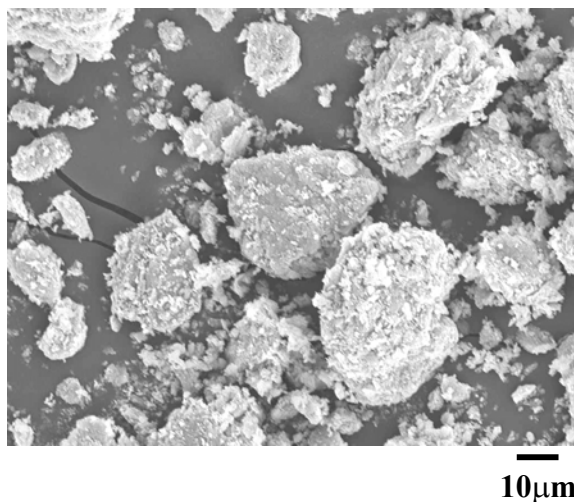


Figure 4-2. Scanning Electron Micrographs of α -Zirconium Phosphate.

4.2.2.2 Intercalation of ZrP with Jeffamine M715

The intercalation reaction [83] of α -ZrP was carried out at room temperature. Twenty mmol of α -ZrP powder was dispersed in 100 ml of methyl ethyl ketone (MEK) for six hours. Forty mmol of monoamine surface modifier (M715) was first dissolved in 100 ml MEK, and then added dropwise into the α -ZrP/MEK mixture. A transparent yellowish ‘gel’ was obtained. It was not possible to wash off the excess monoamine modifier and to dry the resulting compound completely due to its gelatinous nature. The

X-ray diffraction powder pattern of the intercalated α -ZrP (M- α -ZrP) is presented in Figure 4-3.

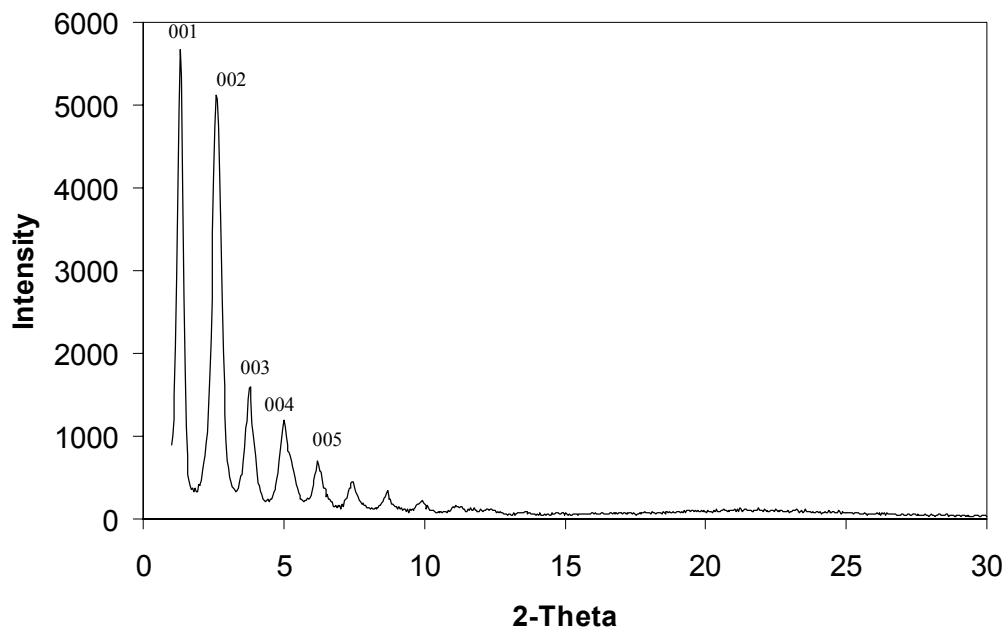


Figure 4-3. X-ray Powder Pattern of α -Zirconium Phosphate Intercalated with Jeffamine M715.

4.2.2.3 Preparation of ZrP-Based Epoxy Nanocomposites

The M- α -ZrP was poured into the epoxy to achieve 1.9 vol. % (5.2 wt %) of α -ZrP in epoxy (M- α -ZrP/Epoxy). After removing MEK with a Rotavapor[®] in a water bath at about 90°C under vacuum, no aggregation or precipitation was found in the

viscous mixture. The mixture was then heated at 130°C, and the curing agent, DDS added at stoichiometric ratio. This mixture was stirred until a transparent yellowish solution was obtained. The mixture was degassed under vacuum and poured into a preheated glass mold. A plaque with dimensions 200 mm (8") x 200 mm (8") x 3.12 mm (0.125") was cast. The resin mixture was cured in an oven at 180°C for 2 hours, followed by 2 hour of post-cure at 220°C.

Table 4-1. Compositions of α -ZrP-Epoxy Nanocomposites (Vol.%)

	α -zirconium phosphate	Jeffamine M715
Neat (DGEBA/DDS)	None	None
M/Epoxy	None	18.7
α -ZrP/Epoxy	1.9	None
M- α -ZrP/Epoxy	1.9	18.7

For comparison, a neat epoxy panel (Neat/Epoxy), an epoxy panel with only the Jeffamine (M/Epoxy) and an epoxy panel (α -ZrP/Epoxy) with 1.9 vol. % of α -ZrP were prepared. The density of α -ZrP is much higher than DGEBA epoxy; the α -ZrP particles were dispersed in MEK and stirred overnight to achieve good dispersion in the resin

matrix. Then, the mixture was blended with DGEBA and the same procedure as above was followed. Table 4-1 presents the composition in vol. % of the different panels.

4.2.3 Characterization

X-Ray diffraction powder patterns were recorded using a Bruker D8 diffractometer with Bragg-Brentano θ - 2θ geometry (40 kV and 40 mA) and a graphite monochromator. The data were recorded between 1° and 30° in 2θ , with a step increment of 0.04° and a count time of 2s per step for the intercalated compound and the polymers. For the M- α -ZrP, the samples were prepared by putting a drop of the mixture on the surface of a flat holder. By slow evaporation of the solvent, a thin film was formed on the surface of the holder for analysis. For α -ZrP the data were taken between 5° and 75° in 2θ , with a step size of 0.04° and a count time of 2s per step. The powder was packed into plastic holder.

The Solid-state NMR was performed with magic angle spinning (MAS) on a modified Bruker MSL-300 MHz machine, operating at 121.5 MHz for ^{31}P . Eighty five percent H_3PO_4 (0 ppm) was used as an external standard.

The infrared spectra were recorded on a Nicolet Nexus 470 FTIR spectrometer with a spectral resolution of 2.000 cm^{-1} . A small amount of the sample was put between two blocks of KBr for analysis. Optical microscopy (OM) was performed using an Olympus optical microscope (model BX60) under both bright field and crossed-polarized fields. Scanning electron microscopy (SEM) investigations were performed (on the fracture surface of the SEN-3PB specimen) using a JEOL JSM-6400, operated at

20 kV, (to observe the overall α -ZrP particle distribution and the homogeneity of the dispersion in epoxy). Transmission Electron Microscopy (TEM) was performed on a JEOL JEM-2010A, operated at 200 kV. A Reichert-Jung Ultracut-E microtome was utilized to prepare thin-sections with 70 ~ 100 nm in thickness for TEM observation.

4.2.4 Mechanical Property Characterization

Dynamic mechanical analysis (DMA) was performed using a Rheometrics[®] (RDS-II) at a fixed frequency of 1 Hz and a temperature sweep of 5°C per step, ranging from -150°C to 250°C. A sinusoidal strain-amplitude of 0.10 % was chosen for the analysis. The dynamic storage modulus (G') and $\text{Tan}\delta$ against temperature curves were recorded and plotted. The temperature at which the $\text{tan}\delta$ curve shows a maximum peak is recorded as the glass transition temperature (T_g).

Tensile test (ASTM D638-98) was performed using a screw-driven mechanical testing machine (Sintech[®]-2) at a crosshead speed of 0.508 mm/min (0.2"/min) at room temperature. An average of at least five tests per sample was performed to report modulus, yield stress, and elongation at break. The fracture toughness measurements of the α -ZrP-based epoxy nanocomposites were conducted based on the linear elastic fracture mechanics (LEFM) approach. Single-edge-notch 3-point-bending (SEN-3PB) test, following the ASTM D5045-96 method, was used to obtain mode-I critical stress intensity factor (K_{IC}) of the neat epoxy and epoxy/ α -ZrP nanocomposite systems. Care was taken to make sure the starter crack exhibits a thumbnail shape crack front before testing. An average of at least five specimens was used to determine K_{IC} of the samples.

4.3 RESULTS AND DISCUSSION

4.3.1 Characterization of M-ZrP

The X-ray powder pattern of the Jeffamine intercalate shown in Figure 4-3 present only the 00ℓ reflections due to the severe preferred orientation exhibited by the Jeffamine intercalate resulting from its layered structure. Ten orders of 00ℓ were present and these were averaged to obtain the basal spacing of 73.27 Å. This value is almost ten times the value of α -ZrP interlayer spacing (7.6 Å).

The intercalate, being a 'gel', where the excess Jeffamine was not able to be washed out, made it very difficult to analyze. In a previous paper, we studied the intercalation of different Jeffamines in α -ZrP [83]. For example, thermogravimetric analysis and elemental analyses on the α -zirconium phosphate intercalated with Jeffamine M300 (this compound formula is $C_7H_{15}O(CH_3CH(CH_3)O)_2CH_2CH_2NH_2$), allowed us to conclude that only one mole of the Jeffamine M300 was intercalated into one mole of α -zirconium phosphate. Structural evidence confirms this hypothesis. It is well known that even when as little as one mole of amine is intercalated into α -ZrP a bilayer is formed [45]. Presumably only every other -POH group interacts with an amine molecule. However, no interpenetration occurs but rather the angle at which the amine is inclined to the layers is smaller decreasing the interlayer distance. In the case of M715 intercalation the very large interlayer spacing also indicates the presence of a bilayer with no interpenetration.

The ^{31}P NMR spectra of the M- α -ZrP intercalate [Figure 4-4] shows two peaks at -18 and -16 ppm against the -18.9 ppm before the intercalation, which suggests that only a portion of the phosphate group is reacted with the amine (a shift of 2 ppm). Similar shifts have been observed on intercalation of n-alkyl amines [84, 85]. This supports the previous conjecture of the bilayer structure formation with every other -POH groups.

The infrared spectra shown in Figure 5 present the following bands: 3448 cm^{-1} , 2873 cm^{-1} , 1710 cm^{-1} , 1639 cm^{-1} , 1456 cm^{-1} , 1106 cm^{-1} and 971 cm^{-1} , which are assigned as water (O-H stretching), C-H stretching, C=O stretching due to the remaining MEK trapped in the gel, water bending motion, -CH₂, C-O stretching from the ether and P-O stretching, respectively. Bands corresponding to protonated nitrogen were not detected. These bands are located at $3400\text{-}3100\text{ cm}^{-1}$ for stretch and 1520 cm^{-1} for bend and are difficult to detect. Thus, it can be assumed that the amine is hydrogen-bonded to the free hydroxide of the phosphate group.

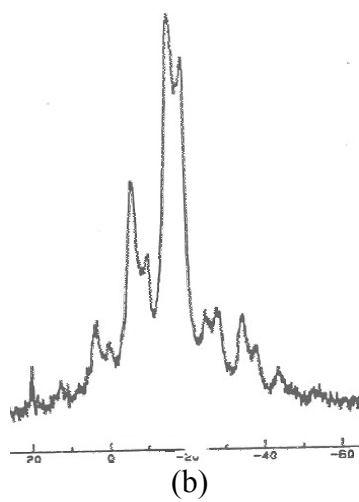
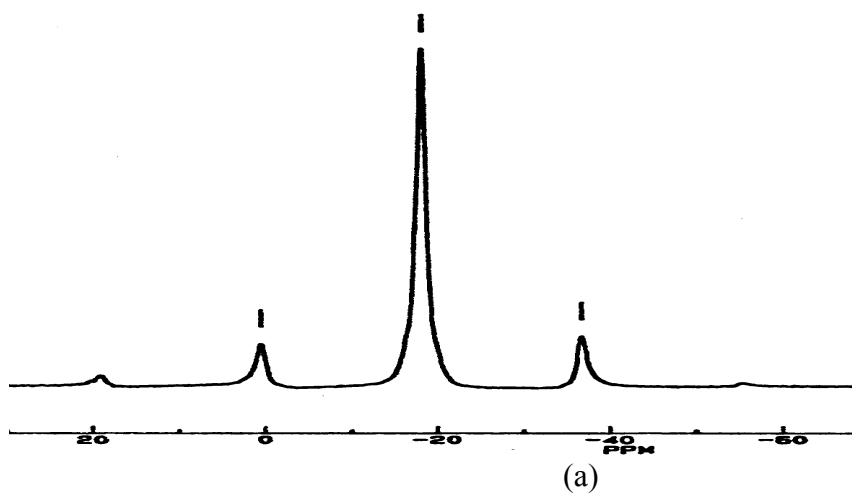


Figure 4-4. (a) ^{31}P NMR of α -Zirconium Phosphate. (b) ^{31}P NMR of α -Zirconium Phosphate Intercalated with M715.

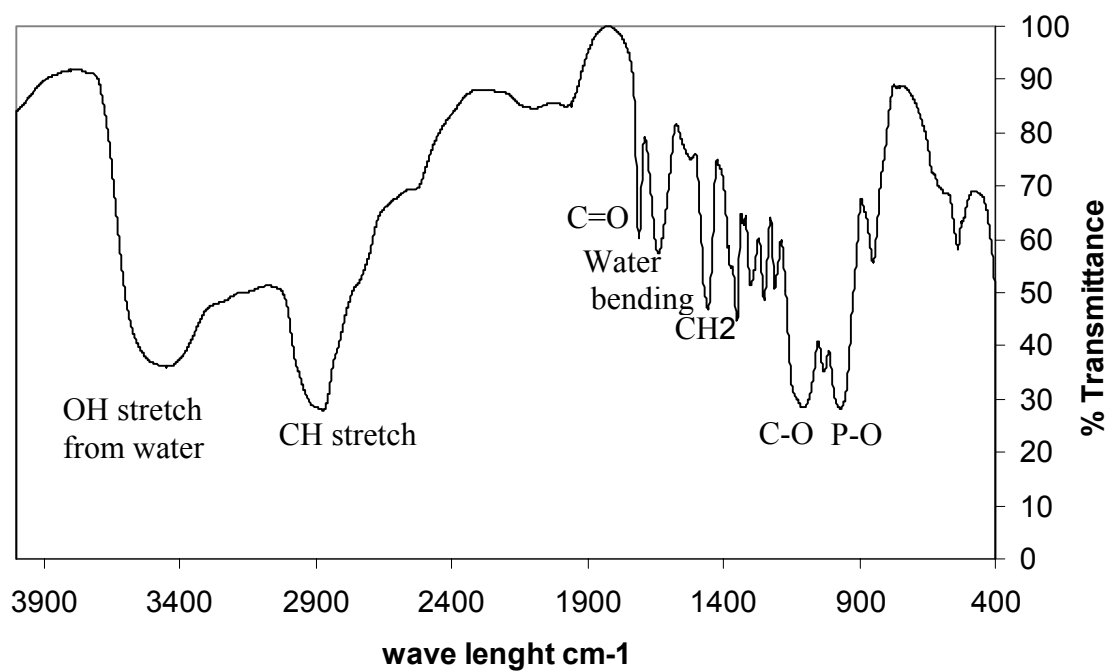


Figure 4-5. Infrared Spectrum of Jeffamine M715 and α -Zirconium Phosphate

Intercalated with Jeffamine M715

4.3.2 Characterization of M-ZrP/Epoxy Nanocomposites

Figure 4-6 presents respectively the powder patterns of M- α -ZrP/Epoxy, Neat/Epoxy and α -ZrP/Epoxy. The X-Ray diffraction powder pattern of the M- α -ZrP/Epoxy nanocomposite shows broad humps around 2° , 10° and 20° in 2θ which is different from M- α -ZrP. This powder pattern exhibits the amorphous nature of the nanocomposite material. The first two humps can be assigned to the inorganic matrix, while the third large broad hump is assigned to the epoxy matrix. In the case of α -ZrP/Epoxy the powder pattern shows a peak at 7.34 \AA , this value was 7.58 \AA in the starting α -ZrP. This change in the interlayer spacing is probably due to the loss of the water molecule, induced by the heating during the polymerization process, and shows that the layer structure has not been disturbed by the epoxy.

To directly investigate the dispersion and the state of intercalation/exfoliation of α -ZrP in the epoxy matrix, OM, SEM, and TEM observations were performed. The SEM images of α -ZrP powder before intercalation are shown in Figure 4-2 and showed aggregated primary particles having sizes in sub-micrometers range. After intercalation α -ZrP particles with the monoamine and dispersed in epoxy, the nanocomposite panel becomes transparent with a slight yellowish color induced by surface oxidation, which is commonly found in cured epoxies. M- α -ZrP/Epoxy panel showed no visible aggregation [Figure 4-7a]. In comparison, the composite α -ZrP/Epoxy is opaque and dark-brown in color, indicating the existence of sub-micron size α -ZrP aggregates [Figure 4-7b].

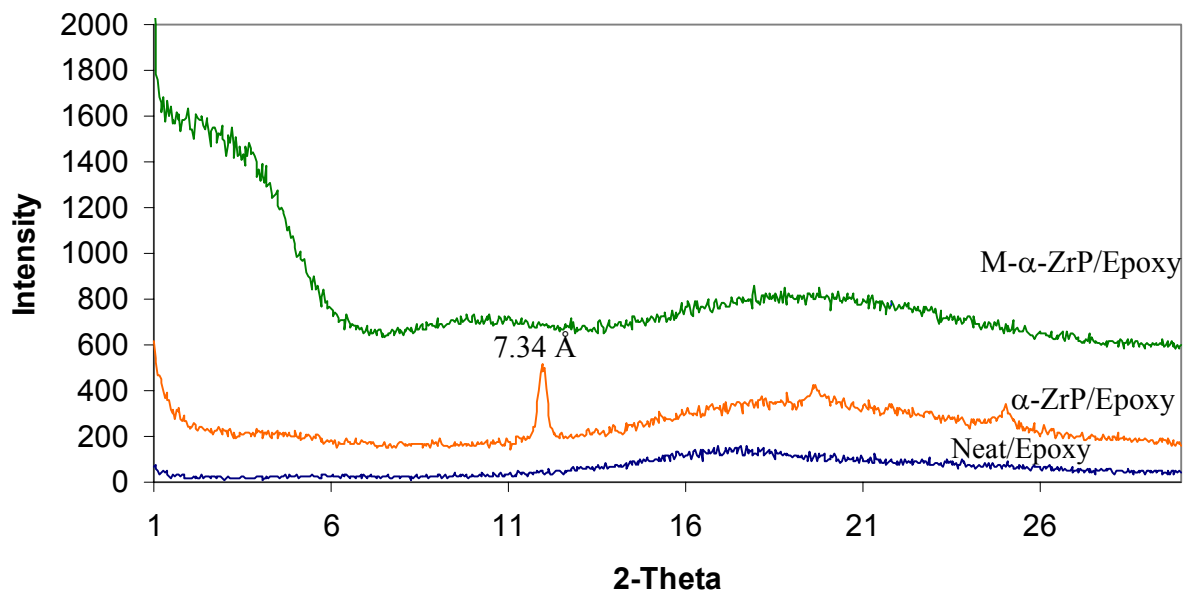


Figure 4-6. X-ray Powder Pattern of (a) α -ZrP/Epoxy (b) Neat/Epoxy (c) M- α -ZrP/Epoxy

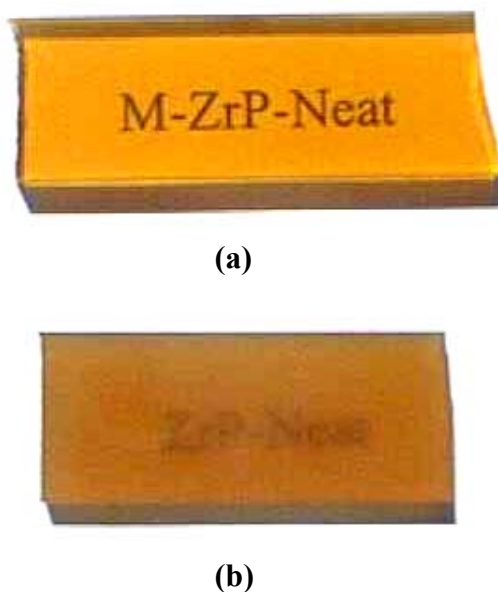
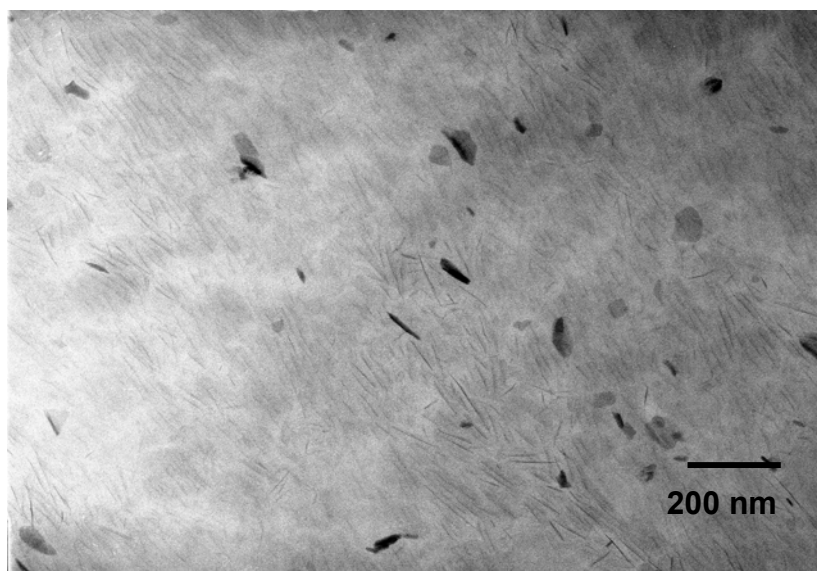


Figure 4-7. Photographs of (a) Transparent M- α -ZrP/Epoxy and (b) Opaque α -ZrP/Epoxy Samples

To make sure that no M- α -ZrP aggregates are present and the overall dispersion of M- α -ZrP in epoxy is uniform, additional OM and SEM investigations were performed. Even after exhaustive examination at high magnifications, no signs of α -ZrP aggregates were found in the matrix. Therefore, no OM and SEM micrographs are presented here since their morphologies investigated are simply featureless.

TEM observation of M- α -ZrP/Epoxy shows widespread exfoliated α -ZrP particles in the epoxy [Figure 4-8]. The state of dispersion and exfoliation of α -ZrP particles in the epoxy matrix is uniform throughout the sample. It is noted that the plane view images of the α -ZrP particles, i.e., the TEM thin section is parallel to the α -ZrP platelet surface, are observed (see arrows in Figure 4-8). It is also noted that, with only 1.9 vol. % of α -ZrP inorganic loading, the area fraction of α -ZrP in epoxy appears to be much higher than 1.9 vol. %. This apparent higher percentage of α -ZrP particles in the micrograph is due to the tilting of the α -ZrP platelets from the plane of the TEM thin section, and to the good dispersion and exfoliation of the α -ZrP in epoxy. In contrast, the TEM micrograph of α -ZrP/Epoxy clearly shows aggregated α -ZrP layer structures, exhibiting much lower apparent area fraction than that of the M- α -ZrP/Epoxy system [Figure 4-9].

The aspect ratio of the α -ZrP layer can be also obtained by dividing the observed length of each α -ZrP layer by the thickness of α -ZrP layer (0.75nm). The estimated aspect ratio of the α -ZrP ranges from about 100 to 200. Another interesting finding of the exfoliated α -ZrP is that α -ZrP platelet structure does not bend or curve [Figure 4-8], as opposed to the curved clay structure frequently observed in epoxy nanocomposites [32]. This implies that the α -ZrP structure is more rigid than clay since they both have approximately the same thickness and aspect ratio.

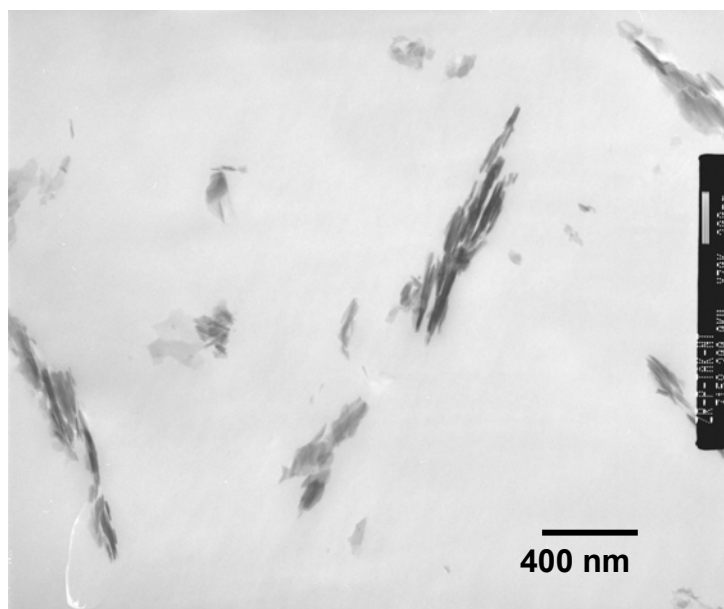


(a)

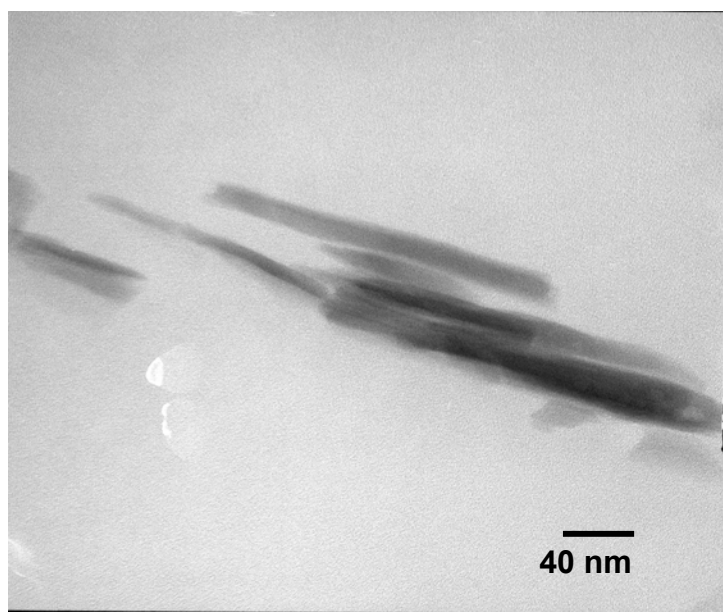


(b)

Figure 4-8. TEM of M- α -ZrP/Epoxy Showing (a) Low Magnification and (b) High Magnification of Uniform Dispersion and Exfoliation of α -ZrP Layers.



(a)



(b)

Figure 4-9. TEM of α -ZrP/Epoxy (a) Low Magnification and (b) High Magnification

4.3.3 Dynamic Mechanical Behavior

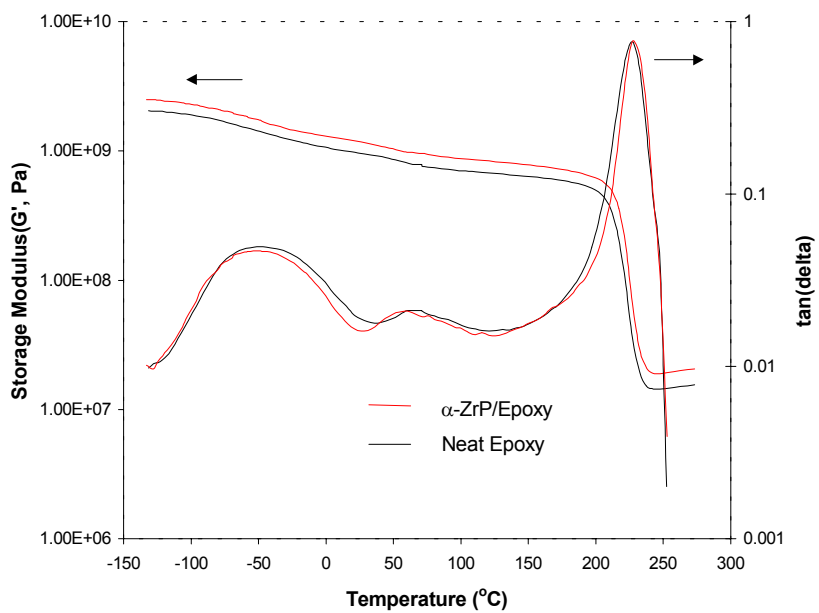
The glass transition temperature (T_g) of the DGEBA/DDS epoxy system is significantly decreased by addition of M- α -ZrP. This value drops from 227°C in the case of neat epoxy to 90°C for the M- α -ZrP/Epoxy [Figure 4-10]. C. S. Triantafyllidis et al.[86], also observed a drop in T_g when they used Jeffamine D2000 as surface modifier for an epoxy-clay nanocomposite; this drop was attributed to the large number of propylene oxide segments in D2000. The drastic difference observed in M- α -ZrP/Epoxy is likely due to the unintended reactions between the excess amount of monoamine and DGEBA epoxy. This excess monoamine M715 renders the formation of many dangling chain ends in the cured epoxy network. This speculation is supported by directly adding monoamine M715 to DGEBA/DDS system before curing. Upon curing, the monoamine-modified DGEBA/DDS (M/Epoxy) shows a significant drop in T_g , from 227°C down to 68°C. To make a more fair comparison, the properties of M/Epoxy are compared to those of M- α -ZrP/Epoxy nanocomposite system. In this case, the T_g of M/Epoxy is significantly increased from 68°C to 90°C after the addition of M- α -ZrP. However, the quantity of the monoamine M715 involved in the M- α -ZrP/Epoxy curing process responsible for the significant drop in T_g , is still uncertain. Therefore, it is unclear if indeed the presence of exfoliated α -ZrP actually leads to a greatly enhanced T_g in the nanocomposite, as compared to M/Epoxy. This issue is currently being addressed by altering the level of monoamine and the type of surface modifiers utilized. The results will be published in a separate paper.

In the case of using unmodified α -ZrP for reinforcement, the DMA plot shows that there is no shift in T_g for the α -ZrP/Epoxy system. The storage moduli of α -ZrP/Epoxy system are only slightly higher than those of DGEBA/DDS throughout the temperature range studied [Figure 4-10]. This suggests that without surface modification, α -ZrP would act as an ordinary filler.

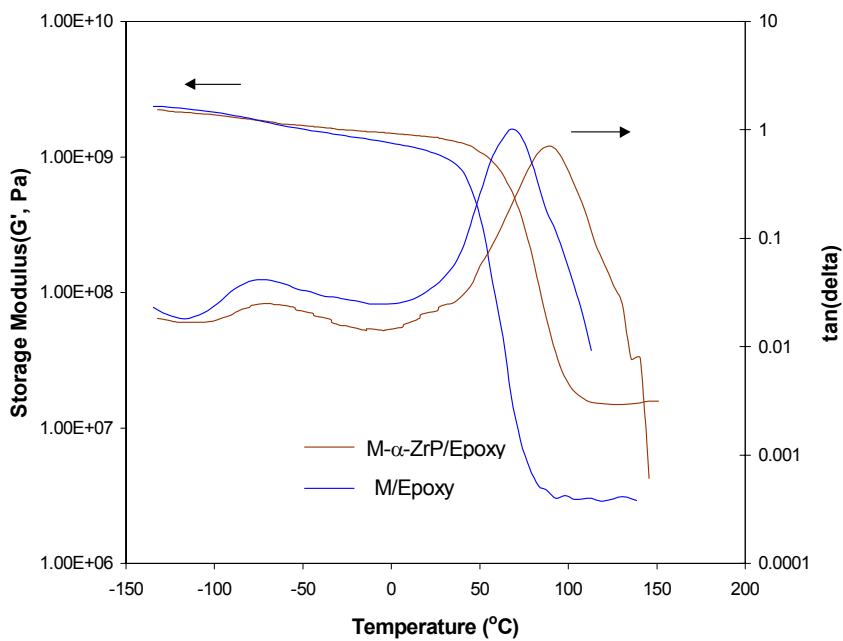
It is interesting that the storage modulus, G' , increases more significantly at a temperature above T_g than at temperatures below T_g . In comparison to M/Epoxy, the addition of M- α -ZrP to epoxy, the storage modulus, G' , of the M/Epoxy matrix at 25°C is only increased from 1.03 GPa to 1.38 GPa. However, a significant increase of the rubbery plateau modulus from 2.90 MPa to 15.8 MPa is observed at temperatures above their respective T_g values. The 4.5 times increase in rubbery plateau modulus [Table 4-2] is probably because the rigid α -ZrP particles serves as physical cross linkers to elevate the rubbery plateau modulus of the epoxy [5, 32]. It is also possible that the significant increase in rubbery plateau modulus is due to the decreased amount of free monoamine in the epoxy matrix due to the adsorbed, immobile monoamine molecules on the α -ZrP surfaces.

Table 4-2. DMA Results of α -ZrP-Epoxy Nanocomposites

	Neat	M/Epoxy	M- α -ZrP/Epoxy	α -ZrP/Epoxy
T_g (°C)	227	68	90	227
G' at 25 °C (Pa)	9.69E+08	1.03E+9	1.38E+09	1.17E+9
Rubbery plateau modulus (Pa)	1.55E+07	2.90E+6	1.58E+07	1.99E+7



(a)



(b)

Figure 4-10. . DMA of (a) Neat and α -ZrP/Epoxy (b) M/Epoxy and M- α -ZrP/Epoxy Systems.

Most interestingly, the increase in G' due to the presence of α -ZrP diminishes as the temperature decreases and becomes non-distinguishable with the neat epoxy when the temperature approaches the γ -relaxation peak of the epoxy, i.e., about -80°C . The recent molecular dynamics modeling work of Gersappe [87] suggests that the above phenomenon can be explained based on the comparable sizes and mobility between the matrix molecule and the nanofiller. The ability of the nanofiller to carry and redistribute the applied stress field depends strongly on the mobility and the size of the nanofiller. As a result, the more mobile the nanofiller is, the easier for the nanofiller to contribute to the stiffening of the matrix. Since the nanofiller is small and can be easily mobilized by the surrounding mobile molecules, the stiffening effect would be maximized when the temperature is above T_g and minimized when the temperature is below the γ -relaxation peak.

The above argument seems reasonable since the molecular size of the epoxy, i.e., the distance between crosslinks in this case, is about 10-20 nm. When the filler size is far greater than the molecular size, the conventional composite principle would take effect, as in the case of the α -ZrP/Epoxy system. Nevertheless, the actual physical origin of such unusual behavior is still not known, which warrants further research in the future. Additional designed experiments are underway to validate the above conjecture.

4.3.4 Mechanical Property Characterization

By adding the monoamine surface modifier to DGEBA/DDS neat resin, the tensile modulus is decreased by about 10 %, and yield stress decreased by 30%. After

the addition of 1.9 vol. % M- α -ZrP to the epoxy, the corresponding properties are increased by 50% and by 10%, respectively [Table 4-3]. The addition of M- α -ZrP to epoxy substantially increases the tensile modulus, while the elongation at break decreases significantly [Figure 4-11]. This big drop in elongation-at-break is possibly caused by the low molecular mobility of the epoxy network structure induced by the presence of the rigid, immobile α -ZrP platelet structure, as evidenced by the significantly suppressed damping behavior in the nanocomposite [Figure 4-11]. This is also why α -ZrP is effective in stiffening the epoxy matrix.

Table 4-3. Mechanical Properties and Fracture Toughness

	Neat	M/Epoxy	M- α -ZrP/Epoxy	α -ZrP/Epoxy
Modulus (GPa)	2.9	2.6	3.9	3.2
Yield strength (MPa)	77.6	54.0	61.0	65.9
Elongation at Break (%)	4.8	13.5	1.8	2.6
K_{IC} (MPa*m ^{1/2})	0.80	0.83	0.77	0.79

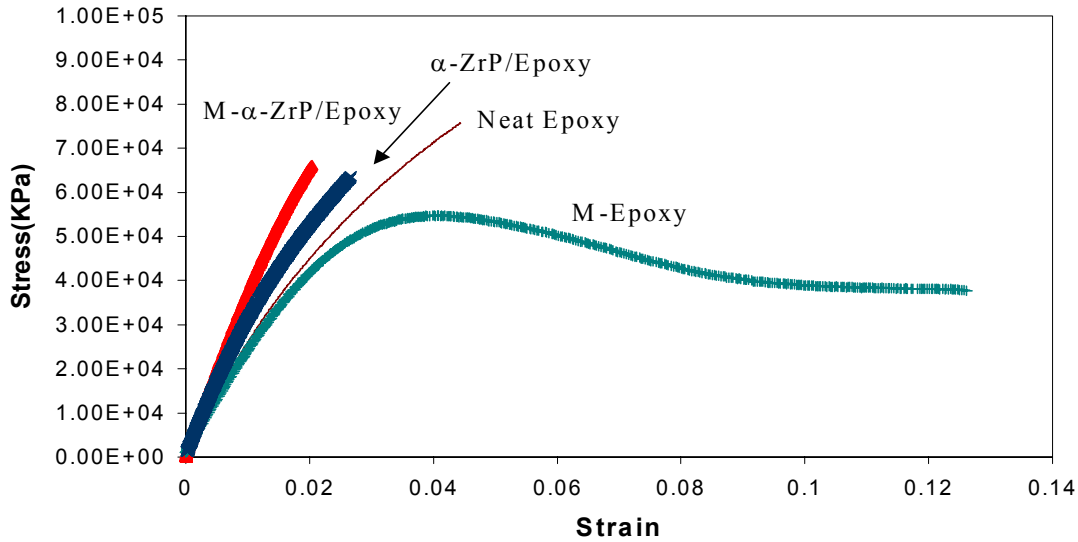


Figure 4-11. Tensile Behavior of Neat and α -ZrP-Modified DGEBA/DDS Epoxy Systems .

Mode-I critical stress intensity factor, K_{IC} , values from the SEN-3PB tests show that the fracture toughness is not significantly changed by the addition of either the monoamine modifier or M- α -ZrP [Table 4-3] since epoxy resin is inherently brittle and/or notch-sensitive. This finding is consistent with our earlier study on clay-filled epoxy nanocomposites systems [32]. This implies that when the nanofiller phase is well

dispersed and in small quantities, it would not act as defects to cause premature failure of the epoxy matrix.

The present research clearly shows that α -ZrP-based epoxy nanocomposites are ideal for gaining fundamental knowledge on the physics of how and why nanoparticles alter the physical and mechanical properties of polymer matrices. The versatility and simplicity of α -ZrP synthesis to control the surface functionality, size and aspect ratio of α -ZrP particles would allow the establishment of unambiguous fundamental relationships between nanoparticle material parameters and the physical and mechanical properties of polymer nanocomposites. We are currently working on altering the aspect ratios, sizes, and surface functionalities of α -ZrP to further investigate how and why nanofiller change the properties of polymers.

4.4 CONCLUSIONS

M- α -ZrP with wide interlayer spacing has been successfully prepared using commercially available monoamines intercalate. The intercalate is hydrogen bonded to the host and exhibits a bilayer structure into the interlayer spacing. Uniformly dispersed and exfoliated α -ZrP-based epoxy nanocomposites were prepared. The mechanical property study of M- α -ZrP/Epoxy nanocomposites shows that rubbery plateau modulus of the M- α -ZrP/Epoxy nanocomposite is about 4.5 times higher than that of the M/Epoxy. The tensile modulus of the M- α -ZrP/Epoxy nanocomposites is increased by 50 % of the reference epoxy, while the ductility is decreased drastically. The

fundamental physics behind the change in mechanical property of the nanocomposite was discussed.

CHAPTER V

MECHANICAL PROPERTY OF α -ZIRCONIUM PHOSPHATE-EPOXY NANOCOMPOSITES AND THEIR TOUGHENING MECHANISMS

5.1 INTRODUCTION

Montmorillonite clay is widely used for polymer nanocomposite preparation with nanolayer exfoliation to study the fundamentals of polymer nanocomposite and to achieve many enhanced materials properties of polymers [1-13]. The possibility of the delamination of layer structure of the montmorillonite clay allows the intercalated or exfoliated polymer nanocomposite with proper surface treatment or with appropriate process to disperse the nanolayer in polymer matrix. By the intercalation or especially the exfoliation of the nanolayers in polymer matrices reported that they are efficiently improve many materials physical or mechanical properties at relatively small amount of addition of the nanofillers [6]. However there are several limits to perform fundamental researches on polymer nanocomposite with montmorillonite clay particles. A few major obstacles for the fundamental nanocomposite research with montmorillonite include the wide size and shape distribution of the particles and the impurity in the clay particles. The montmorillonite clay is obtained from nature with purification and further treatment for commercial applications. Therefore the impurity in the montmorillonite clay is

always involved some extent, and the exact composition, the shape and size, and its distribution can hardly be characterized accurately.

To overcome these obstacles while retaining the layer structure to be exfoliated, the synthesized α -zirconium phosphate (ZrP) particles can be a good candidate nanofillers for polymer nanocomposite preparation. It was first synthesized and characterized by Clearfield at 1964, and its crystal structure is extensively studied, and the size and shape can be controlled by the reaction condition [43, 44]. Therefore, with ZrP particle, the study of the fundamental nanofiller effects on the nanocomposite properties can be systematically investigated including the effects of the aspect ratio, the size, and the size distribution of the nanofillers.

Previous reports on epoxy nanocomposites with synthetic ZrP [88] addressed the intercalation of ZrP particles and the preparation of ZrP epoxy nanocomposites with fully exfoliated ZrP. The improved tensile modulus and yield strength of ZrP epoxy nanocomposites was discussed with a fundamental structure-property relationship of ZrP-based epoxy nanocomposites. But the drastic decrease of the glass transition temperature of ZrP epoxy nanocomposites needs to be further investigated to understand the effects of the surface modifiers on the material properties of this nanocomposite system.

In this study, the mechanical properties and toughening mechanisms of synthetic ZrP - epoxy nanocomposites with different amounts of surface modifiers are studied. To achieve this purpose, two different systems of ZrP - epoxy nanocomposites were prepared with a commercially available monoamine-terminated polyether as a surface

modifier. The influences of the surface modifier on the morphology and mechanical properties of the ZrP - epoxy nanocomposites are studied. A ZrP - epoxy nanocomposite system with CSR particles is also investigated for its mechanical property changes and toughening mechanisms.

5.2 EXPERIMENTAL

5.2.1 Materials

Diglycidyl ether of bisphenol-A (DGEBA) epoxy resin (DER332[®], Dow Chemical) was mixed with 4,4'-diamino-diphenyl sulfone (DDS, Aldrich), which is a curing agent, to prepare the epoxy matrix for this study. The DGEBA epoxy monomer has a narrow monomer molecular weight distribution of about 172~176 g/mole.

The reagents were used to prepare ZrP as received: Zirconium oxychloride octahydrate ($\text{ZrOCl}_2 \cdot 8\text{H}_2\text{O}$), 98% (Aldrich), Phosphoric Acid (EM), Jeffamine M715 (Huntsman Chemical) and Methyl ethyl ketone (Merck).

Preformed CSR particles from KANEKA Corporation were used to investigate the toughening ability of clay-epoxy nanocomposites. These CSR particles have a rubber core size of 80~90 nm in diameter and are covered with a compatibilizer copolymer shell of 10~20 nm in thickness [26]

5.2.2 Surface Modification of α -ZrP.

The detailed chemistry and preparation of ZrP followed procedures described elsewhere [47, 81, 82]. The interlayer spacing of a α -ZrP crystal is 7.6 Å. The prepared ZrP particles' characterization and their intercalation was investigated and reported in a previous article [88]. Monoamine-terminated polyether amine, Jeffamine M 715 is used for surface modification of prepared ZrP particles.

5.2.3 Preparation of α -ZrP-Based Epoxy Nanocomposites

The procedure for preparation of M1- α -ZrP/Epoxy nanocomposite is the same as the procedure to prepare the M2- α -ZrP/Epoxy nanocomposite system, described in detail in the previous report. [88] Only a brief explanation is given here as follows. The M1- α -ZrP in solvent MEK was poured into the liquid epoxy to prepare panel with 1.9 vol. % (5.2 wt %) of α -ZrP in epoxy (M1- α -ZrP/Epoxy). After removing MEK with a Rotavapor[®] in a water bath at about 90°C, under vacuum, no aggregation or precipitation was found in the viscous mixture. When the mixture was ready, it was heated at 130°C, and the curing agent, DDS powder was added at a stoichiometric ratio. This mixture was stirred until a transparent yellowish solution was obtained. After degassing the prepared mixture under vacuum, it was poured into a preheated glass mold to make a plaque with dimensions of 200 mm (8") x 200 mm (8") x 3.12 mm (0.125"). The resin mixture was cured in an oven at 180°C for 2 hours, followed by 2 hours of post-cure at 220°C. For the Epoxy-II system, the curing schedule was 130°C for 3 hours, 180°C for 2 hours, then followed by 2 hours of post-cure at 220°C. For epoxy panels of the second system

(Epoxy-II) the surface modifier amounts of 1 to 1 mole ratio is used rather than 2-to-1 mole ratio.

For the preparation of toughened nanocomposites with CSR, the liquid epoxy with well-dispersed CSR from Kaneka-Texas was added into the mixture of liquid epoxy with M1- α -ZrP or α -ZrP to make CZE or CMZE nanocomposites, respectively. Two neat epoxy panels (Neat, Neat-II), two epoxy panels with only the Jeffamine (M1/Epoxy and ME), two epoxy panels (M1-ZrP/Epoxy and MZE) with 1.9 % vol. of modified α -ZrP, and a toughened epoxy panel with only CSR with Epoxy-II (CSR/Epoxy-II) were prepared. The compositions of the prepared nanocomposite panels are shown in Table 5-1a and b.

5.2.4 Characterization

X-ray diffraction (XRD) powder patterns for the prepared nanocomposite panels were taken between 1 and 30° in 2 θ , with a step size of 0.04° and a count time of 2s per step. with a Bruker D8 diffractometer with Bragg-Brentano θ -2 θ geometry (40 kV and 40 mA) and a graphite monochromator. Optical microscopy (OM) was performed using an Olympus optical microscope (model BX60) under both bright field and crossed-polars. Scanning electron microscopy (SEM) investigations were performed to observe the overall α -ZrP particle distribution and the homogeneity of the dispersion in epoxy on the fracture surface of the SEN-3PB specimen using a JEOL JSM-6400, operated at 20 kV. TEM with a JEOL JEM-2010A, operated at 200 kV were used to characterize the

Table 5-1 Compositions of ZrP-Epoxy System-1, -2

a) Compositions of ZrP-Epoxy System-1 [Vol.%]

	α -ZrP	Jeffamine M715
Neat Epoxy(DDS/DER332)	None	None
M1-Epoxy	None	7.8 (20 mmol)
M2-Epoxy	None	18.7 (40 mmol)
M1-ZrP-Epoxy [*]	1.9 (5.2wt%)	7.8
M2-ZrP-Epoxy ^{**}	1.9	18.7
ZrP- Epoxy ^{***}	1.9	None

^{*}Twenty mmol of α -ZrP was intercalated with 20 mmol of Jeffamine M715: d-spacing of 50.0 Angstrom

^{**}Twenty mmol of α -ZrP was intercalated with 40 mmol of Jeffamine M715: d-spacing of 73.3 Angstrom

^{***}No surface treatment on α -ZrP: α -ZrP was added into DER332 after overnight dispersion in MEK with stirring

b) Compositions of ZrP-Epoxy System-2 [Vol.%]

	α -ZrP	Jeffamine M715 [*]	CSR
Neat Epoxy-II(E) ^{**}	None	None	None
M1-Epoxy-II (ME)	None	7.8 (20 mmol)	None
M1-ZrP-Epoxy-II (MZE)	2.0 (5.4 wt%)	7.8	None
CSR-M1-Epoxy-II (CME)	None	8.3	3.3wt%
CSR-M1-ZrP-Epoxy-II (CMZE)	2.0	7.8	3.2wt%

^{*} Jeffamine M715 is used as a surface modifier.

^{**} Neat Epoxy-II: DER332/DDS system with 3 step curing at 130°C/3hr+180°C/2hr+220°C/2hr

morphology and the ZrP layer exfoliation in the epoxy resin matrices. These XRD, OM, SEM, and TEM conditions were described in detail at a previous report [88].

5.2.5 Mechanical Property Characterization

From dynamic mechanical analysis (DMA), using a Rheometrics[®] (RDS-II) at a fixed frequency of 1 Hz and a temperature sweep of 5°C per step from -150°C to 250°C, the dynamic storage modulus (G') and loss $\tan\delta$ against temperature curves were plotted. The temperature at which the $\tan\delta$ curve shows a maximum peak is recorded as the glass transition temperature (T_g).

Tensile test as ASTM D638-98 was performed with a screw-driven mechanical testing machine (Sintech[®]-2) at a crosshead speed of 0.508 mm/min (0.2"/min) at room temperature. An average of at least five tests per sample was performed to report modulus, yield stress, and elongation at break.

5.2.6 Viscosity Measurement

The viscosities of the neat liquid epoxy resin, the liquid epoxy with unmodified ZrP particles, and the liquid epoxy with modified ZrP particles are measured with RDS-II (Rheometrics) at 26 °C. A parallel plate with 50 mm diameter is utilized with 10% strain and frequency from 1×10^{-1} to 1×10^2 rad/sec. The viscosities of three different samples are recorded with increasing shear rate.

5.2.7 Toughening Mechanism Investigation

A single-edge-notch 3-point-bending (SEN-3PB) test, following the ASTM D5045 method, was used to obtain the mode-I critical stress intensity factor (K_{IC}) of the neat epoxy and epoxy/ZrP nanocomposite systems based on the linear elastic fracture mechanics (LEFM) approach.

Fracture toughness values alone do not allow for the observation of damage zones or toughening mechanisms. The sequence of damage or events leading to the toughening of the polymer is crucial to understanding the role the toughener plays. It is imperative that an additional method be utilized to validate the values obtained from other mechanical tests.

The widely accepted, common approach used to determine toughening mechanisms involves the observation of the damage zones from developed by partially fractured specimens. To generate these fracture zones, double-notched 4-point bend (DN-4PB) samples are used. Through this technique, one crack fails while the other is arrested right before its failure. This arrested crack tip can be used to analyze the toughening mechanism(s) occurring. Using OM and TEM, the crack tip damage zone can be observed along with operative toughening mechanisms. Transmission optical microscopy (TOM) is used to observe evidence of shear banding around the crack tip.

5.3 RESULTS AND DISCUSSION

5.3.1 Characterization of the Intercalate α -ZrP and M1-ZrP/Epoxy Nanocomposites

In the previous study with synthetic ZrP epoxy nanocomposites, the amount of surface modifier was 40 mmol for 20 mmol of ZrP. The amount of surface modifier was decreased to 20 mmol for 20 mmol of ZrP in the current study to investigate the effect of the surface modifier amount on the morphology and properties of prepared nanocomposites. It was observed that the basal spacing for the intercalated ZrP with 20 mmol of surface modifier is 50.04 angstrom as shown in Figure 5-1, from the average of 5 orders of 00ℓ . The X-ray powder pattern of the intercalated ZrP with 40 mmol of Jeffamine M715 showed a basal spacing of 73.27 Å [88], which is longer than the one with 20 mmol of surface modifier.

The X-ray diffraction result for the modified ZrP epoxy nanocomposite (M1-ZrP/Epoxy) is presented in Figure 5-2 (bottom). If the relative intensities of the peaks are considered, it can be claimed that most of all ZrP layer-structures are exfoliated though some small amount of repeated layer-structures remained to give corresponding small peaks to the original ZrP layer structures as shown in Figure 5-2 (top).

SEM and TEM observations were used as methods for direct investigation of the dispersion and the state of intercalation/exfoliation of α -ZrP in the epoxy matrix. To the naked eye, the M1- and M2-ZrP/Epoxy nanocomposite panels are yellowish and

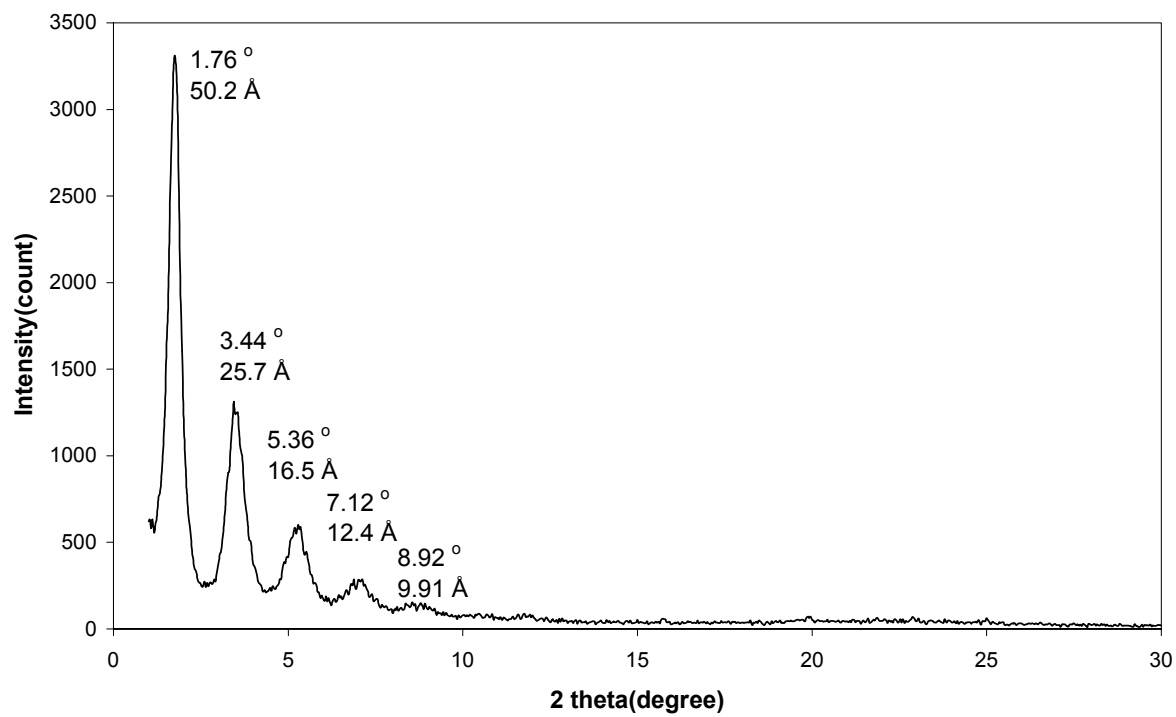


Figure 5-1. WAXD of Intercalated ZrP particles with 20 mmol of Monoamine M715.

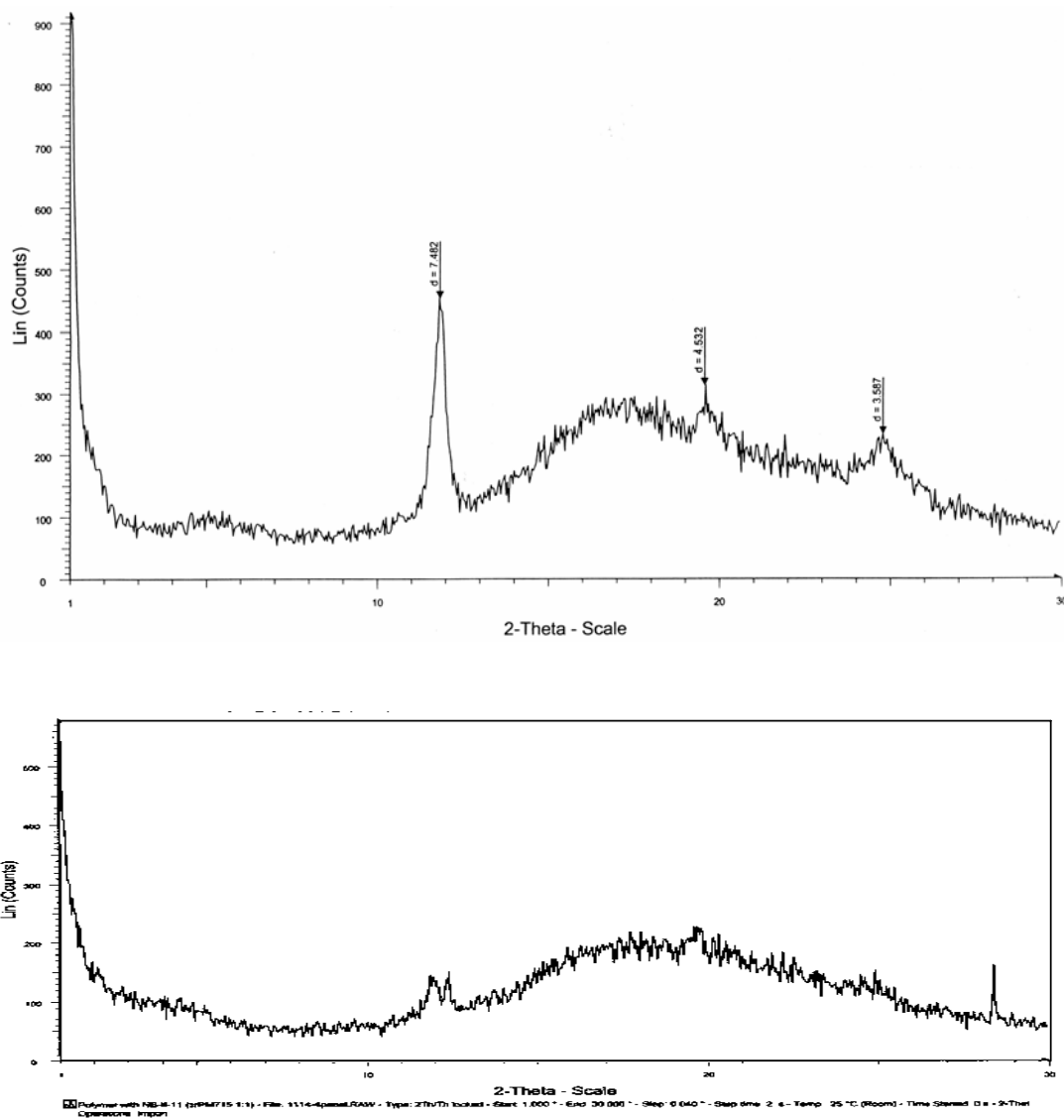


Figure 5-2. WAXD of ZrP/Epoxy Composite (top) and M1-ZrP/Epoxy Nanocomposite (bottom).

transparent without visible aggregation in the panels, however the prepared ZrP/Epoxy composite without ZrP surface modification is opaque and dark-brown in color.

The SEM of the ZrP/Epoxy composite and the M2-ZrP/Epoxy nanocomposite in Figure 5-3 (taken on the failed surface from SEN-3PB test) shows the significant change in the particles' size or their aggregation in the matrices. The finer particle distributions are found in the SEM picture (bottom of Figure 5-3) for the M2-ZrP/Epoxy nanocomposites. The more direct piece of evidence of ZrP layer exfoliation is found from TEM observations for the M1-ZrP/Epoxy nanocomposites in Figure 5-4. If the added amount of the ZrP particles in the M1-ZrP/Epoxy, which is only about 2.0 Vol.% (5.4 wt%), are considered, the uniform and overall presence of the layer structures in the matrix resin [Figure 5-4, top] is evidence of their good dispersion of particles. The exfoliation of layer structure is shown in Figure 5-4, bottom. The dark platelets observed in the top picture of Figure 5-4 possibly caused the small peaks corresponding to the original ZrP particle structures. However, the exfoliation and the distribution of the ZrP particles in M1-ZrP/Epoxy is apparently not as good as in the M2-ZrP/Epoxy nanocomposite system [88].

5.3.2 Dynamic Mechanical Behavior

The unmodified ZrP fillers behave as conventional fillers and there is no shift in T_g , and the storage modulus increased slightly than those of the neat epoxy system throughout the tested temperature range [Figure 5-5, top]. The T_g drop after the addition of surface modifier for nanofiller was reported for a few cases of epoxy nanocomposites,

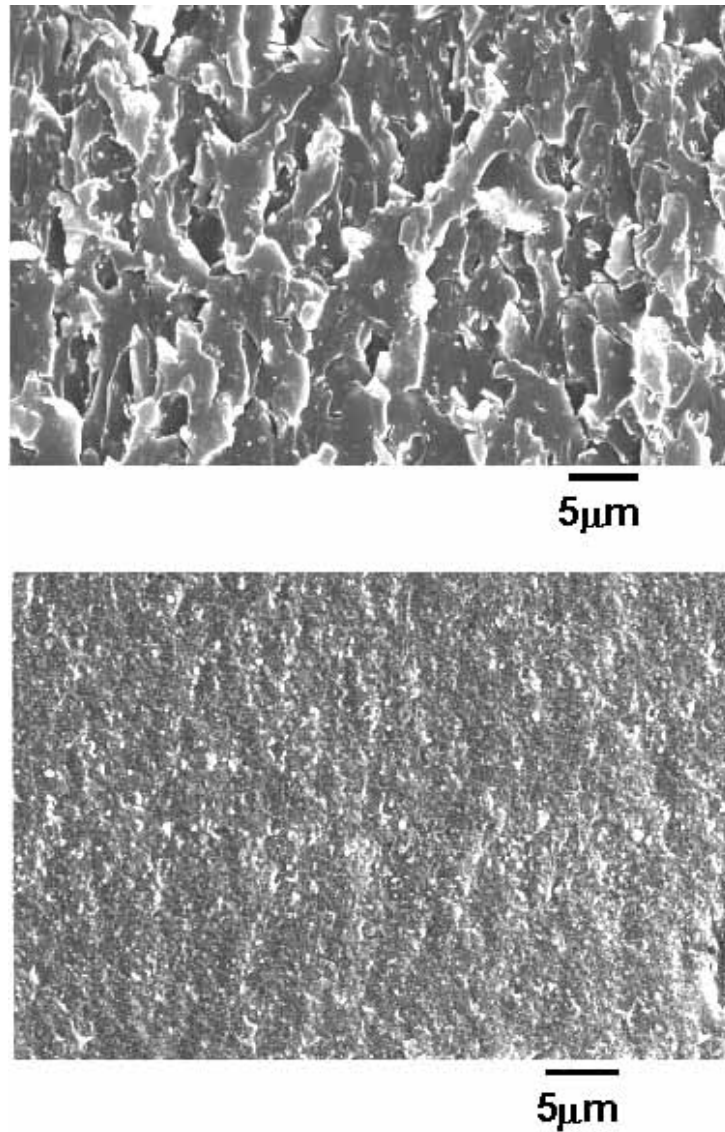


Figure 5-3. SEM Pictures on the Failed Surface from SEN-3PB Test (Top: ZrP/Epoxy Composite, bottom: M2-ZrP/Epoxy Nanocomposite)

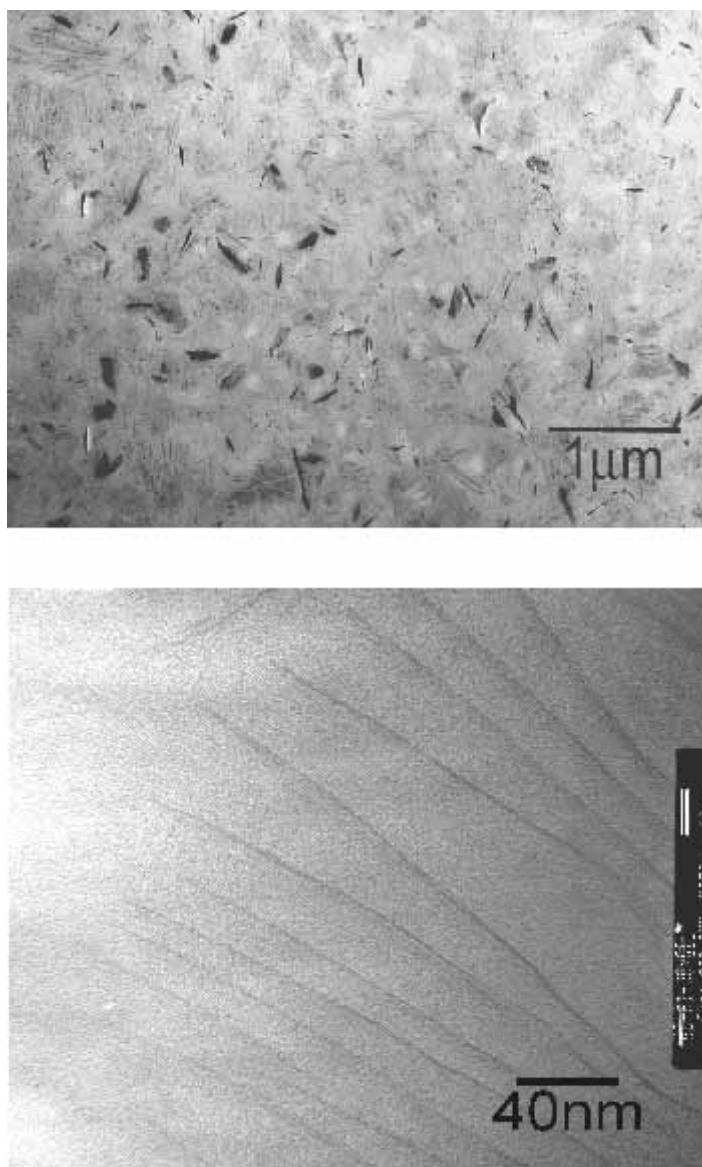


Figure 5-4. TEM Pictures of M1-ZrP/Epoxy Nanocomposite Showing (a) Low Magnification and (b) High Magnification of Dispersion and Exfoliation of ZrP Layers.

because of unexpected reactions between the surface modifier and the curing agents. [86, 88] The epoxy system with monoamine M715 (40 mmol used for 20 mmol of ZrP) -

modified DGEBA/DDS (M2/Epoxy) shows a significant drop in T_g , from 227°C down to 68°C, while the M2-ZrP/Epoxy has its T_g at 90 °C [Figure 5-5, bottom]. This figure shows that the increase in G' due to the presence of ZrP diminishes as the temperature decreases and becomes non-distinguishable with the neat epoxy when the temperature approaches the γ -relaxation peak of the epoxy, i.e., about -80°C. As discussed in the previous reports [87, 88] the above phenomenon can be explained based on the comparable sizes and mobility between the matrix molecule and the nanofiller. The nanofiller is small and can be easily mobilized by the surrounding mobile molecules, the stiffening effect would be maximized when the temperature is above T_g and minimized when the temperature is below the γ -relaxation peak.

The DMA plot of the DGEBA/DDS epoxy system with reduced amount of monoamine surface modifier (20 mmol for M1/Epoxy) [Figure 5-6] shows same phenomenon for the storage modulus behavior of nanofiller-added epoxy system, while the system M2-ZrP/Epoxy shows a bigger increase (from 2.90×10^6 to 1.58×10^7 Pa) than the system M1-ZrP/Epoxy (from 7.59×10^6 to 1.39×10^7 Pa).

The same plot shows the change of T_g from 227°C of neat DGEBA/DDS epoxy to 132°C, which is much higher T_g than the T_g of M2/Epoxy, 68°C. The influence of the surface modifier on the T_g drop is clearly observed at this plot, and the T_g drop appears to be decreased by the addition of smaller amounts of surface modifier.

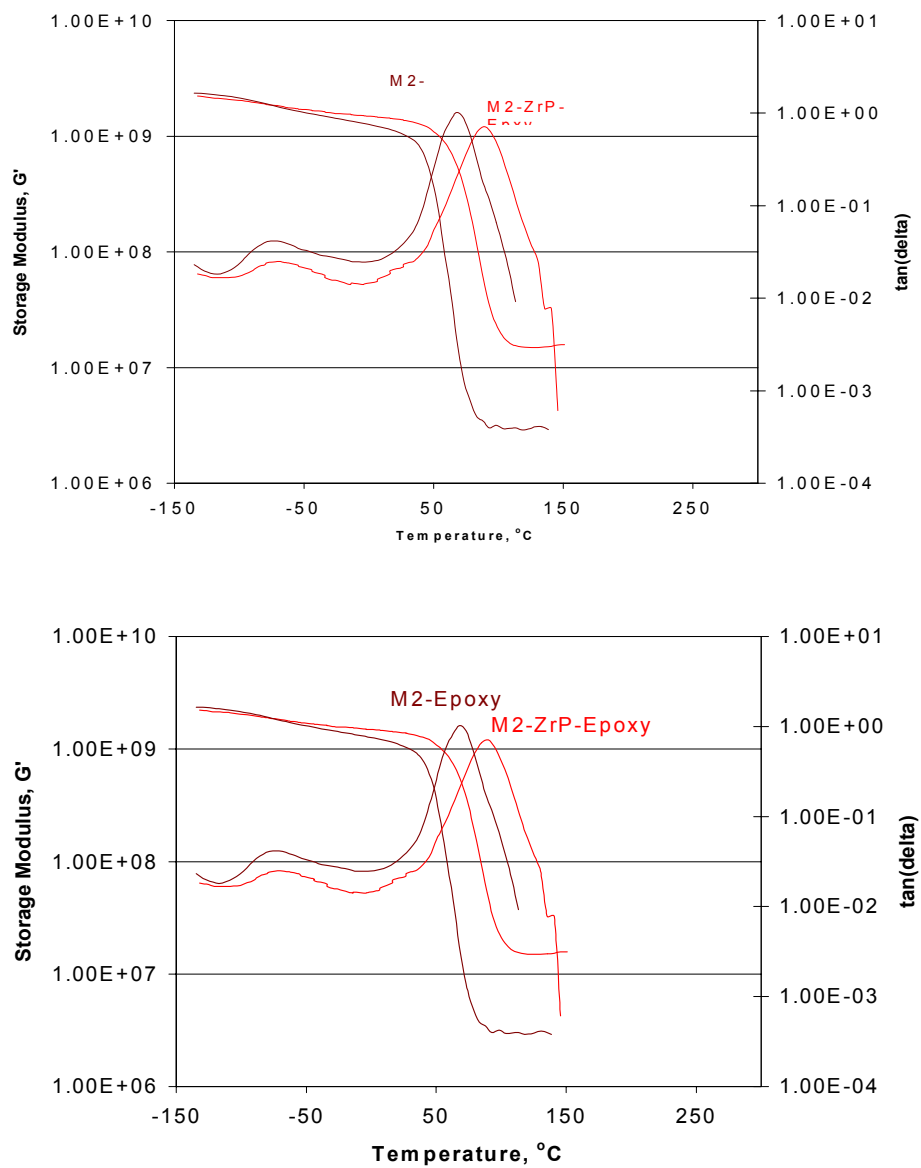


Figure 5-5. DMA plots of (a) Neat Epoxy and ZrP/Epoxy (b) M2/Epoxy and M2-ZrP/Epoxy Systems.

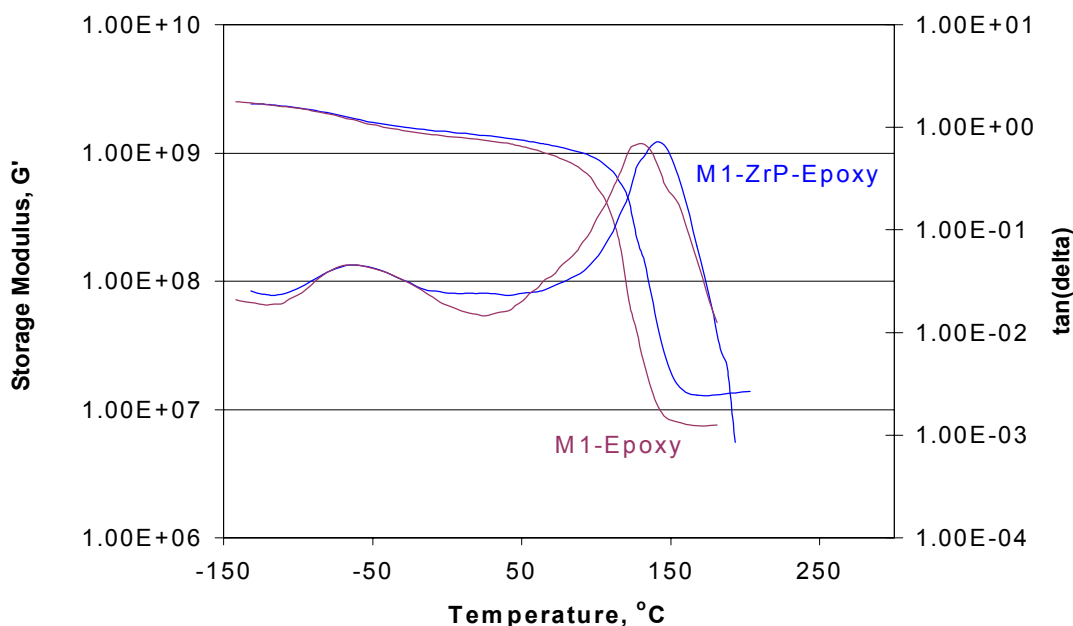


Figure 5-6. DMA Plots of M1/Epoxy and M1-ZrP/Epoxy Systems.

To understand the nanofiller effect on the prepared nanocomposite materials, the data from M1-ZrP/Epoxy can be compared with the result from the M1/Epoxy system. In this case, the increment of T_g due to nanofiller addition is about 10°C from 132 to 142°C for M1/Epoxy and M1-ZrP/Epoxy, respectively. This is smaller than the increment in T_g of the nanocomposite system with 40 mmol of surface modifier, which is from 68 to 90°C for M2/ Epoxy and M2-ZrP/Epoxy, respectively.

There are reports of the effects of nanofillers in T_g of the matrix resins [30, 59, 89~93], but the nanofiller effect is not clearly understood yet. Some reports claim that

the exfoliation of the nanolayer structure caused the increase in T_g of matrix resin, and it is found that the T_g is effectively increased only with enough amount of the exfoliated or intercalated nanolayers [30, 89, 90]. It is reasonable, because the constraint by the nanolayer structures in the matrix resin restricts the mobility of the chain of molecules, which cause the increase of T_g . In regard to this role of the nanolayer structure in the matrix resin, the more rigid layer must be the more effectively affect the increase in T_g , because it works as constraining nano-walls more effectively against the chain molecule movements in the matrix resin. In other words, if the nanolayer is not stiff enough it may not play the role as constraining nano-walls. This may be the reason why some of the exfoliated nanolayer does not effectively increase the T_g of matrix resin, as reported by some researchers who claim that the nanofiller does not affect the increase in T_g [89, 91]. The ZrP layers appear to be stiffer than clay layers as shown in TEM pictures [32, 88], so ZrP layers effectively contribute to increase in T_g of matrix more than the clay layers.

5.3.3 Mechanical Property of ZrP/Epoxy Nanocomposites

The tensile modulus results of the M1-ZrP/Epoxy nanocomposite and M2-ZrP/Epoxy nanocomposite systems show that they have similar values about 3.9 GPa, which is increased from 3.1 GPa of M1/Epoxy and from 2.4 GPa from M2/Epoxy resin systems [Figure 5-7, Table 5-2]. If we focus on the M1-ZrP/Epoxy system, there is an interesting result of the increase in both modulus (25%) and yield stress (17%) by the addition of ZrP to the epoxy resin system.

The elongation at break for the M1-ZrP/Epoxy is around 9%, which is a higher value than that of the M1/Epoxy resin system. This result is quite different from the elongation at break value of M2-ZrP/Epoxy nanocomposite system (1.8%), which was drastically decreased by the addition of ZrP from 13.5% of M2/Epoxy resin system and was discussed in previous report [88].

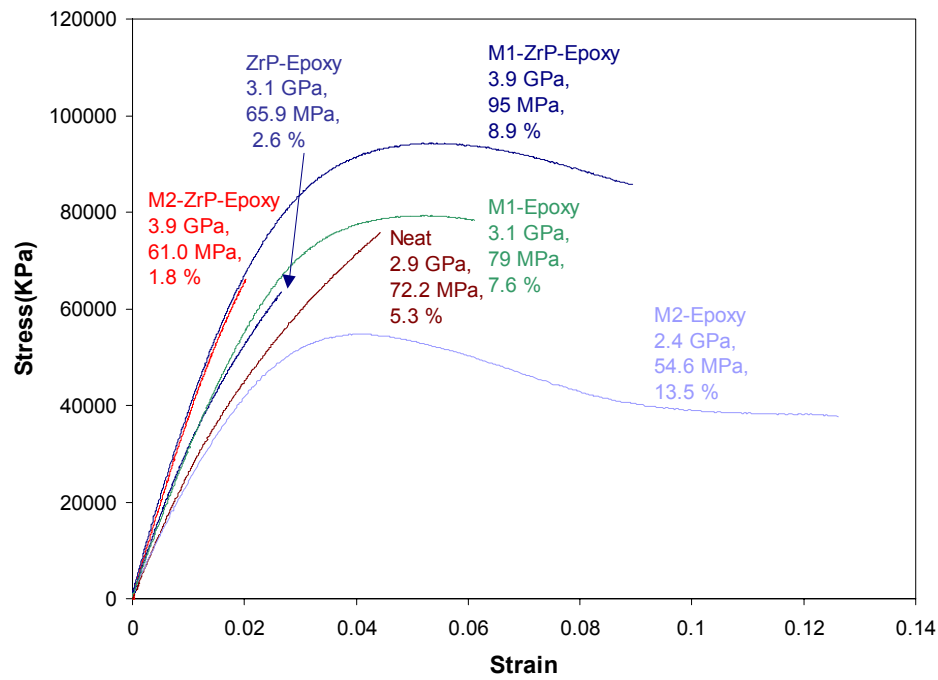


Figure 5-7. Tensile Behavior of M1-, M2-ZrP/Epoxy Nanocomposites.

Table 5-2. Tensile Properties and Fracture Toughness of ZrP-Epoxy Nanocomposites

	Neat	M1-Epoxy	M2-Epoxy	M1-ZrP-Epoxy	M2-ZrP-Epoxy	ZrP-Epoxy
Modulus (GPa)	2.9	3.1	2.4	3.9	3.9	3.1
Yield strength(MPa)	72.2	79.0	54.6	95.0	61.0	65.9
Elongation at Break(%)	5.3	7.6	13.5	8.9	1.8	2.6
K_{IC} (MPa*m ^{1/2})	0.80	-	0.83	-	0.77	0.79

5.3.4 Viscosity of Liquid Epoxy Resin with ZrP Particles

The viscosity behavior is one of the most important factors to be considered for practical industry applications. From the data sheet [94] of the DGEBA we used (DER332, Dow), the liquid epoxy has complex viscosity in the range of 4.0~6.0 Pa·sec at 25 °C, and the test results for the liquid epoxy with samples are shown in Figure 5-8. At first, the viscosity of the liquid epoxy resin, DER332 at 26 °C is around 2.83-3.17 Pa·sec, and they behave as a Newtonian, the viscosity is independent of the shear rate (1/sec). If the ZrP without surface modification is added to the liquid epoxy resin, the viscosity is slightly decreased with the increased shear rate and the viscosity is lower than the DER332 liquid epoxy resin. When the surface modified ZrP is added to the

liquid epoxy resin, it shows the shear thinning effect; the complex viscosity is increased significantly to over 13.3 Pa·sec at low shear rate (2.65×10^{-1} /sec) and decreased to 7.09 Pa·sec at higher shear rate (1.09×10^2 /sec). This is possibly because of the successful exfoliation of the ZrP layer structure with matrix resin, which uniformly dispersed layers among the matrix resin with similar scale level of the molecules increase the viscosity of the matrix resin. Though it may not be compared directly, similar effect was reported for the nanotube filled polycarbonate nanocomposite systems [95]. This result is consistent with the fiber-reinforced composite materials from theoretical expectations and experimental observations [96~98]. The complex viscosity values of the liquid epoxy with modified ZrP is high relative to the values of the viscosity of liquid epoxy resin without modified ZrP or resin with unmodified ZrP. It can be expected because the conventional filler such as the unmodified ZrP behaves as the viscosity reducing agent in the liquid epoxy resin matrix, while the modified ZrP particles increase the viscosity of the matrix resin at tested shear rate range. The shear-thinning effect as shown in the Figure 5-8 is also good for this mixture to be processed in industrial applications.

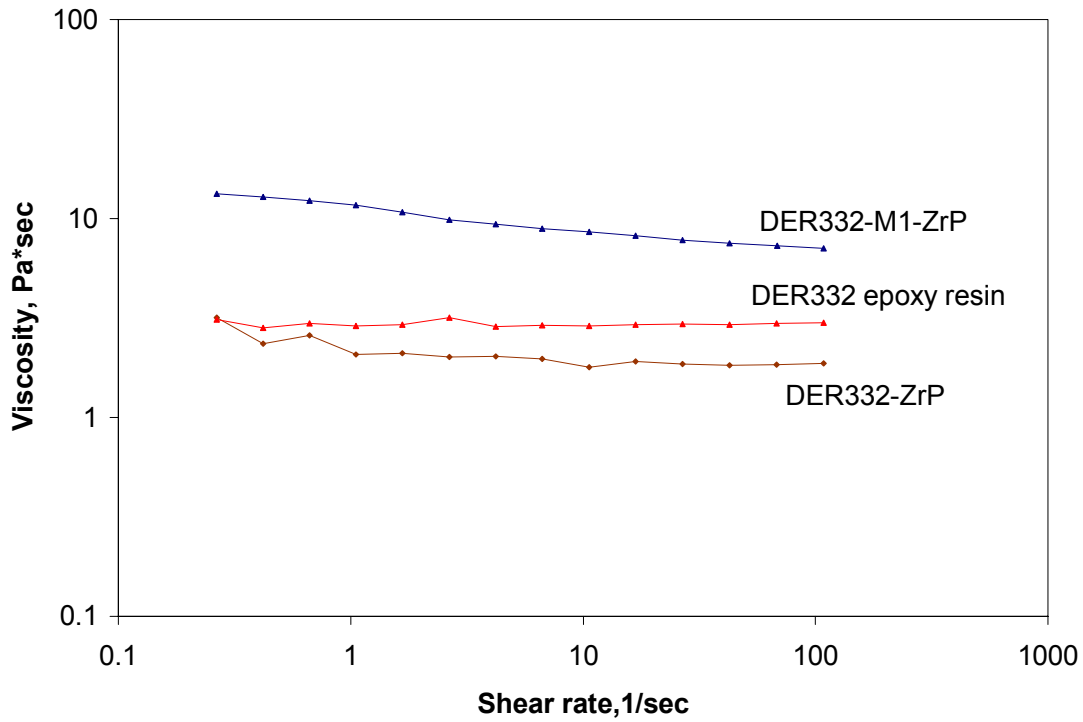


Figure 5-8. Viscosity of the ZrP and M1-ZrP in Liquid Epoxy (DER332) at Different Shear Rate.

5.3.5 Epoxy-II Nanocomposite System with CSR

5.3.5.1 Mechanical Properties

The modulus of the ME, modifier added system, is slightly increased to 3.1 GPa from 2.9 GPa of the neat Epoxy-II system [Figure 5-9]. By the addition of the exfoliated ZrP into ME, the modulus is increased to 4.1 GPa. By additional CSR adding to the MZE system, the CMZE system has modulus of 3.6 GPa. As a reference, CME system

with modifier with CSR without ZrP particles has modulus of 2.6 GPa, which is smaller than the neat Epoxy-II system.

The yield stress for the ME system, 89.7 MPa, is increased to 103.4 MPa (MZE system) by adding the exfoliated ZrP particles. The CSR addition to the MZE system lowers the yield stress to 93.3 MPa. When CSR is added to ME, the yield stress is decreased to 78.8 MPa. The elongation at break for the ZrP Epoxy-II nanocomposite systems, i.e., ME, MZE, CME, and CMZE have similar values around 6.3 to 7.1 %. The neat Epoxy-II resin has relatively smaller value of elongation at break, which is 3.5 %.

5.3.5.2 Toughening Mechanisms of CMZE System

The modified ZrP Epoxy-II nanocomposites with and without CSR are prepared to study the role of nanofiller and CSR in their fracture behavior and the toughening mechanisms by CSR addition. The SEN-3PB tests for these Epoxy-II systems revealed a significant increase in the mode I critical fracture toughness values (K_{IC}) in the case of the addition of ZrP and CSR together in the epoxy resin system. It is increased to 1.64 $\text{MPa}\cdot\text{m}^{0.5}$ of CMZE nanocomposite system from 0.69 $\text{MPa}\cdot\text{m}^{0.5}$ of ME epoxy system, which is over a 130 % increase in K_{IC} . It is very interesting that this dramatic increase of fracture toughness by small amount of CSR addition into epoxy nanocomposite with exfoliated layer-structure is observed also for the clay-epoxy nanocomposites [89].

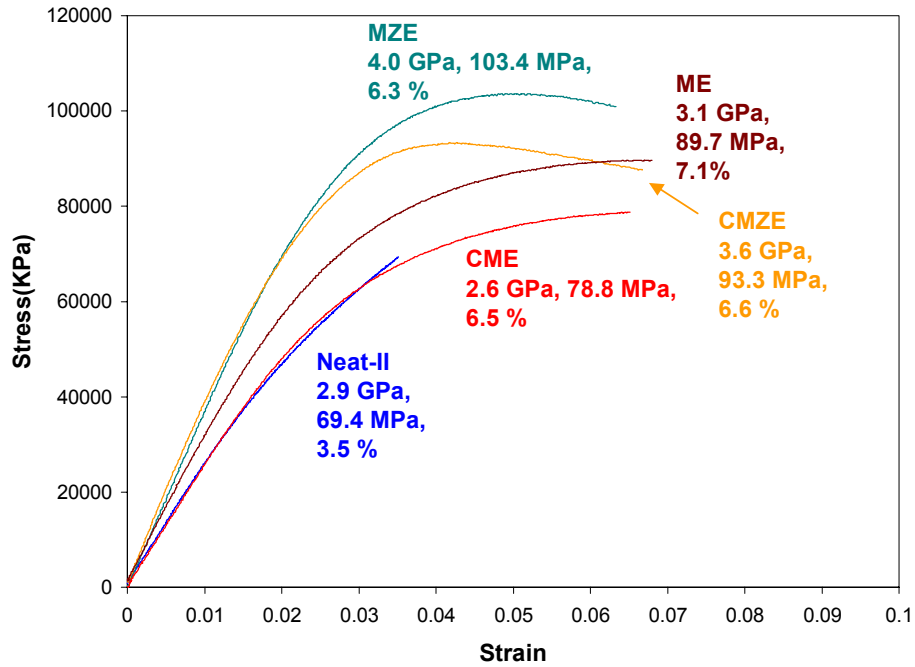


Figure 5-9. Tensile Behavior of M-ZrP/Epoxy-II Nanocomposites.

On the other hand, the K_{IC} value is not significantly changed by the addition of either the surface modifier or the exfoliated ZrP into the epoxy resins as shown in Table 5-3. It is consistent with previous research that exfoliated layer nanofillers do not affect the fracture toughness of epoxy resin [32].

The CSR addition to ME system increases the K_{IC} value about 33 %, which is not as significant as the increment in CMZE but it is still a meaningful increase for the

brittle epoxy resin system. Very interesting results are observed from the microscopy observation on the DN-4PB test specimens. The OM from MZE has no plastic deformation at the crack tip damage zone and failed as brittle manner, so it is not presented here. However when the crack tip area of the MZE specimen from the DN4PB test is observed with TEM, there are some voids along with dispersed nano-layer structures [Figure 5-10]. The magnified TEM picture on the void clearly shows the void is developed adjacent of the ZrP layers. Another TEM picture [Figure 5-11] with arrows also supports this claim, and layer structures from ZrP nanofillers are observed around the developed crack. Similar fracture behavior was observed from other epoxy nanocomposites with clay nanofillers and they do not induce any significant toughening mechanism but fail in brittle manner [32].

When the CSR particles are added to the MZE system, a massive plastic deformation at the crack tip damage zone is clearly observed from the OM picture of CMZE specimen under bright field and cross-polarized conditions as shown in Figure 5-12. Big area of birefringence along the developed crack is also detected as evidence of the possible shear deformation around the developed crack and crack tip region. For further characterization on the toughening mechanisms of epoxy nanocomposites by CSR addition, TEM pictures are taken along the crack development direction and at the crack tip damage zone. Several pictures are taken before CSR staining, because the small cavities of CSR may not be clearly observed once the CSR particles are stained [Figures 5-13~14]. Figure 5-13 shows a TEM picture along the crack development direction and

many cavities from CSR particles are observed besides the developed crack, and they are elongated with angle.

Table 5-3. Tensile Properties and Fracture Toughness of ZrP-Epoxy-II Nanocomposites

	Neat II E	M-Epoxy-II ME	M-ZrP-Epoxy-II MZE	CSR-M-Epoxy-II CME	CSR-M-ZrP-Epoxy-II CMZE
Modulus (GPa)	2.9	3.1	4.0	2.6	3.6
Yield strength(MPa)	69.4	89.7	103.4	78.8	93.3
Elongation at Break(%)	3.5	7.1	6.3	6.5	6.6
K_{IC} (MPa*m ^{1/2})	0.76	0.69	0.70	0.92	1.64

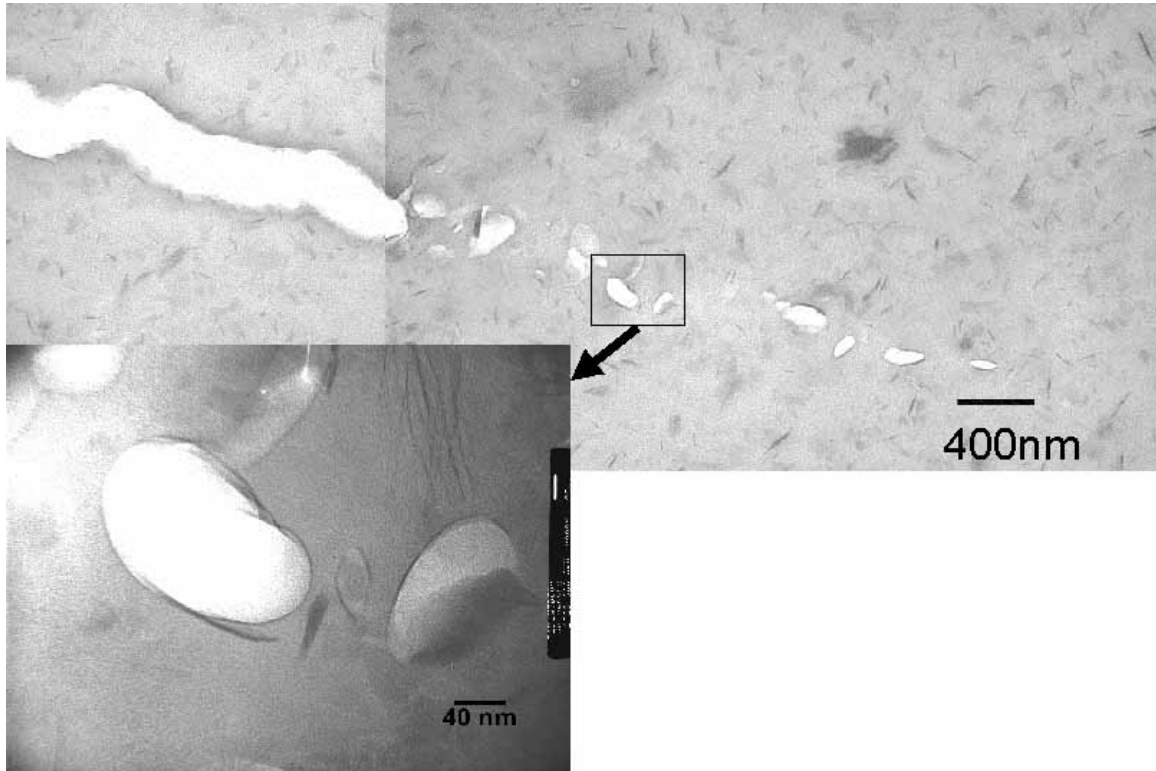


Figure 5-10. TEM of Crack Tip Damage Zone from DN-4PB Test Sample of MZE Epoxy Nanocomposites.

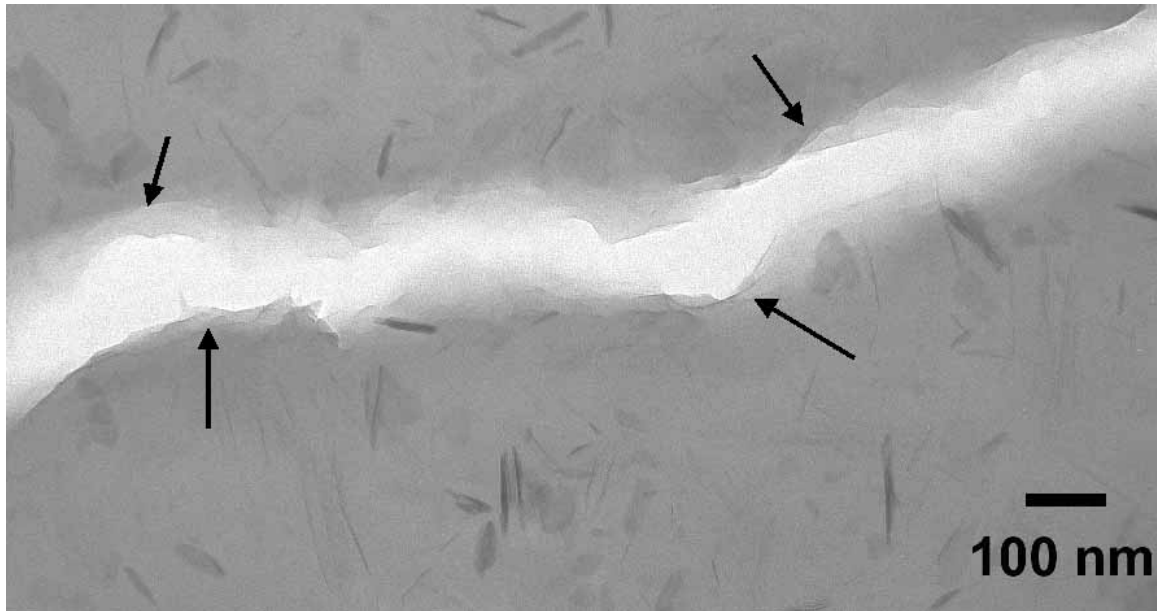


Figure 5-11. TEM of Crack from DN-4PB Test Sample of MZE Epoxy Nanocomposites.

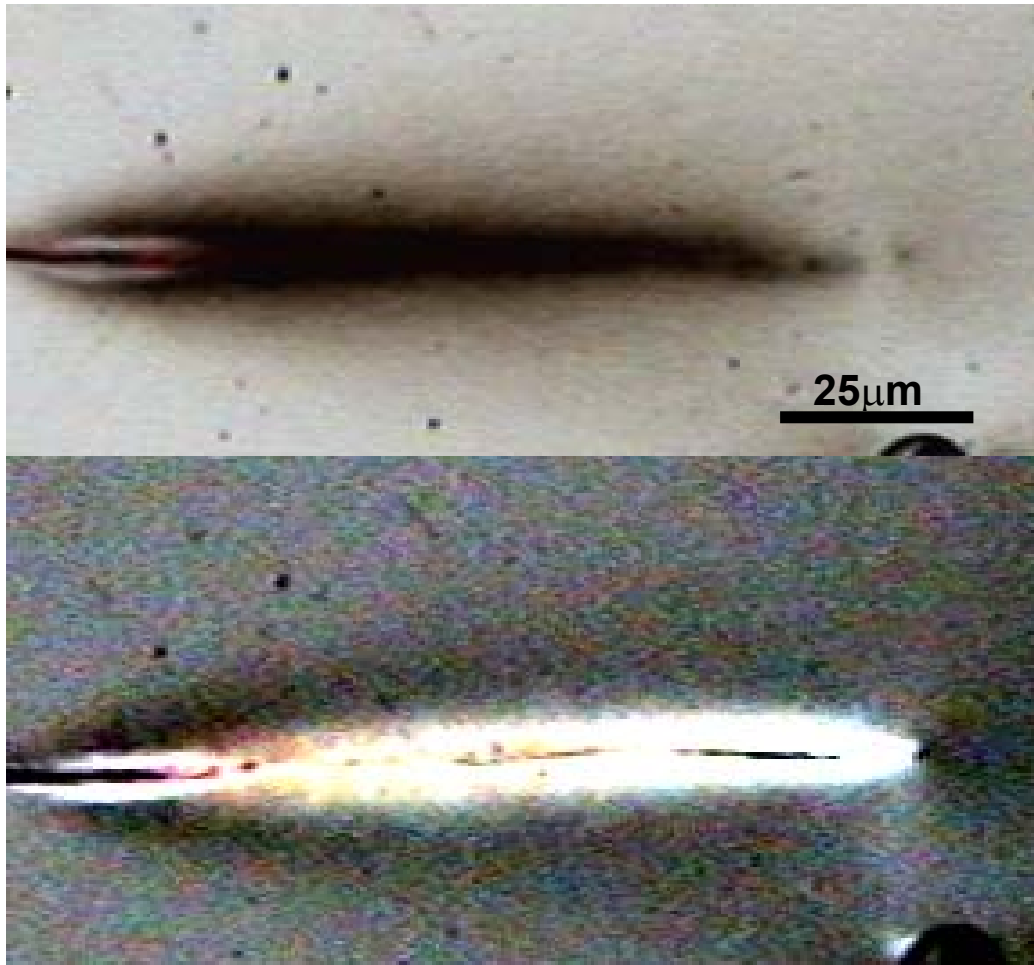


Figure 5-12. OM of Crack Tip Damage Zone from DN-4PB Test Sample of CMZE Epoxy Nanocomposite. (top) Bright Field and (bottom) Cross-polarized Field.

The CSR particles in the CMZE nanocomposite are stained with OsO_4 to give enough hardness for better thin-sectioning and for the enhanced contrast for taking pictures. In Figure 5-15, the stained CSR and exfoliated ZrP layers far from the crack are observed. The round shape of a CSR particle has its size of slightly smaller than 100 nm diameter. From the Figure 5-16, which shows besides the crack, most of CSR near the crack are cavitated and elongated, and some intact and elongated CSR particles are also observed. The exfoliated ZrP layer structures observed near CSR do not involve any void or cavity generation, which is different from the MZE fracture behavior. Figure 5-17 is a TEM picture from the crack tip damage zone, and it shows the blunted crack tip and similar features with those from beside the cracks and the ZrP layer structures are not involved with the cavity generation. However, the elongated cavities and intact CSR's more severe elongations are perpendicular to the direction of the crack development.

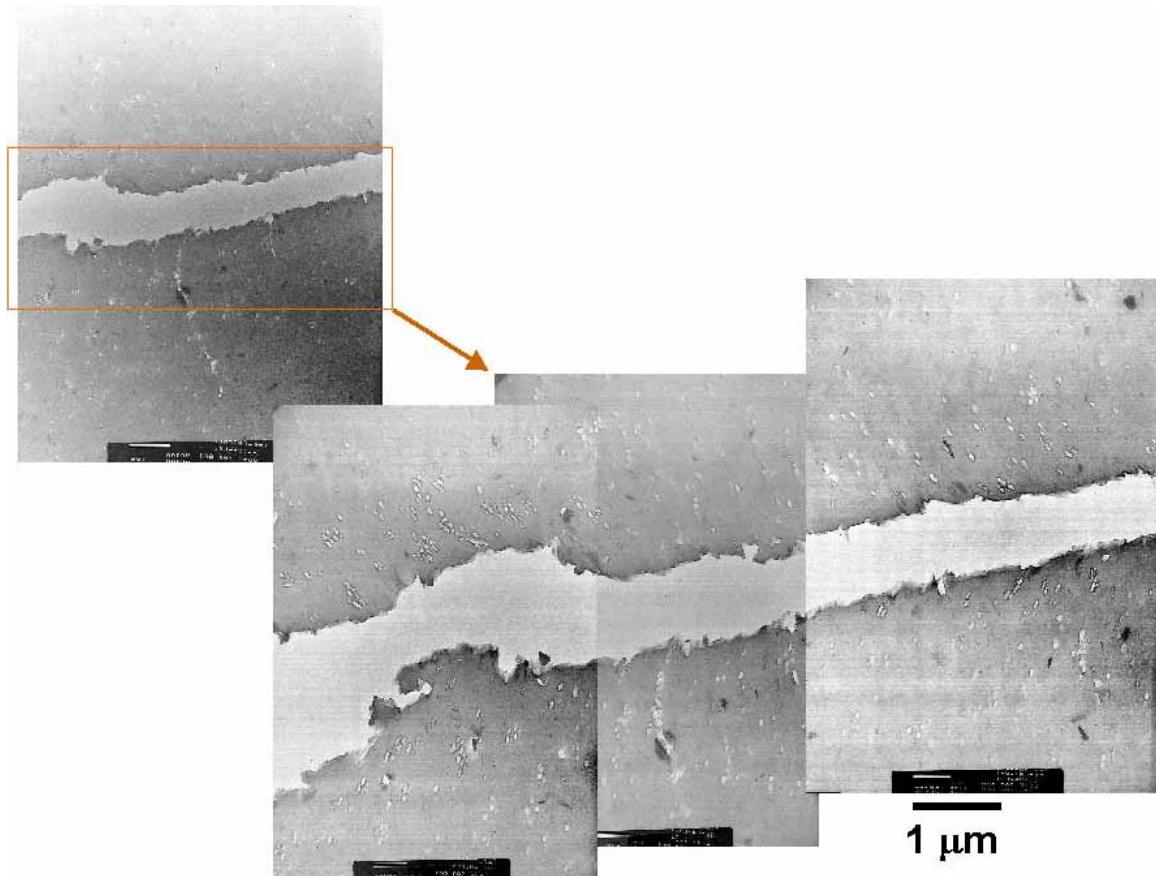


Figure 5-13. TEM of Crack from DN-4PB Test Sample of CMZE Epoxy Nanocomposite before CSR Staining.

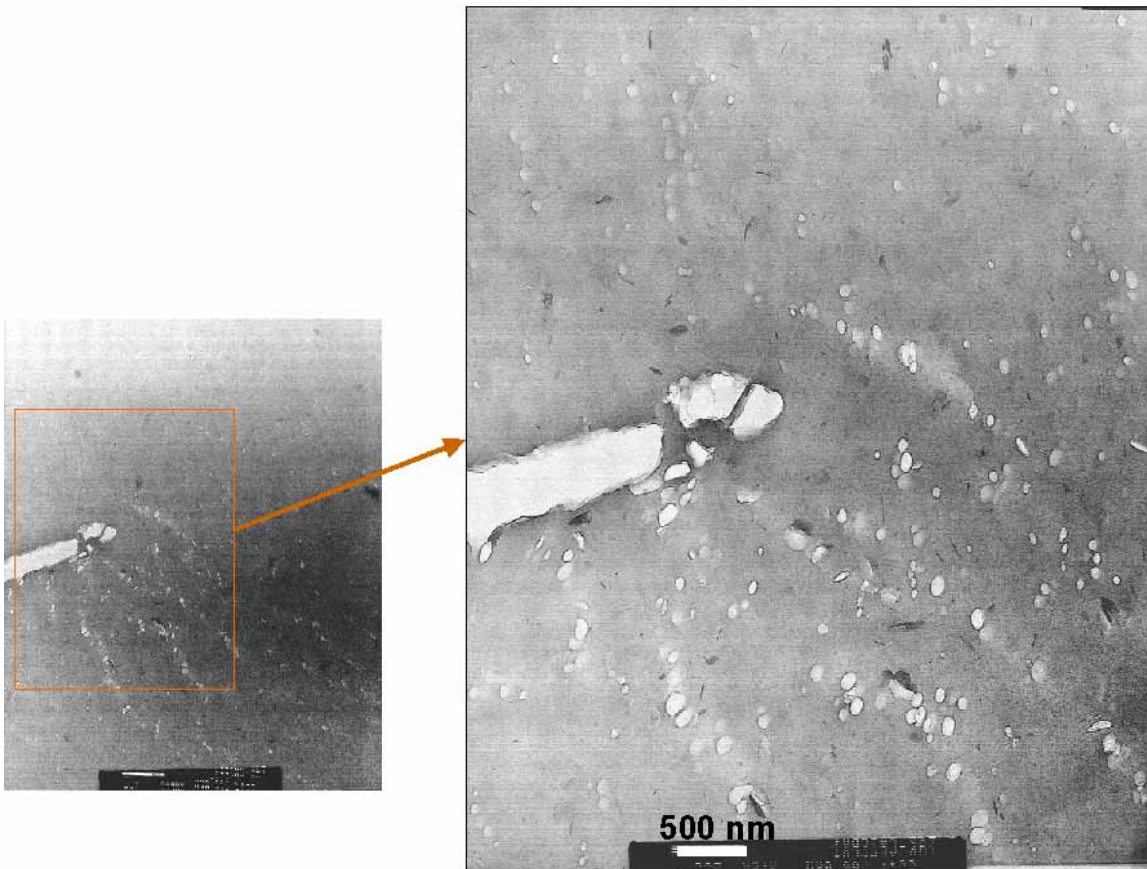


Figure 5-14. TEM of Crack Tip Damage Zone from DN-4PB Test Sample of CMZE Epoxy Nanocomposite before CSR Staining.

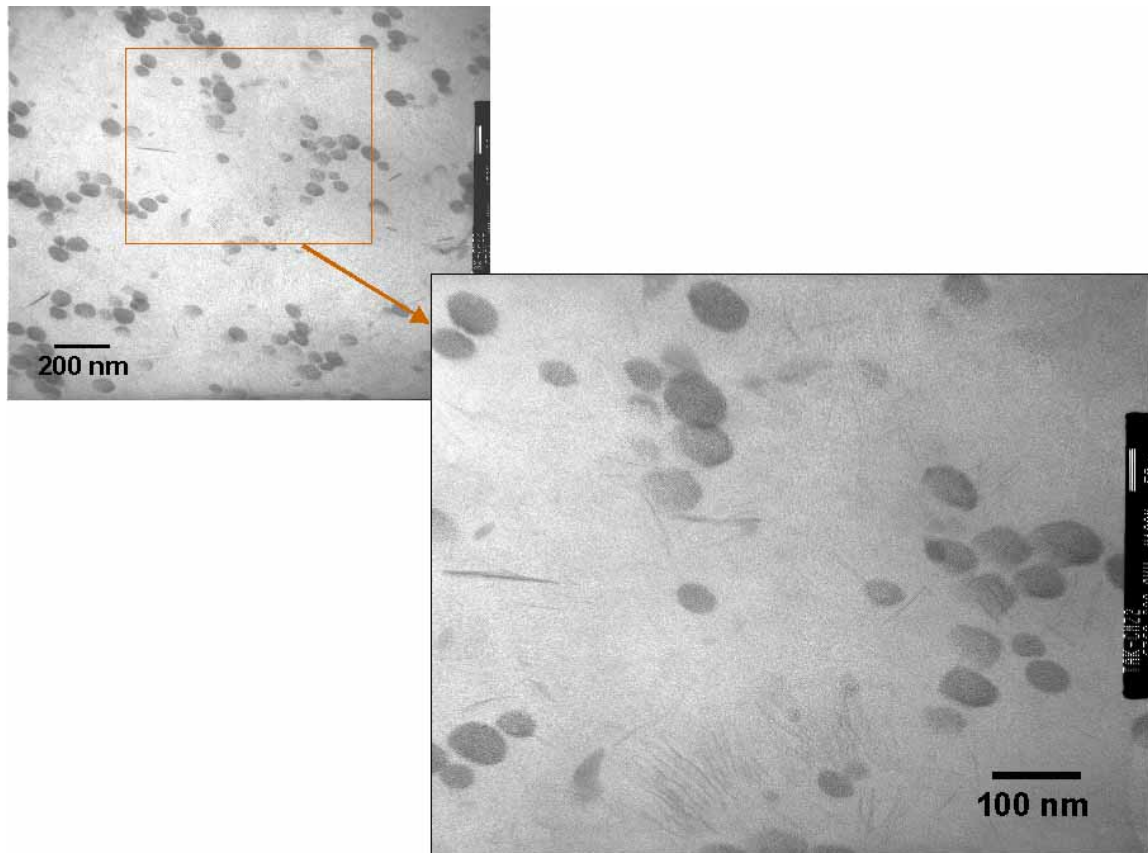


Figure 5-15. TEM of CMZE Epoxy Nanocomposite after CSR Staining Far from Crack.

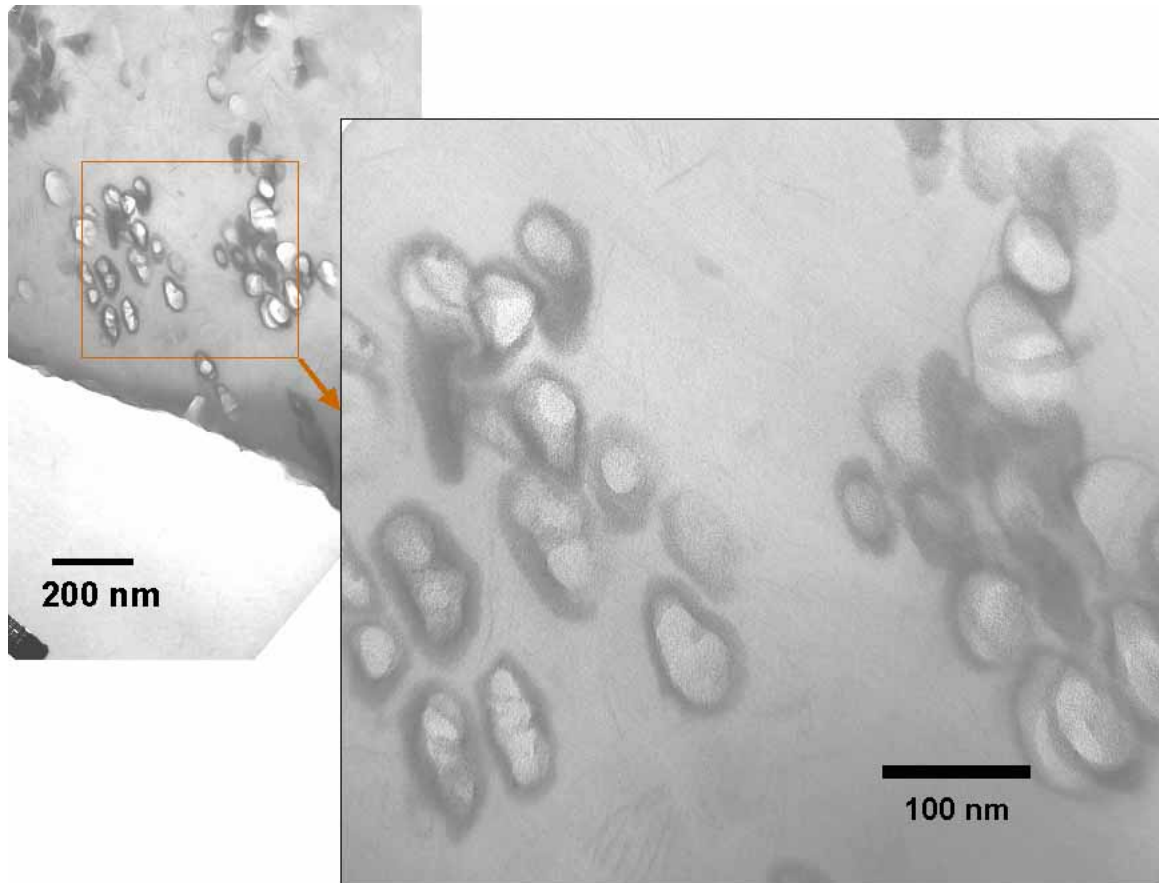


Figure 5-16. TEM of Crack from DN-4PB Test Sample of CMZE Epoxy Nanocomposite after CSR Staining.

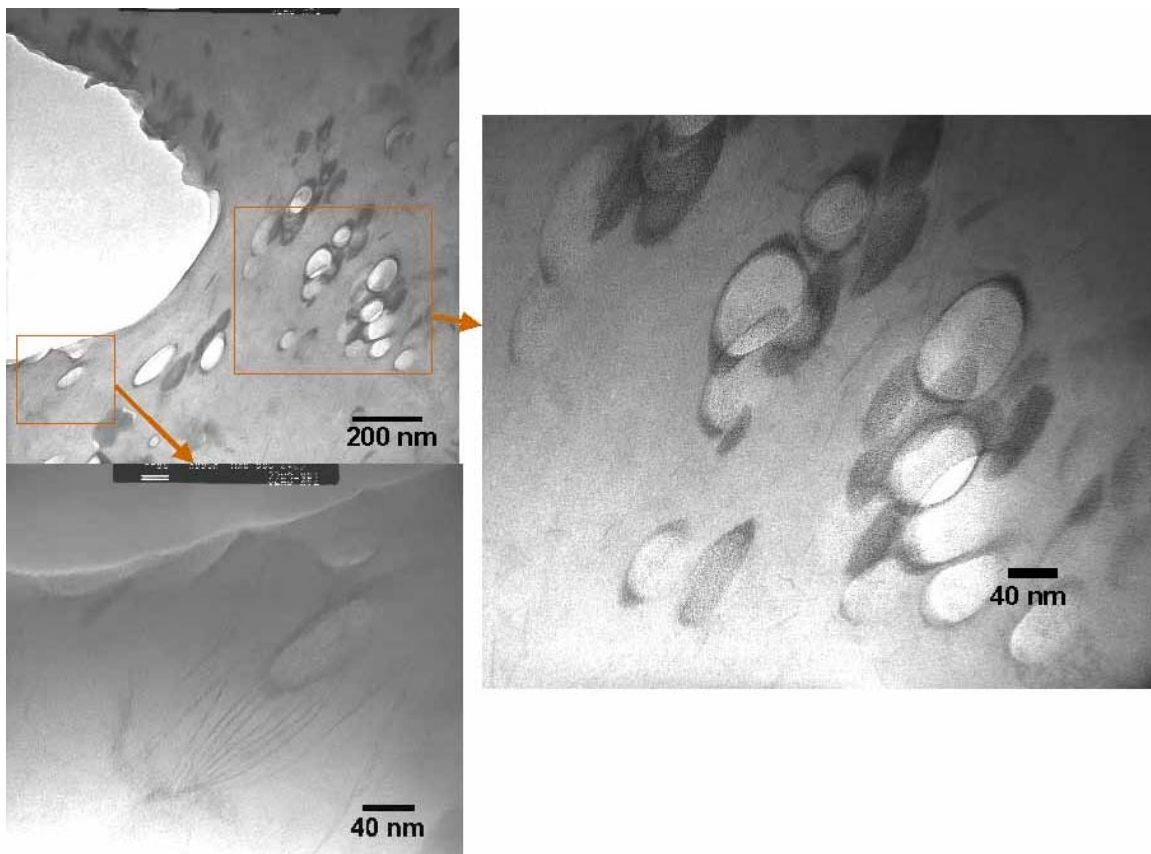


Figure 5-17. TEM of Crack Tip Damage Zone from DN-4PB Test Sample of CMZE Epoxy Nanocomposite after CSR Staining.

5.4 CONCLUSIONS

The mechanical properties and fracture behavior of synthetic ZrP - epoxy nanocomposites with different amounts of monoamine surface modifiers and the toughening mechanisms of ZrP-Epoxy nanocomposites with CSR particles are

investigated. The prepared ZrP-epoxy nanocomposites, M1- and M2-ZrP/Epoxy were characterized with WAXD and TEM for the nanofiller exfoliation and good dispersion in matrices. The nanocomposite with more surface modifier has a lower rubbery plateau modulus and lower glass transition temperature than the nanocomposite with less amounts of modifier. Exfoliated ZrP nanofillers increase the storage moduli of the matrices, especially at temperatures above T_g . The M1-ZrP/Epoxy system and the M2-ZrP/Epoxy system have similar tensile modulus values, while the M1-ZrP/Epoxy system has higher yield stress and elongation at break values than M2-ZrP/Epoxy system. Fracture toughness, K_{IC} , for these systems, i.e., neat epoxy, M2/Epoxy, ZrP/Epoxy, and M2-ZrP/Epoxy system have similar values around $0.8 \text{ MPa}\cdot\text{m}^{0.5}$.

The fracture toughness behavior of the ZrP epoxy nanocomposite system and the toughening mechanisms of CSR added ZrP epoxy nanocomposite are studied with another epoxy system. The CSR added ZrP epoxy nanocomposite (CMZE) has decreased tensile modulus (3.6 GPa) than the ZrP epoxy nanocomposite system (MZE) without CSR (4.1 GPa). The fracture toughness of the MZE is remarkably increased by CSR addition to 230 % (from 0.70 to $1.64 \text{ MPa}\cdot\text{m}^{0.5}$). The fracture behavior of the MZE system is in brittle manner with no major toughening mechanism, and a crack developed between ZrP layers in the matrix resin. Delamination of layers is observed with TEM. When the CMZE system failed, the CSR particles adjacent to the developing crack are elongated and cavitated to alter the stress state, and the matrix resin is shear deformed. Usually, the ZrP layer delamination makes cavities in between the layers, but this was not found in the CMZE system.

CHAPTER VI

CONCLUDING REMARKS AND RECOMMENDATIONS

The structure-property relationships of epoxy nanocomposites with inorganic layer-structure nanofillers have been studied in this dissertation. The fracture behavior and toughening mechanisms of epoxy nanocomposites with CSR particles were also investigated with several epoxy nanocomposite systems.

6.1 Intercalation and Exfoliation of the Inorganic Layer Structures in Epoxy Matrices

Morphology in two nanoclay-filled epoxy systems was investigated using both microscopy and spectroscopy tools. Clay exfoliation was achieved using a series of sample preparation steps, and confirmed using small and wide angle X-ray scattering and transmission electron microscopy (TEM) techniques.

The interlayer surfaces of α -ZrP can be easily modified because of its high surface ion exchange capacity characteristics. The α -ZrP structure is layered clay-like and possesses aspect ratios of at least 100. M- α -ZrP with wide interlayer spacing has been successfully prepared using commercially available monoamines intercalate. The intercalate is hydrogen bonded to the host and exhibits a bilayer structure into the interlayer spacing. The state of uniform dispersion and exfoliation has been confirmed

using WAXD and direct transmission electron microscopy observation at various locations of the sample.

6.2 Mechanical Properties of the Epoxy Nanocomposites

6.2.1 Clay Epoxy Nanocomposites

Significant modulus improvement was obtained when clay exfoliation was achieved. The T_g of the epoxy nanocomposites based on DMA was nearly identical to that of neat epoxy. The rubbery plateau moduli of the nanocomposites were increased with the addition of a nanofiller.

The tensile moduli of both System-1N and System-1NR were significantly higher than that of neat resin. The additions of clay and CSR improved modulus and fracture toughness.

6.2.2 ZrP-Epoxy Nanocomposites

The dynamical mechanical analysis study of M2-ZrP/Epoxy nanocomposites shows that the rubbery plateau modulus of the M2-ZrP/Epoxy nanocomposite is about 4.5 times higher than that of the M2/Epoxy. The nanocomposite with the greater amount of surface modifier has a lower rubbery plateau modulus and a lower glass transition temperature than that of the nanocomposite with a lesser amount of modifier.

The M1-ZrP/Epoxy system and the M2-ZrP/Epoxy system have similar tensile modulus values, but the M1-ZrP/Epoxy system has a higher yield stress and elongation at break value than the M2-ZrP/Epoxy system. With an addition of only 1.9 vol.% α -

ZrP, the tensile modulus of the α -ZrP-reinforced epoxy nanocomposite (M2-ZrP/Epoxy) is increased by 50% of the reference epoxy, and the yield strength improved by 10%. However, ductility of the matrix (elongation at break) is drastically reduced after the α -ZrP reinforcement. The CSR added ZrP epoxy nanocomposite (CMZE) has decreased tensile modulus (3.6 GPa) when compared to the ZrP epoxy nanocomposite system (MZE) without CSR (4.1 GPa).

6.3 Fracture Behavior and Toughening Mechanisms of Epoxy Nanocomposites

6.3.1 Clay Epoxy Nanocomposites

Incorporation of core-shell rubber (CSR) in both the clay-filled epoxy systems leads to greatly enhanced fracture toughness. Optical microscopy and TEM observations of the CSR-modified nanocomposites suggest that the toughening mechanisms in System-2NR include cavitation of CSR, followed by limited shear yielding of the matrix. Crack bifurcation, deflection, and crack bridging are also observed. In the more ductile System-1NR system, the major toughening mechanisms involve a large-scale CSR particle cavitation and/or debonding between the intercalated clay layers, followed by massive shear banding of the matrix. The present study has shown that the ductility of a polymer matrix can significantly influence the toughening effect from using CSR. CSR is effective in improving the fracture toughness of epoxy nanocomposites.

6.3.2 ZrP-Epoxy Nanocomposites

Fracture toughness, K_{IC} , for these systems, i.e., neat epoxy, M2/Epoxy, ZrP/Epoxy, and M2-ZrP/Epoxy systems has similar values around $0.8 \text{ MPa}\cdot\text{m}^{0.5}$. The CSR added ZrP epoxy nanocomposite (CMZE) has a decreased tensile modulus as compared to the ZrP epoxy nanocomposite system (MZE) without CSR. Following CSR addition, fracture toughness of MZE increased by 230 %.

The fracture behavior of the MZE system is classified in a brittle manner with no major toughening mechanisms. A crack developed between ZrP layers in the matrix resin and delamination of layers was observed. When the CMZE system failed, the CSR particles adjacent to the developing crack are elongated and cavitated to alter the stress-state and the matrix resin becomes shear deformed. The ZrP layer delamination, which makes cavities in between layers, is not found in the CMZE system.

6.4. Recommendations for Future Research

The nanocomposite with a greater amount of surface modifier has a lower rubbery plateau modulus and a lower glass transition temperature than the nanocomposite with a lesser amount of modifier. However, the quantity of the monoamine M715 involved in the M1-, M2-ZrP/Epoxy curing process responsible for the significant drop in T_g , is still uncertain. This issue can be addressed by altering the level of monoamine and the type of surface modifiers utilized.

The present research clearly shows that α -ZrP-based epoxy nanocomposites are ideal for gaining fundamental knowledge on the physics of how and why nanoparticles alter the physical and mechanical properties of polymer matrices. The versatility and simplicity of α -ZrP synthesis to control the surface functionality, size and aspect ratio of α -ZrP particles would allow the establishment of unambiguous fundamental relationships between nanoparticle material parameters and the physical and mechanical properties of polymer nanocomposites. Research on altering the aspect ratios, sizes, and surface functionalities of α -ZrP, to further investigate how and why nanofillers change the properties of polymers, is necessary.

The ability of the nanofiller to carry and redistribute the applied stress field depends strongly on the mobility and the size of the nanofiller. As a result, the more mobile the nanofiller is, the easier it is for the nanofiller to contribute to the stiffening of the matrix. Since the nanofiller is small and can be easily mobilized by the surrounding mobile molecules, the stiffening effect would be maximized when the temperature is above T_g and minimized when the temperature is below the γ -relaxation peak. When the filler size is far greater than the molecular size, the conventional composite principle would take effect, as in the case of the α -ZrP/Epoxy system. Nevertheless, the actual physical origin of such unusual behavior of nanofiller is still not known, which warrants further research in the future. Additional designed experiments need to be done.

In summary, several epoxy nanocomposite systems are successfully prepared and show enhanced materials properties. The CSR particles are used as an effective toughening product for epoxy nanocomposite systems to achieve desirable toughness without loss in

other mechanical properties, and the fracture behavior and major toughening mechanisms are investigated in relation with the role of the nanofillers in the epoxy matrices. The application of nanofillers, especially ZrP particles, and CSR particles for epoxy nanocomposite materials preparation and for study the fundamental structure-property relationships is promising.

REFERENCES

1. Y. Kojima, A. Usuki, M. Kawasumi, A. Okada, T. Kurauchi and O. Kamigaito, *J. Polym. Sci. Part A: Polym. Chem.* **31** (1993) 983.
2. Y. Kojima, A. Usuki, M. Kawasumi, A. Okada, T. Kurauchi and O. Kamigaito, *J. Polym. Sci. Part A: Polym. Chem.* **31** (1993) 1755.
3. Y. Kojima, A. Usuki, M. Kawasumi, A. Okada, Y. Fukushima, T. Kurauchi and O. Kamigaito, *J. Mater. Res.* **8** (1993) 1185.
4. Z. Wang and T. J. Pinnavaia, *Chem. Mater.* **10** (1998) 1820.
5. J. Massam and T. J. Pinnavaia, *Mater. Res. Soc. Symp. Proc.* **520** (1998) 223.
6. H. Z. Shi, T. Lan and T. J. Pinnavaia, *Chem. Mater.* **8** (1996) 1584.
7. Z. Wang, T. Lan and T. J. Pinnavaia, *Chem. Mater.* **8** (1996) 2200.
8. T. Lan, P. D. Kaviratna and T. J. Pinnavaia, *Chem. Mater.* **7** (1995) 2144.
9. T. J. Pinnavaia, T. Lan, P. D. Kaviratna and M. S. Wang, *Mater. Res. Soc. Symp. Proc.* **346** (1994) 81.
10. K. Masenelli-Varlot, E. Reynaud, G. Vigier and J. Varlet, *J. Polym. Sci. Part B-Polym. Phys.* **40** (2002) 272.
11. H. Wang, C. C. Zeng, M. Elkovitch, L. J. Lee and K. W. Koelling, *Polym. Engr. Sci.* **41** (2001) 2036.
12. T. D. Fornes, P. J. Yoon, H. Keskkula and D. R. Paul, *Polymer.* **42** (2001) 9929.
13. L. M. Liu, N. Qi and X. G. Zhu, *J. Appl. Polymer Sci.* **71** (1999) 1133.

14. C. A. May (ed.), *"Epoxy Resin Chemistry and Technology"*, 2nd ed. (Marcel Dekker, New York, 1988).
15. a) A.F. Yee and R.A. Pearson, *J. Mater. Sci.* **21** (1986) 2462.
b) R.A. Pearson and A.F. Yee, *J. Mater. Sci.* **21** (1986) 2475.
16. C.B. Bucknall, *"Toughened Plastics"*, (Applied Science Publishers Ltd., London, 1977).
17. S.C. Kunz, Ph.D. Thesis, Churchill College, Cambridge, 1978.
18. A.J. Kinloch, "Relationship between Chemistry, Microstructure and Properties of Toughened Thermosetting Polymers", *Proc. PMSE Div. 194th ACS National Meeting* (Aug., 1987).
19. H. Breuer, F. Haaf and J. Stabenow, *J. Macromol. Sci.-Phys.* **B14(3)** (1977) 387.
20. S. Wu, *Polymer* **26** (1985) 1855.
21. J. Sultan and F. McGarry, *Polym. Eng. Sci.* **13** (1973) 19.
22. A.J. Kinloch, S.J. Shaw, D.A. Tod and D.L. Hunston, *Polymer* **24** (1983) 1341.
23. A.S. Argon, R.E. Cohen, O.S. Gebizlioglu and C.Schwier, in *"Advances in Polymer Science: crazing in Polymers"*, edited by H.H. Kausch, (Springer, Berlin, 1983), vol. 52/53, p.275.
24. R.J.M. Borggreve and R.J. Gaymans, "7th International Conference on Deformation, Yield and Fracture of Polymers", (Cambridge, England, 1988), p.34.
25. W.D. Bascom, R.Y. Ting, R.J. Moulton, C.K. Riew and A.R. Siebert, *J. Mater. Sci.* **16** (1981) 2657.

26. H.-J. Sue, E. I. Garcia-Meitin and D. M. Pickelman, in *Elastomer Technology Handbook*, edited by N. P. Cheremisinoff, *CRC Press*, chapter 18 (1993) 662.
27. H.-J. Sue, E. I. Garcia-Meitin, D. M. Pickelman and P. C. Yang, *Advances in Chemistry Series No. 223, Toughened Plastics I: Science and Engineering*, Chapter 10 (1993).
28. H.-J. Sue, J. L. Bertram, E.I. Garcia-Meitin, J. W. Wilchester and L. L. Walker, *Colloid Polym. Sci.* **272** (1994) 456.
29. T.J. Pinnavaia, T. Lan, Z. Wang, H. Shi and P. D. Kaviratna, *Nanotech. ACS*, chapter 17 (1996) 250.
30. P.B. Messersmith, and E. P. Giannelis, *Chem. Mater.* **6** (1994) 1719.
31. S. D. Burnside, and E. P. Giannelis, *Chem. Mater.* **7** (1995) 1597.
32. K. T. Gam, T. Miyamoto, R. Nishimura and H.-J. Sue, *Polym. Eng. & Sci.* in press.
33. N. Nasegawa, M. Kawasumi, M. Kato, A. Usuki and A. Okada, *J. Appl. Polym. Sci.* **67** (1998) 87.
34. N. Hasegawa, H. Okamoto, M. Kawasumi and A. Usuki, *J. Appl. Polym. Sci.* **74** (1999) 3359.
35. C. B. Ng, B. J. Ash, L. S. Schadler and R. W. Siegel, *Advanced Comp. Letters* **10** (2001) 101.
36. C. M. Chan, J.S. Wu, J.X. Li and Y. K. Cheung, *Polymer.* **43** (2002) 2981.
37. M. Z. Rong, M. Q. Zhang, Y. X. Zheng, H. M. Zeng, R. Walter and K. Friedrich, *Polymer.* **42** (2001) 167.

38. G. Borchardt, "*Smectites, Minerals in Soil Environments*", edited by J.B. Dixon and S.B. Weed, Soil Science Society of America, Madison, Wisconsin, chapter 14 (1989) 675.
39. A. Usuki, Y. Kojima, M. Kawasumi, A. Okada, Y. Fukushima, T. Kurauchi and O. Kamigaito, *J. Mater. Res.* **8** (1993) 1179.
40. M. S. Wang and T. Pinnavaia, *Chem. Mater.* **6** (1994) 468.
41. T. Lan and T. Pinnavaia, *Chem. Mater.* **6** (1994) 2216.
42. Y. Kurokawa, H. Yasuda, M. Kashiwagi and A. Oyo, *J. Mater. Sci. Lett.* **16** (1997) 1670.
43. A. Clearfield and J. A. Stynes, *J. Inorg. Nucl. Chem.* **26** (1964) 117.
44. a) A. Clearfield and G. D. Smith, *Inorg. Chem.* **8** (1969) 431.
b) J. M. Troup and A. Clearfield, *Inorg. Chem.* **16** (1977) 3311.
45. A. Clearfield and R. M. Tindwa, *J. Inorg. Nucl. Chem.* **41** (1979) 871.
46. Y. Ding, D. J. Jones, P. Maireles-Torres and J. Roziere, *Chem. Mater.* **7** (1995) 562.
47. H. Kim, S. W. Keller, T. E. Mallouk, J. Schmitt and G. Decher, *Chem. Mater.* **9** (1997) 1414.
48. M. L. Jackson, Soil Chem. Analysis, Advanced Course, Dept. Soil Sci., Univ. of Wisconsin (1969)
49. J. W. Jordan, *J. Phys. Chem.* **59** (1949) 294.
50. G. W. Beall and S. J. Tsipursky, Proc. of Additives 98, (Orlando), Feb. (1998).
51. F. L. Beyer, N. C. Tan, A. Dasgupta and M. E. Galvin, *Chem. Mater.* **14** (2002) 2983.

52. A. Clearfield, *Ann. Rev. Mater. Sci.* **14** (1984) 205.
53. X. Kornmann, H. Lindberg and L. A. Berglund, *Polymer* **42** (2001) 1303.
54. X. Kornmann, H. Lindberg and L. A. Berglund, *Polymer* **42** (2001) 4493.
55. Y. C. Ke, L. Wang and Z. N. Qi, *Acta Polymerica Sinica* **6** (2000) 768.
56. G. S. Sur, H. L. Sun, S. G. Lyu and J. E. Mark, *Polymer* **42** (2001) 9783.
57. J. H. Chang and D. K. Park, *J. Polym. Sci.: Part B: Polymer Physics* **39** (2001) 2581.
58. K. E. Strawhecker and E. Manias, *Chem. Mater.* **12** (2000) 2943.
59. H. Tyan, Y. Liu and K. Wei, *Chem. Mater.* **11** (1999) 1942.
60. Y. Chen and J. Iroh, *Chem. Mater.* **11** (1999) 1218.
61. T. Agag, T. Koga and T. Takeichi, *Polymer* **42** (2001) 3399.
62. H. L. Tyan, K. H. Wei and T. E. Hsieh, *J. Polym. Sci.: Part B: Polymer Physics* **38** (2000) 2873.
63. Z. Wang and T. J. Pinnavaia, *Chem. Mater.* **10** (1998) 3769.
64. Y. I. Tien and K. H. Wei, *Macromolecules* **34** (2001) 9045.
65. K. J. Yao, M. Song, D. J. Hourston and D. Z. Luo, *Polymer* **43** (2002) 1017.
66. D. A. Brune and J. Bicerano, *Polymer* **43** (2002) 369.
67. J. M. Gloaguen and J. M. Lefebvre, J. M., *Polymer* **42** (2001) 5841.
68. G. Wei and H.-J. Sue, *J. Appl. Polym. Sci.* **74** (1999) 2539.
69. G.-X. Wei, H.-J. Sue, J. Chu, C. Huang and K. Gong, *Polymer* **41** (2000) 2947.
70. G.-X. Wei, H.-J. Sue, J. Chu, C. Huang and K. Gong, *J. Mater. Sci.* **35** (2000) 555.
71. H.-J. Sue, P. M. Puckett, J. L. Bertram, L. L. Walker and E. I. Garcia-Meitin, *J. Polym. Sci.: Part B: Polymer Physics* **37** (1999) 2137.

72. A.C. Garg and Y. W. Mai, *Composite Sci. and Tech.* **31** (1988) 179.
73. A.M. Donald and E.J. Kramer, *J. Appl. Polym. Sci.* **27** (1982) 3729.
74. B. Z. Jang, D. R. Uhlmann and J. B. Vander Sande, *Polym. Eng. Sci.* **25** (1985) 643.
75. R. A. Pearson and A. F. Yee, *J. Mater. Sci.* **26** (1991) 3828.
76. C. G. Chen, D. Curliss, *SAMPE J.* **37** (2001) 11.
77. A. S. Holik, R. P. Kambour, S. Y. Hobbs and D. G. Fink, *Microstructure Sci.* **7** (1979) 357.
78. M. Biswas and S. S. Ray, *Advances in Polymer Science Vol. 115, New Polymerization Techniques and Synthetic Methodologies.* (Springer, 2001), p.167.
79. T. K. Chen and Y. H. Jan, *Polym. Eng. Sci.* **35** (1995) 778.
80. K. T. Gam, N. Bestaoui, N. Spurr, A. Clearfield and H. –J. Sue, SPE-ANTEC (Nashville), The Society of Plastics Engineers, May 2003.
81. A. Clearfield, W. L. Duax, A. S. Medina, G. O. Smith and J. R. Thomas, *J. Phys. Chem.* **73** (1969) 3424.
82. A. Clearfield, A. Oskarsson, C. Oskarsson, *Ion exchange and Membranes*, **1** (1972) 91.
83. N. Bestaoui, N. Spurr and A. Clearfield, submitted to *Chem. Mater.*.
84. D. J. Mac Lachlan and K. R. Morgan, *J. Phys. Chem.* **94** (1990) 7657.
85. D. J. Mac Lachlan and K. R. Morgan, *J. Phys. Chem.* **96** (1992) 3459.
86. C. S. Triantifillidis, P. C. LeBaron and T. J. Pinnavaia, *Chem. Mater.* **14** (2002) 4088.
87. D. Gersappe, *Phys. Rev. Lett.* (2002) 89-058301.

88. H. -J. Sue, K. T. Gam, N. Bestaoui, N. Spurr and A. Clearfield, *Chem. Mater.*, submitted.
89. P. B. Messersmith, E. P. Giannelis, "Novel Tech. in Synth.&Proc. of Adv. Mater.", the Minerals, Metals & Mater. Soc. (1995) 497.
90. P. Kelly, A. Akelah, S. Qutubuddin, A. Moet, *J. Mater. Sci.* **29** (1994) 2274.
91. R. A. Vaia, H. Ishii, E. P. Giannelis, *Chem. Mater.* **5** (1993) 1694.
92. E. P. Giannelis, *Adv. Mater.* **8** (1996) 29.
93. J. Massam, Z. Wang, T. J. Pinnavaia, Proc. ACS PMSC Div. 78 (1995) 274.
94. Dow Liquid Epoxy Resins, Dow Chemical Co., Form No.296-224-790-P&M, (1990)
95. P. Potschke, T. D. Fornes, D. R. Paul, *Polymer* **43** (2002) 3247.
96. A.T. Mutel, M. R. Kamal, "Rheological Properties of Fiber Reinforced Polymer Melts", in *Two Phase Polymer Systems*, edited by L. A. Utraki, Munich, chapter 12 (1991) 305.
97. T. Kitano, T. Kataoka, *Rheol Acta* **19** (1980) 753.
98. T. Kitano, T. Kataoka, Y. Nagatsuka, *Rheol Acta* **23** (1984) 20.

VITA

Ki Tak Gam was born on March 2, 1969 in Masan, Kyung-nam, Republic of Korea. He lived in Masan until finishing high school. In 1987, he went to Pusan, the biggest seaport and the 2nd largest city in Korea, and began his college life. He earned his B.S. degree in 1991 from Pusan National University with a major in Polymer Science and Engineering. He then continued his graduate studies at the same university and obtained a M.S. degree in 1994. The focus of his M.S. research was synthesis, characterization, and biological activity study of antitumor polymer drugs. From 1993 to 1998, he worked as a researcher in Film R&D Team, Kolon Ind. Inc., Kumi, Korea. He started his Ph.D. program at Texas A&M University in 1998. After a semester in the Civil Engineering Department, he switched to the field of polymer science and engineering to pursue a Ph.D. in Mechanical Engineering. His research interest is preparation, characterization, and the structure property relationship of polymer nanocomposites. His permanent address is:

500 Nanpo-Ri, Gusan-Myun, Hapcho-Gu

Masan-City, Kyung-sang-nam-Do 641-041

Republic of Korea